Earth's Field Nuclear Magnetic Resonance Measurement of Blood Pressure Metrics in a Compliant Vessel Model

Steven Ronny Frohlich

Johannesburg, 2019

A dissertation submitted to the Faculty of Engineering and the Built Environment, University of Witwatersrand, Johannesburg, in fulfilment of the requirements for the degree of Master of Science in Engineering.

Declaration

I declare that this dissertation is my own unaided work. It is being submitted to the degree of Master of Science in Engineering to the University of the Witwatersrand, Johannesburg. It has not been submitted before for any degree or examination to any other University.

.....

(Signature of Candidate)

……. day of …… year …….

Abstract

The following experimental design and setup have been created by the author and supervisor. Current methodologies for non-invasive blood pressure measurement are flawed due to the subjective nature of measurement. Experimentation has been performed to determine to what degree relevant cardiovascular metrics can be non-invasively extracted from idealised software and hardware models of a human upper limb. The physical model is constructed to replicate the dimensions of major arteries and veins of the upper limb and is filled with water to approximate the vessels in the upper arm. Static water tests are performed to calibrate the model in order to obtain appropriate parameter values. Pulse and collect experiments have been performed on volumes of water flowing through cardiovascular analogues that are polarised upstream by 300 mT annular Halbach arrays. Testing is performed using the *TerraNova-MRI* Earth's Field Nuclear Magnetic Resonance apparatus from *Magritek*. Signal models obtained from literature have been modified to determine the effect of vessel compliance on flow measurements. A direct positive correlation ($p= 0.88$) between signal level received and the increasing pressure and volume of water within the model is observed. The average standard error between measurements is 0.04 μV, or 10% of the magnitude of the smallest measured signal. The relative error between theoretical and measured signals is 30%. The relative error is unreliable as the theoretical model does not include the effects of noise. The compliance of the model's vessel analogues is estimated to be 1.48 ml/mmHg compared to normal healthy young human compliance values of ~ 2 ml/mmHg. An empirical relationship between the pressure and signal captured by the apparatus is found. The problem is ill-posed with many possible pressure-volume relationships able to output the same signal result. Calibration of the signal and model needs to be performed to determine a direct causal relationship between blood pressure and the EFNMR signal captured.

Dedication

The author would like to dedicate this dissertation to his family and friends who endured hours of discussion on this topic. The constant emotional and financial support of my family has helped keep me both motivated and sane during these two years.

To my friends, who constantly questioned what and why I have been doing this research, you have truly helped me understand why I have been asking these questions and why I believe this dissertation can help develop humanity's knowledge of what is possible with what we already know.

Acknowledgements

I would like to acknowledge the help and support of my supervisor, Steven Dinger, who has always been available at the nearest convenience to discuss the direction of my research. He has been a fantastic and responsive supervisor throughout the research period.

Acknowledgement must be given to Jethro Polliack and Shani Feller, who, through the course of their Honour's degree performed research which greatly assisted the research that is given in this dissertation.

I would like to acknowledge the Wits Electrical and Information Engineering faculty who have always been supportive and available to discuss the scope and understanding of this dissertation.

I would also like to acknowledge the support of Wits University through their provision of the Postgraduate Merit Award that funded the first year of my research.

Table of Contents

List of Figures

Glossary of Terms and Abbreviations

Abbreviation/Term	Description
CSPT	Calibrated Subclavian Pulse Tracing
EFNMR	Earth Field Nuclear Magnetic Resonance
IAP	Invasive Arterial Pressure
ICU	Intensive Care Unit
KAM	Korotkoff Auscultatory Method
NIBP	Non-Invasive Blood Pressure

Chapter 1 – Introduction

1.1 Problem Context

Blood Pressure (BP) and arterial compliance are important metrics that assist medical practitioners in the successful diagnosis and treatment of a patient [1]. Blood Pressure and vascular compliance metrics are used by medical practitioners to diagnose or monitor a large array of medical conditions, including kidney/heart conditions, hypertension and Hypovolemia. It is therefore important to have a reliable method for blood pressure measurement.

Current methodologies for the measurement of blood pressure includes use of either invasive (Invasive Arterial Pressure (IAP)) or non-invasive (Non-Invasive Blood Pressure (NIBP)) methods of determining the systolic/diastolic/mean pressure within the artery. Ideally, doctors would want to use non-invasive methods for these measurements, as the invasive measurements introduce routes for infection in the body and may lead to unnecessary blood-loss [1].

1.1.1 Non-Invasive Blood Pressure/Compliance Monitoring

The issue with current indirect methodologies for the estimation of arterial compliance and blood pressure is that most methods make use of the Korotkoff Auscultatory Method (KAM) [2]. KAM is inherently subjective to the measurer, due to the requirement of distinctive sounds to be heard before the measurement can be finalised. The method is subjective and also requires frequent calibration [2], which is non-ideal as measurements of any quantity should be objective and consistent. Therefore there is a need to develop a methodology for the objective non-invasive measurement of blood pressure and other cardiovascular metrics.

1.2 Research Aim

To develop a methodology that can be used to show the relationship between experimental Earth Field Nuclear Magnetic Resonance (EFNMR) measurements of

pulsatile flow and vascular metrics developed in an idealised model of the human upper arm.

Proof-of-concept research has been performed using the *TerraNova-MRI* from *Magritek* to conduct EFNMR experiments for non-invasive determination of blood pressure and flow velocity. The research seeks to show that EFNMR could be used in place of current non-invasive BP measurement techniques for the consistent monitoring of patients in the Intensive Care Unit (ICU).

1.3 Research Objectives

The following objectives will be used to assess the viability of using EFNMR as a novel methodology for blood pressure measurement. These objectives need to be fulfilled to obtain a fundamental understanding of the underlying principles of fluid dynamics in distensible vessels:

- A physical model that adequately represents the cardiovascular characteristics will be explored and used for measurement
- The model will be used to quantitatively determine if current EFNMR technology can be used as a viable tool for small volume measurements on the scale of the Brachial artery and the Basilic/Cephalic veins.
- A relationship between EFNMR experimental data, pressure and compliance within the model is to be determined

1.4 Limitations and Constraints

The experimental setup that is to be used is physically constrained in order to simplify the problem statement. The constraints are determined by cost-to-produce of the pre-polarising magnet arrays, the physical limitations and dimensions of the measurement equipment and the biological constraints of the cardiovascular structures in a typical human upper limb.

Chapter 2 – Background

Blood pressure as a diagnostic tool for medical diagnosis of hypertension, hypotension, Acute Kidney Injury (AKI) and a wide variety of health issues is well documented [3]. Today the Korotkoff sounds are used as a golden standard for recording blood pressure non-invasively [2]. EFNMR can be used to estimate volumes of flowing water [4]. EFNMR can therefore be used as an alternative non-invasive measurement for blood pressure and compliance metrics.

2.1 Blood Pressure Measurement Standards

The use of Korotkoff's sounds to non-invasively determine blood pressure was first implemented in 1905 and has been held as the golden standard of BP measurement [2]. The Korotkoff sounds are generally used in all methods of non-invasively determining blood pressures throughout the body. Oscillometry is an automated technique that has been developed to automatically measure BP using similar Korotkoff sounds to aid in the measurements [3].

Lehman et al. shows that current non-invasive measurements of systolic and diastolic BP's in hypotensive and hypertensive patients are clinically and significantly different (with up to 10% difference) from the intra-arterial BP's [2]. A study by Lehman et al. showed that systolic blood pressure measurements performed using Non-Invasive Blood Pressure (NIBP) techniques for hypotensive patients in the ICU is higher than measurements obtained using Intra-Arterial Pressure (IAP) by an average offset of 10.05 mmHg [3].

The same study also showed that these systolic BP measurements in the hypotensive range can be indicators for acute kidney injury (AKI). The study shows that there is a higher prevalence of AKI in hypotensive patients (systolic pressure < 70 mmHg). The studies indicate that a more robust methodology for non-invasively measuring blood pressure is required to prevent inaccurate diagnoses of patients.

Current non-invasive methods for BP measurement require either a sphygmomanometer or calibrated Subclavian Pulse Tracing (cSPT) to obtain blood pressures within major arteries of the upper limb [3]. While the interpretation of blood pressure results from a sphygmomanometer rely directly on the Korotkoff Auscultatory Method (KAM), the reliance of cSPT on KAM is slightly obfuscated [5]. SPT relies on two separate pressure transducers places along the subclavian artery to capture the deformation of the Subclavian artery due to the heartbeat [5] [6]. The physical distance between the two transducers captures the pulse wave in terms of electrical voltage due to deformation of the transducer, these electrical waveforms are then equated to measurements taken by a sphygmomanometer in order to calibrate the device [6].

Leca and Groza have demonstrated that the Korotkoff Auscultatory Method (KAM) is unscientific and hence inaccurate to be considered as the gold standard [2]. In order to consider a measurement objective and correct, the measurement must have a fundamental basis in science. KAM is subjective to the measurer, this subjectivity introduces bias which prevents the measurement being objective. In addition to this, most of the common procedures to ensure correct auscultation may not be adhered to by medical practitioners and nursing staff responsible for recording these metrics [7] [2].

2.2 Arterial Compliance

Compliance is typically obtained through either direct (angiography, MRI or transcutaneous intravascular ultrasound) or indirect (Stroke Volume over pulse pressure and pulse wave velocity) methods [7]. These techniques for arterial compliance C estimation all in some way require blood pressure measurements to be used according to the relationship following:

$$C = \frac{\Delta V}{\Delta P} \qquad [\mathrm{m.N^{-1}}], \qquad (1)$$

where ΔV is the change in volume and ΔP is the change in pressure. Therefore it is required to create a scientific methodology for the determination of both blood pressure and arterial compliance. The proposed research attempts to show the extent

to which BP and Compliance can be determined using measurements obtained using the *TerraNova-MRI* equipment.

2.3 Earth-Field NMR and System Modelling

Evidence for the use of Nuclear Magnetic Resonance (NMR) principles in measuring volumes of water is well documented [8] [9]. If we want to determine the compliance of an artery we will need to relate these NMR equations and principles to information and equations describing fluid flow, pressure and compliance.

Hydrogen atoms within a sample that will be measured have a resonant spin frequency at which the atoms precess around the static magnetic field vector. This resonant frequency is called the Larmor frequency and can be calculated using:

$$\omega = \gamma B_0 \qquad \text{[Hz]}, \qquad (2)$$

where ω is the Larmor frequency, γ is the gyromagnetic ratio of Hydrogen atoms and B_0 is the magnitude of the static magnetic field.

EFNMR experiments mostly pertain to static sample tests with recent advances in the determination of flow characteristics [10]. Fridjonsson et al. have put forth preliminary results detailing the possibility of using EFNMR equipment for the measurement of flow [8]. Their experiments implemented a pre-polarisation permanent magnet Halbach array upstream from the EFNMR detector coil, with fluid velocities of 0-1 m/s. Equation 3, as obtained from Fridjonsson et al. relates the signal magnitude received to the time taken for the sample to pass from pre-polarising magnet to the measurement equipment:

$$S_d = S_0\left(1 - \frac{t_D + t_a}{\tau_d}\right) e^{\frac{-(t_D+t_a)}{T_2^*}} \left(1 - e^{-\frac{\tau_p}{T_1}}\right) e^{-\frac{\tau_{pd}}{T_1}} \qquad \text{[µV]}, \qquad (3)$$

where S_d is the signal detected (µV), S_0 is the original signal magnitude under steady-state conditions, t_D is the time taken between excitation and detection of the signal (in order to reduce the B_1 coil ring-down time), t_a is the acquisition time of

the signal, τ_d is the fluid residence time within the detector, T_2^* is the combination of spin-spin relaxation and magnetic field inhomogeneity, τ_p is the residence time inside the polarising coil, T_1 is the spin-lattice relaxation time and τ_{pd} is the time taken for the fluid to travel between polariser and detector. Furthermore, according to the paper by Fridjonsson et al. the spins within the detector coil must still be accounted for because the residence time within the detector coil, τ_d, is close to the travel time of the water between polarisation and detection, τ_{pd} [8].

The distance between the polarising magnetic field and the EFNMR device and the rate at which this magnetization decays are controlled parameters [9]. Steady-state bulk magnetization of a water sample is developed according to [8] [9]:

$$M = M_0\left(1 - e^{-\frac{t}{T_1}}\right), \tag{4}$$

where M_0 is the bulk magnetization of water and $M_0 \propto B_0^{\frac{7}{4}}$ [8]. For this experiment the initial signal magnitude, present in the artery, is equal to this magnetization term multiplied by the volume within the artery within the polarizing field [9], as shown in equation 5.

$$S_0 = M_0 \gamma B_E V_{artery} \frac{B_1}{I}, \tag{5}$$

where $\frac{B_1}{I}$ is the ratio of the magnetic field produced by the RF excitation coil, to the current through the coil. V_{artery} is the artery volume within the detector. The product of the B_1/I and Earth's magnetic flux density (B_E) increase the efficacy of the measurement and cannot be omitted [9]. The volume term can then be used to determine the changing volume in order to determine arterial compliance.

Assuming that the only variable quantity in the system is the volume within the artery, we can derive the resulting change in signal term:

$$\Delta S_d = M_0 \gamma B_E \Delta V_{artery} \frac{B_1}{I}\left(1 - \frac{t_D}{\tau_d}\right) e^{-\frac{t_D}{T_2^*}}\left(1 - e^{-\frac{\tau_p}{T_1}}\right) e^{-\frac{\tau_{pd}}{T_1}} \ . \tag{6}$$

Using equation 6, EFNMR can be used to measure flowing volumes of water by setting ΔV_{artery} to a constant. Within a non-compliant vessel, the change in the measured signal due to a changing flow rate only relies on the velocity through the flow setup.

2.4 EFNMR Flow Measurement

The potential use of Nuclear Magnetic Resonance (NMR) for flow metering has previously been recognised [8] [10], with the advantages of NMR techniques for flow analysis (e.g., non-invasive measurement and an ability to accurately probe multi-component systems) demonstrated in a number of high-magnetic-field NMR applications ($B_0 \geq 1$ T) [10]. However, the significant cost and inflexibility of high-field NMR instrumentation has made industrial deployment of NMR flow meters infeasible. In the industry, recent improvements in low field NMR technology [8] have provided opportunities for the development of industrially applicable NMR flow meters.

Previously Fridjonsson et al. [8] demonstrated the use of an Earth's magnetic field excitation and detection r.f. coil within a single phase flow meter. Earth's magnetic field is considered low-field, with a magnetic field intensity of ~30 μT in Johannesburg. Velocity was measured using EFNMR via the use of a mobile permanent magnet (used for pre-polarisation of the sample) located at variable distances upstream of the detection coil, effectively performing a time-of-flight measurement. The NMR signal from this instrument was successfully and quantitatively modelled as a function of both velocity and separation distance between the pre-polarisation magnet and the detection coil as described with equation 2 [4].

The distinguishing factor of the current research is that the volume within the detector coil of the *TerraNova* is variable due to the flow vessel's compliance. A variable volume within the detector cavity influences the V_{artery} and τ_d terms. The effect on the V_{artery} term is evident from Eq. 6, but the effect on τ_d arises from the conservation of fluid flow equation,

$$Q = Av \quad [\mathrm{m^3.s^{-1}}] \tag{7}$$

where Q is the volumetric flow rate, A is the cross-sectional area through which the fluid is flowing and v is the velocity of the flow through the vessel. An increased volumetric flow rate through a compliant vessel leads to an increased accumulation of volume within the vessel. The increased volume in the vessel leads to an increased cross-sectional area of the vessel, which according to (7), infers a decreased flow velocity through the vessel. τ_d is defined by

$$\tau_d = \frac{\mathrm{L_d}}{v_d} \quad [\mathrm{s}]. \tag{8}$$

In terms of the designed model of the arm, the portions of pipe that connect the rest of the model to the flow setup are contained within rigid 5 mm radius PVC pipes. The velocity v_d through these pipes can be calculated using (7) and experimental measured volumetric flow rates.

A RF B_1 excitation pulse is used to rotate the resultant magnetic vector in the water sample, which is initially precessing around the static magnetic field vector produced by the Earth's magnetic field. The orientation of the B_1 pulse is orthogonal to the static magnetic field and the direction of flow. The duration of the excitation pulse determines to what angle the resultant vector will tip. The maximum signal is obtained when the excitation pulse tips the precessing resultant magnetic vector by 90 degrees [9]. After the excitation of the water sample, there is a programmed delay to account for signal ring-down in the B_1 coil. A typical FID is shown in Figure 2-1.

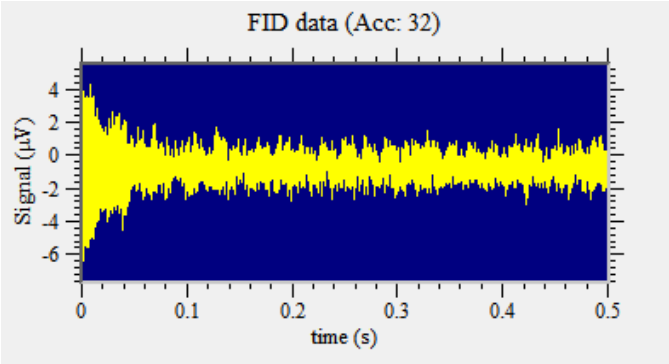

Figure 2-1 A typical FID captured by the EFNMR apparatus using the pre-polarization coil with 500 ml static water and 32 averages

The delay time is non-adjustable as the ring-down of the B_1 coil can influence the magnitude of signal measured by the *TerraNova* as shown in Figure 2-2:

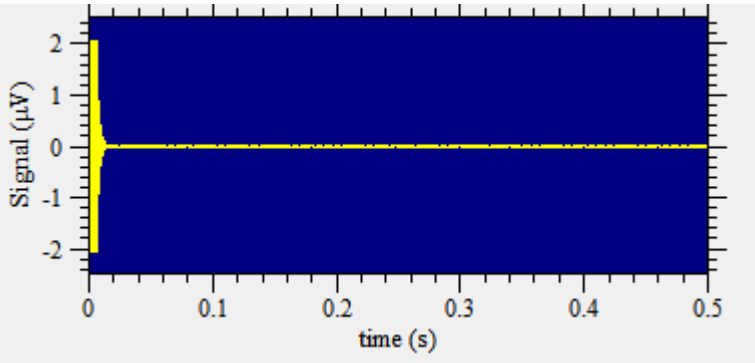

Figure 2-2 - Ring-down of the B_1 coil captured by the EFNMR apparatus, Ring-down must be de-energised before the signal is captured. A delay prevents ring-down interference during signal measurement.

The length of time this excitation pulse is activated affects the measured signal, due to the dynamic nature of the volumes being measured. A portion of the volume that is excited by the B_1 pulse will flow out of the detection chamber before a measurement is taken. The *TerraNova* apparatus has functionality built into it that allows for the length of the B_1 pulse to be reduced while still achieving the same tipping angle, by increasing the B_1 transmission gain. This functionality allows for the B_1 excitation pulse time to be reduced for specific application to this research.

Chapter 3 – Idealized Vessel Model of the Upper Limb

An idealized model replacement for the human upper limb is designed for experimental purposes. The following chapter outlines the design considerations used when constructing a model for EFNMR blood pressure measurement.

3.1 Upper-Limb Approximation

In order to design a proof of concept experiment for the purpose of blood pressure measurement, approximations have been made to create an idealized model of the human upper limb. The vascular network of the upper limb consists of many arteries and veins. To simplify these networks, we consider that all of the arteries flowing from proximal to distal on the limb, can be approximated as one artery using a WindKessel (WK) model. The same procedure can be used with respect to veins that carry blood from distal to proximal, giving rise to 2 fluid-carrying vessels in the model

The proposed solution uses two Halbach arrays placed equidistant from the *TerraNova-MRI* device, on either side of the device. Using previous works performed using the *TerraNova*, Halbach arrays are used in place of a pre-polarising coil field acting on fluids before entering the *TerraNova* device. The arrays pre-polarise the water that flows through. The upstream array will polarise arterial flow, before flowing into the *TerraNova* and the distal Halbach array will polarise any venous return flow.

The vast network of arterial and venous vascular structures in the upper limb have been simplified into two fluid containing vessels (an artery and a vein) using a 2-element WindKessel model.

The WK model lumps all arteries and veins together and assumes that the valves and peripheral resistance of the vessels are what result in a consistent peripheral flow rate [11].

3.2 Physical Model Design

The model used for this research utilises two flow-carrying pipes (static patent bore radius of 4-5 mm), which are analogous to the lumped-parameter WK approximations for arteries and veins in the upper limb. The model container is approximately the length of the *TerraNova* device. The model has been constructed using hard, clear plastic tubing. Either end of the plastic tubing is sealed, with two connection points for the flow system into the model. The connection points allow the tubes analogous to major blood carrying vessels of the upper arm (artery and vein) to connect to the flow system external to the model. A third connection point is used to connect a MPX10DP series gauge pressure sensor to the model, which is used to measure the change in pressure within the model caused by the change in arterial size. The setup of the flow carrying pipes and entry points into the model is illustrated in Figure 3-1.

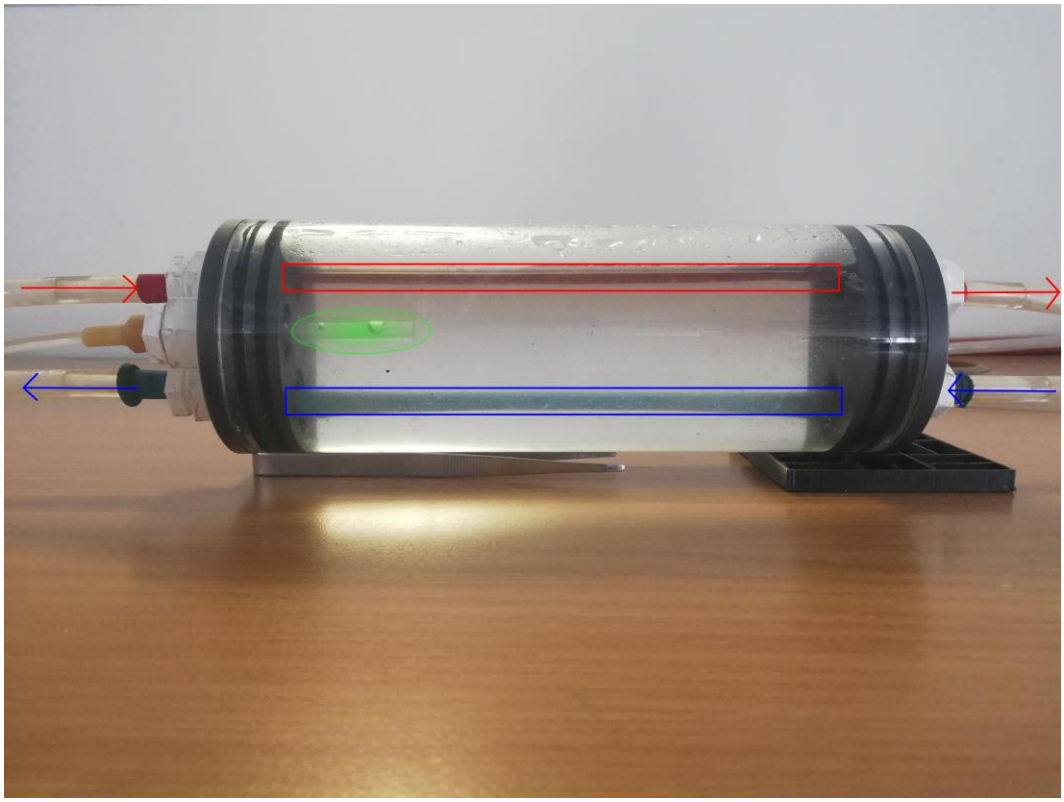

Figure 3-1 Model setup with the arterial analogue pipe and entry points into the model highlighted in red, the venous analogue and entry points highlighted in blue and the pressure sensor entry point into the model highlighted in green

Since the model has been constructed using non-distensible PVC piping, when the model is filled entirely with water, the cardiovascular analogues will not be able to expand. An air bubble of known volume is left within the model to allow for the cardiovascular models to expand and collapse within the clear PVC pipe. The pressure sensor measures the change in pressure within the air bubble in the model. The change in pressure in the air is related to a changing volume of air within the chamber according to the ideal gas law. The air bubble is shown in Figure 3-2.

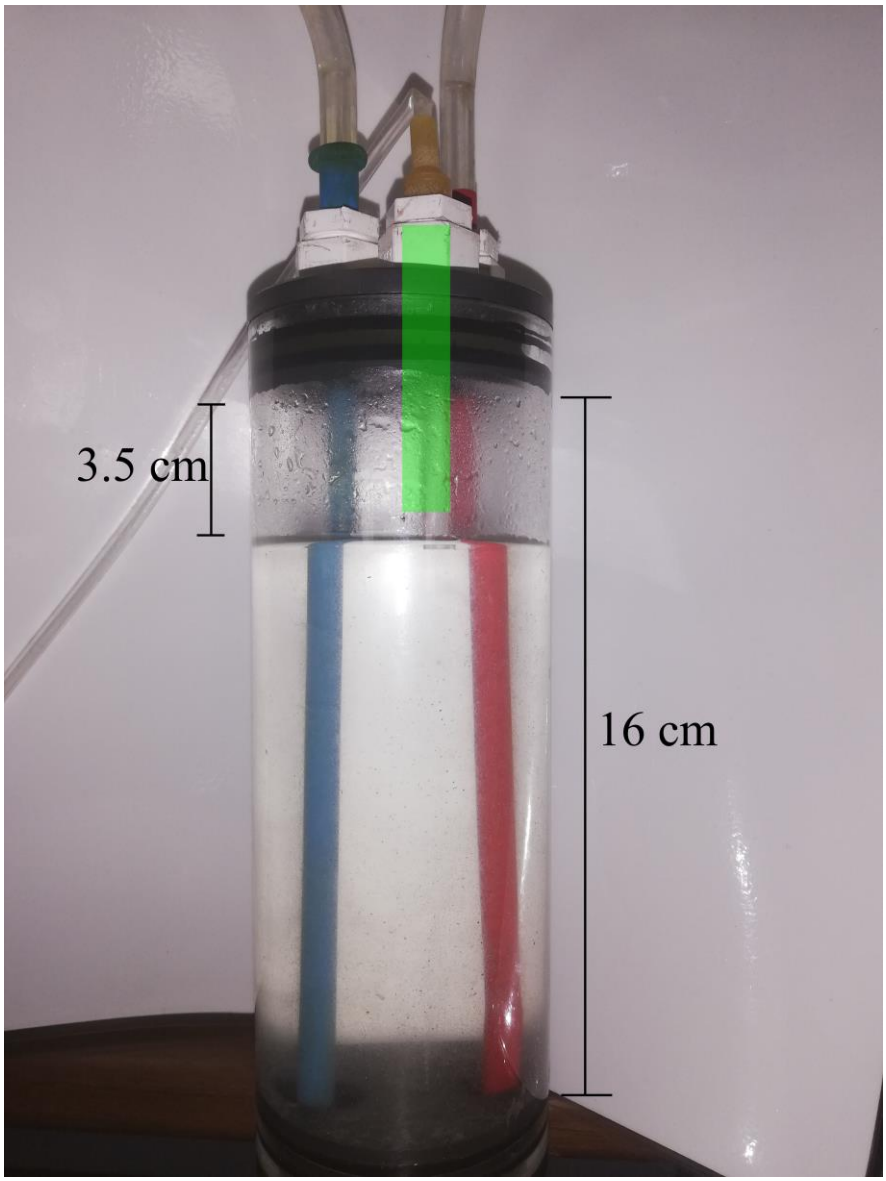

Figure 3-2 Model setup illustrating the air bubble dimensions and the pressure measurement port and tube into the model highlighted in green

The change in volume of air due to the measured static pressure change within the model is directly proportional to the volume of water in the cardiovascular analogue pipes. Using the measured static pressure within the model and a calculated volume, the compliance of the total model can be calculated.

3.2.1 Compliance

The compliance of arteries and veins refers to the distensibility of these vessels when internal pressure within the vessel is altered. Compliant and non-compliant medical balloons are used in surgical practice to either occlude or expand tissues in angioplasty procedures [12]. Non-compliant balloons refers to the case of a balloon that only expands to a specified size even if the internal pressure increases beyond the specified point [12].

The Young's modulus of the common carotid arterial walls has been experimentally calculated by Gamble et al. to be approximately 314.5 kPa [13]. The same research stated that the Young's modulus increases with age at a rate of +13.9 kPa multiplied by the patient's age [13].

The model therefore needs to incorporate pipes that can change in volume as fluid flows. Thin long rubber balloons have been used to approximate the arteries and veins in the upper limb, as they have an un-dilated internal diameter similar to that of the major blood-carrying vessels of the upper arm at approximately 5-9 mm [14] [15]. The Young's modulus of silicone rubber that is used in these balloons is ~ 1000 kPa [16]. The Young's modulus of silicone rubber can be approximated to the Young's modulus of a 50 year old human individual (~1005 kPa) according to results by Gamble et al. [13].

The balloons used in this study are non-medical but compliant balloons that increase in diameter as internal pressure increases. These balloons have been used as the Young's modulus of silicone rubber is within an order of magnitude to the experimental moduli determined by Gamble et al. [13]. Due to the distensibility of the balloons, they provide an analogue of arteries as they have an implicit volume/pressure (hence compliance) relationship [12].

3.2.2 Blood Analogue

Blood contains many substances which can be used for NMR imaging, i.e. Hydrogen, Sodium, Flourine and Nitrogen. Hydrogen has the lowest nuclear mass (it consists of one proton) and the largest nuclear moment (1.41×10^{-26} J/T) [9]. Therefore Hydrogen is the ideal molecule for NMR applications. Water is the main contributor of Hydrogen atoms in NMR applications and blood plasma is 55% of blood and the plasma is approximately 90% water, this means that blood is ~50 % water [17]. The human body is also approximately 70% water including the blood, muscles and cells [17]. Therefore the model makes use of regular tap water as an analogue to blood.

In the upper arm, blood and water are perfused throughout the limb. This essentially static volume of fluid within the arm is incorporated within the model by filling the model with tap water. In a human limb, the perfusion of blood indicates that some of the polarized flowing water will diffuse into the musculature of the arm before moving into the detector. The phenomenon is not modelled, however the relaxation rate is relatively fast and can therefore be neglected.

3.2.3 Flow Generation

External to the *TerraNova*, the fluid flows through 5mm I.D clear PVC tubing. The tubing passes through the Halbach arrays both proximal and distal to the *TerraNova* device and allows for the water to be polarised. The water used during the experimentation is stored in a reservoir and pumped through the model using a RS-360SH micro-water pump [18].

Chapter 4 – Methodology

The idealised model of the human upper limb discussed in the previous chapter has been constructed and the system diagram is shown below in Figure 4-1. As mentioned above, the model incorporates an air bubble within the model through which pressure and volume changes can be measured and calculated. The model is then placed within the *TerraNova-MRI* device and the Halbach arrays are placed 20 cm away on opposite sides of the *TerraNova*, along the bore of the device. The "feed" tubing that carries the flow into the model, passes through the Halbach arrays in order to polarise the flow prior to entering the *TerraNova*.

With the experimental setup shown in Figure 4-1, data can now be obtained to investigate the research question.

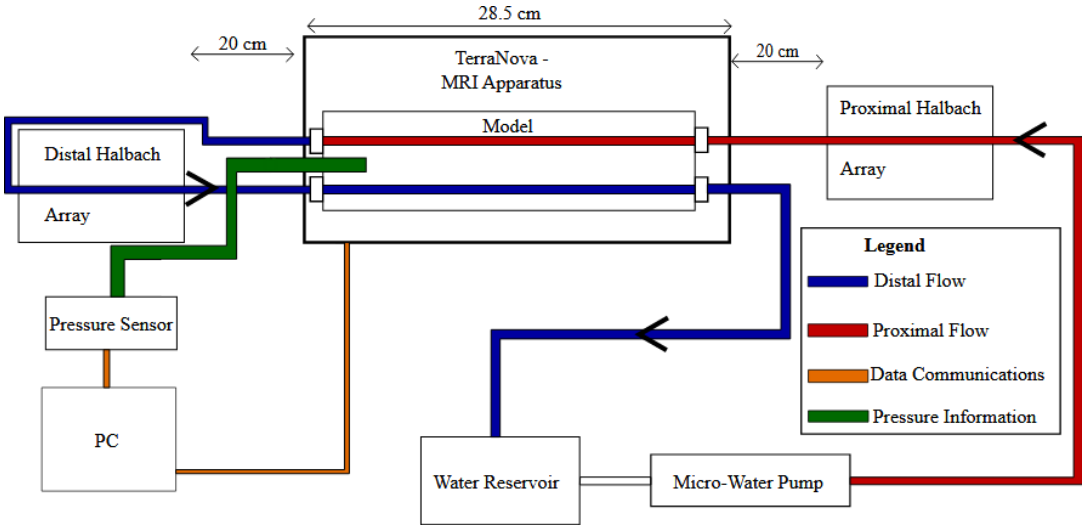

Figure 4-1 Block flow diagram of the model and flow

Before the entire model and system is constructed, model simulations are constructed using the modified Fridjonsson mathematical model. These simulations will be used to determine whether the *TerraNova-MRI* can measure the small signals that are expected to be returned from the model.

4.1 Model Simulations

A mathematical relationship for determining the changes in pressure and volume within an artery using a theoretical setup has been developed. An experimental setup and model can be used to define the system. First, the model used to describe EFNMR interactions using rigid, non-compliant tubes is presented. The model has been constructed to verify previous works performed by the author [19]. Next, a simulation has been created that will be used to model the fluid and EFNMR dynamics through the major arteries of a human arm.

4.1.1 Previous Model and Results

The first procedure in order to determine whether EFNMR can be used to detect blood flow is to investigate whether the device can detect the small volumes of polarised flow medium, comparable to the volume that would be inside a vessel 20 cm long with radius 0.5 cm (or 15 – 20 ml).

The ability of the *TerraNova-MRI* to detect small volumes of flowing water has been tentatively breached in previous works by the author [19], where detectable signal levels (0.1 ~ 1 μV) were obtained from water in lengths of 12 mm radius PVA pipe [19]. The paper states that a 300 mT annular Halbach array is used to polarise the flowing water upstream from the *TerraNova-MRI*.

The Vensim PLE simulation environment is used to model, develop and analyse real-world problems using rate-level (stock-flow) modelling techniques [20]. *Vensim PLE* simulations have been constructed to model the experiment in order to verify that the software can predict what has been experimentally measured. In addition, Vensim offers real-time output responses to changing variables within the model through the SyntheSim simulation interface.

Using the designed model with rigid pipes it is possible to simulate the experiment and verify that the results correlate with the measured results. The designed model simulation yielded results that correlated well (correlation coefficient = 0.88) with the experimentally obtained data, as shown in Appendix A.

4.1.2 Simulation of Vessel Compliance and Results

An experimental simulation is used to see the relationship between pulsatile polarised blood flow and EFNMR signal. The simulation will be used to see the signal magnitude ranges received by the EFNMR device in response to changing arterial and venous volumes typical of human cardiovascular structures. The simulation model is constructed using the *Vensim PLE x32* software package.

The model only takes into account blood flowing through the EFNMR apparatus through the arterial system with no polarized venous flow. The simulation of only polarised arterial flow enables insights into the approximate range of signal magnitudes that would be measured by the *TerraNova*. The signal magnitude that is shown in these simulations must then be smaller than the signal magnitude measured if 2 separate flow carrying vessel are used.

As stated in section 2, the model being used to describe the characteristics of flow through arteries of interest is the 2-element Windkessel [11]. The simulation makes use of a modelled pressure waveform from the heart to determine the pressures within the system that drive flow.

Blood flows from the left ventricle into the aorta at the pressures developed by a normotensive heartbeat (120/80 mmHg or 16/11 kPa). Blood then flows into the axillary arteries, followed by the brachial artery which then splits into radial and ulnar arteries. The route of flow from the Aorta to the Ulnar and Radial arteries are given in figure 4-2.

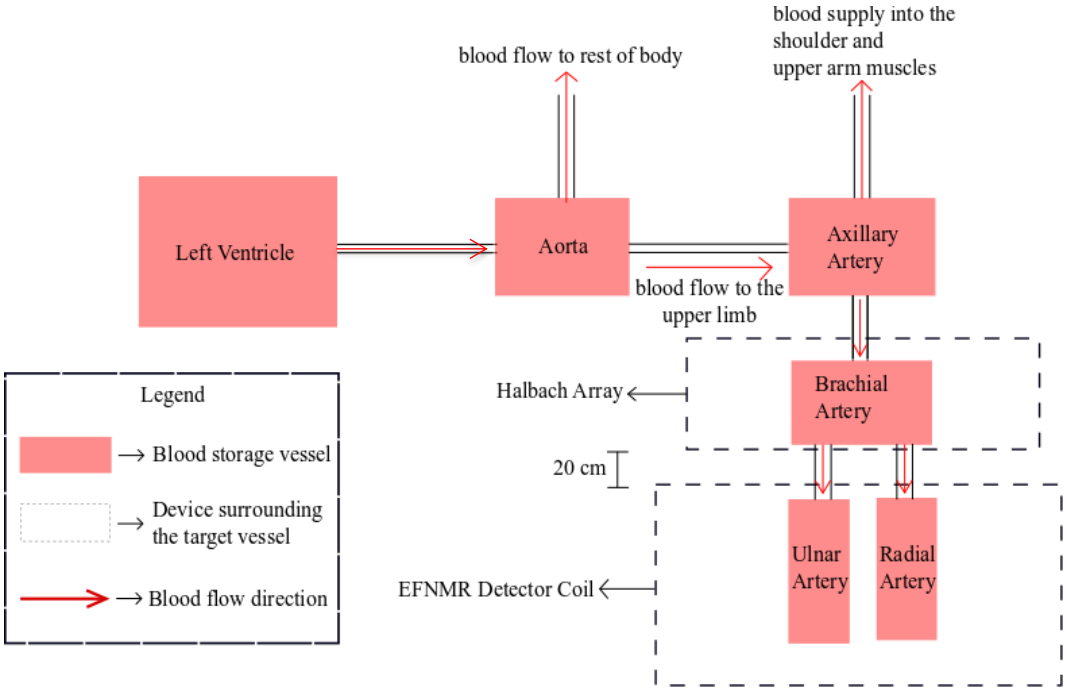

Figure 4-2 Route of blood flow through the body highlighting the route of blood from the left ventricle to the major blood carrying arteries of the forearm

The output from the simulation is within the range experimentally obtained from previous works. The model for EFNMR signal detection in *Vensim PLE* is then applied to the model of the major arteries in the arm and forearm. Figure 4-3 illustrates the changing signal magnitude received by the *TerraNova-MRI* from the polarised blood flowing within the radial and ulnar arteries.

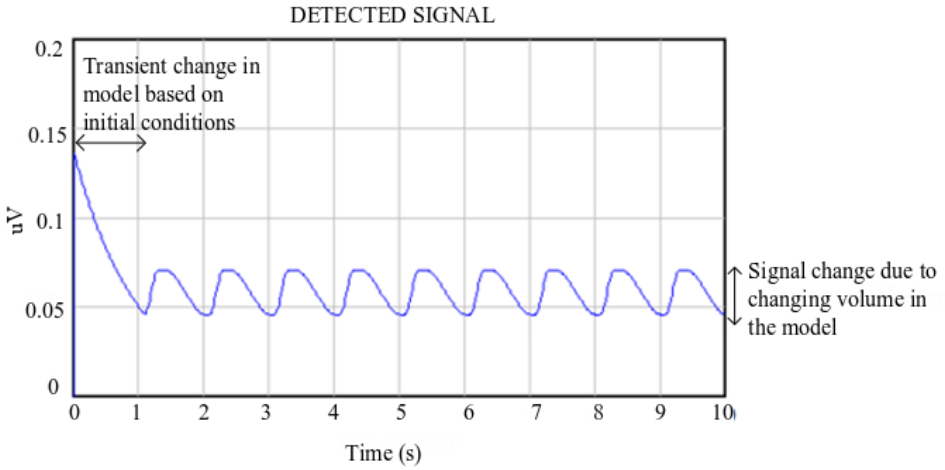

Figure 4-3 Model simulation results for the signal obtained by the *TerraNova* on the volume within the arteries of the forearm using 1 Hz pulsatile flow within these arteries

These simulation results indicate that the device will be able to detect changes in signal based on these changing volumes during a blood pulsatile flow. The above simulation of the detected signal indicates that the resolution of the *TerraNova-MRI* need to be set to 0.1 µV or less to view the difference between diastole (minimum volume within the artery) and systole (maximum volume within the artery) in the pulse waveform.

4.1.3 Fourier Analysis of the Signal Model

Previous work in flow metering using the *TerraNova* apparatus utilises equation 6 to determine the flow rate within a tube in the time domain [8] [4]. This proposes a challenge to the current research, as the Free-Induction-Decay (FID) signal emitted from the sample within the *TerraNova* does not generate a larger typical time-domain FID response. The FID in the time-domain is distorted by noise, as the RMS noise levels (~ 4 µV), are equatable or even larger than the signal being measured. The proposed research suggests that the frequency magnitude spectrum can be used to capture the required information to determine a changing volume and pressure within the modelled vessels. The inverse Fourier transform is then used to estimate the peak signal in the time-domain and the SNR is calculated as:

$$SNR = \frac{x_p}{\sigma_{ave}} \quad \text{[dB]}, \quad (11)$$

where x_p is the measured signal at a given point and σ_{ave} is the averaged standard deviation of the set of experiments, given the same experimental conditions. Figure 4-4 shows a typical time-domain FID captured by the TerraNova-MRI apparatus,

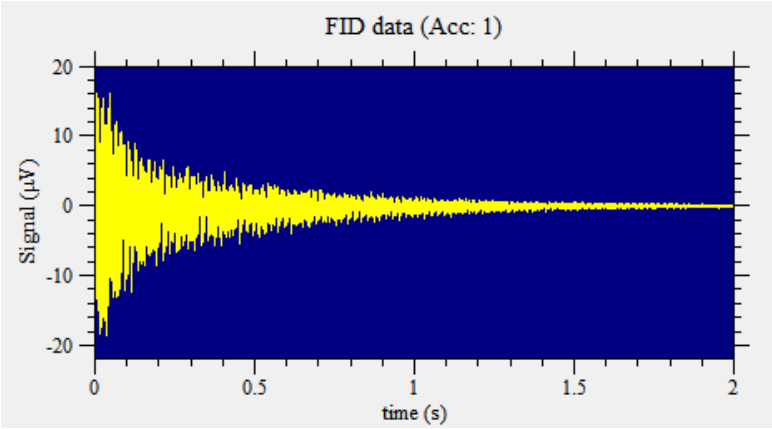

Figure 4-4 A 2 second acquisition time FID captured by the *TerraNova* apparatus using a 500 ml phantom and the pre-polarisation coil with no Halbach arrays

This research proposes that the frequency magnitude spectrum can be used to capture the required information to determine a changing volume and pressure within the modelled vessels. In order to show that this methodology is valid, a MATLAB script has been written to demonstrate the effect a changing volume and velocity has on the frequency response of the signal model. Equation 6 has been modified to incorporate a changing time variable in the terms that influence the signal capturing within the *TerraNova*, as shown by

$$\Delta S_d = M_0 \gamma B_E \Delta V_{artery} \frac{B_1}{I}\left(1 - \frac{t}{\tau_d}\right) e^{-\frac{t}{T_2^*}}\left(1 - e^{-\frac{\tau_p}{T_1}}\right) e^{-\frac{\tau_{pd}}{T_1}}. \quad (12)$$

As can be seen in equation (12), the Larmor frequency component, γB_E, is not contained within a sinusoid. The sinusoid term is required to place the peak signal at the correct frequency in the Fourier domain. This has been done due to previous research utilising only the time-domain characteristic of the FID and not being

concerned with the frequency response. In order to extract an appropriate frequency signal, a cosine term is added to equation 10 according to the theoretical signal expression provided in the *TerraNova-MRI* User Manual [9],

$$\Delta S_d = M_0 \gamma B_E \Delta V_{artery} \frac{B_1}{I}\left(1 - \frac{t}{\tau_d}\right) e^{-\frac{t}{T_2^*}} \left(1 - e^{-\frac{\tau_p}{T_1}}\right) e^{-\frac{\tau_{pd}}{T_1}} \cos(\gamma B_E t) \tag{13}$$

Where γB_E comes from equation (2) and indicates the Larmor Frequency of the precessing Hydrogen nuclei in the sample. The MATLAB code and the parameter values used for all of the components in Equation 11 is presented in Appendix B. A sample output from the MATLAB script is given in Figure 4-5:

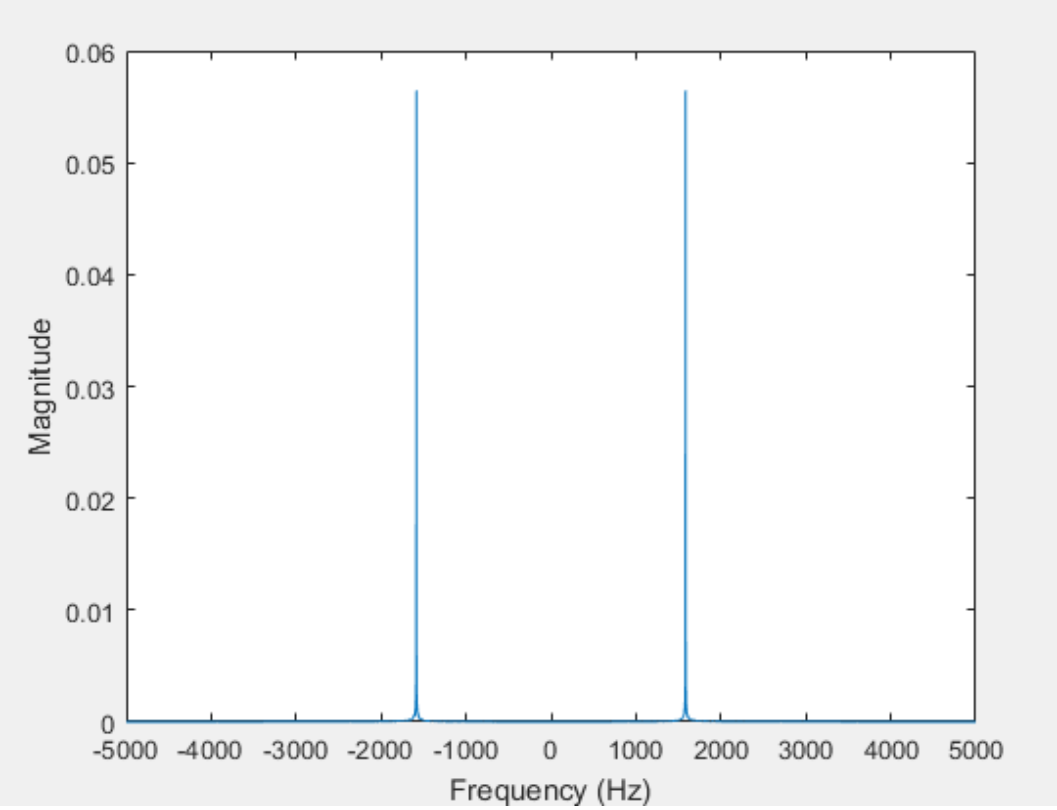

Figure 4-5 MATLAB script output showing the predicted EFNMR signal frequency and magnitude captured by the TerraNova at a flow rate of 9.5 ml/s

The magnitude of the frequency response is within the ranges measured with the *TerraNova* apparatus. Correlation suggests that the frequency response of the signal measured using the *TerraNova* can be used to measure the resulting change in the

Fourier magnitude of the signal obtained during varied volumetric flow rate experiments.

4.2 Hardware

4.2.1 Pre-Polarisation

The *TerraNova-MRI* device from *Magritek Ltd* is designed for relatively large static water applications (~500 ml). Large signal models describing the relationship between EFNMR signals and flowing water have been developed by Fridjonsson et al. [8]. Fridjonsson's papers investigate using Annular Halbach arrays as pre-polarisation mechanisms for flowing water experiments within relatively large, rigid pipes with diameters of approximately 10 cm.

Previous works by Fridjonsson and Stanwix et al. state that Halbach arrays should be placed, at minimum, 50 cm from the *TerraNova*, as the magnetic field from the arrays interferes with the *TerraNova* [8]. The *TerraNova* device makes use of 3-axis shim coils to ensure a uniform magnetic field within the bore. Halbach arrays introduce high order non-uniform magnetic fields to the experimental procedure. The shimming procedure of the *TerraNova* cannot remove these irregularities within the device, which results in a greatly diminished received signal magnitude according to the relationship, $\Delta B \propto \frac{1}{L^3}$, where L is the distance of the Halbach arrays from the *TerraNova*.

The aim of this research is to show that this concept can be used on a model of a human limb. A 50 cm separation distance is therefore non-ideal for these applications. Previous works using the *TerraNova-MRI* at the University of the Witwatersrand has shown that the arrays can be placed within the 50cm limit. The cost of placing the arrays within 50cm of the device is a decreased signal magnitude and a shift in the Larmor frequency of the precessing protons within the device.

4.2.2 Vessel Diameters

Previous experiments that were performed to model flowing water through the *TerraNova* used pipe diameters with an internal diameter of 3cm which is six times larger than the diameter of flow carrying arteries and veins of approximately 5mm. EFNMR measurement depends on the number of precessing protons in a sample, which translates to vessel diameter and volume.

4.2.3 Vessel Compliance

In addition, previous experiments performed in the field of flowing water EFNMR measurements have used large rigid pipes. Experiments to determine cardiovascular metrics need to take the compliance of a pipe into account, as the volume within the flow carrying tube changes with respect to time.

4.2.4 Budget

All of the equipment used for the experiment and the model constructed have been acquired at a reasonable price due to budget constraints. The *TerraNova-MRI* is already available from the University of the Witwatersrand.

4.3 Experimental Procedure

The flow rate through the system is kept constant while results are obtained from the *TerraNova* device and the pressure sensor. In order to ensure that the measurements taken are consistent, when the flow rate through the system is modified, measurements are only taken after the system has been flowing for 2 minutes. This ensures that the flow in the distensible tubes is able to fully develop and the transients in the system are allowed to dissipate before measurement is performed.

The flow rate is then incremented by increasing the voltage over the pump's motor in increments of 0.5 V. The flow rate associated with the voltage over the motor is known through previous experiments and is measured iteratively throughout the experimental procedure. A relationship between flow rate through the system and

the voltage measured by the *TerraNova* is to be determined. The experimental setup, Halbach arrays and model of the upper limb can be seen in Figure 4-6.

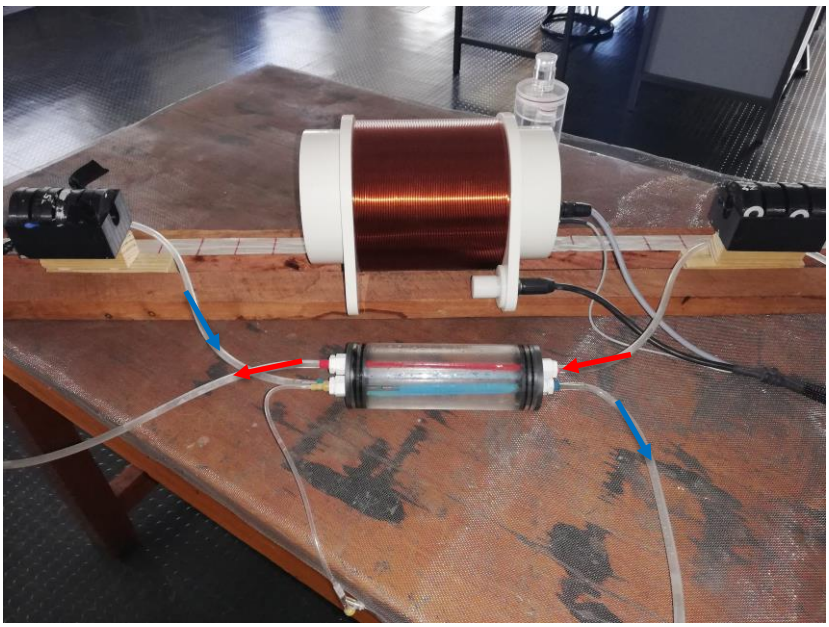

Figure 4-6 Model and setup used to perform the experiments, the model has been removed from the *TerraNova* for display purposes. Arrows have been included to indicate direction of flow

This experimental setup that will be used to determine the effect compliant vessels have on EFNMR flow measurements.

4.3.1 Fluid Flow Setup

The flow system is created using a RS-360SH centrifugal micro water pump connected to the model using 5mm I.D clear PVC pipe according to Figure 4-1. The centrifugal pump has been used due to its consistent volumetric outflow rate. The flow proceeds from a water reservoir into the pump. The flow then progresses through a Halbach array, into the model through the “arterial” analogous pipe, indicated through use of a red balloon. The flow then proceeds out of the model through a loop created using more 5mm I.D clear PVC piping. The piping passes the Halbach array distal to the *TerraNova* device and re-enters the model, which is analogous to the “venous” system and is indicated through use of a blue balloon. The flow then continues back into the water reservoir, a 5 litre container.

4.3.2 Pressure Sensor

A MPX10DP series gauge pressure sensor is connected to the model through a third port on one side of the model. The sensor is low-cost with a differential pressure range of 0-10 kPa. The resolution of the sensor is 3.5 mV/kPa, with a response time of 1 ms [21]. The sensor accuracy is equal to the measurement 3.5 mV ± 0.1 %. The pressure is measured and recorded using an Arduino Uno programmed using the sensor's Transfer Function, given in equation 9,

$$P = (V_{ADC}/1024 - 0.04)/0.009 \quad \text{[kPa]} \ (9)$$

The third port, through which the pressure gauge is attached, is exposed to a static air bubble within the model. The sensor monitors the air pressure changes within the bubble caused by the increase in the diameters of both the arterial and venous analogues due to increasing volumetric flow rates.

4.3.3 Halbach Array Orientation

The experimental setup proposed makes use of annular Halbach arrays similar in magnetic flux density (300 mT) to those designed and described by Fridjonsson et al. The arrays are used to pre-polarise the flowing water before it enters the *TerraNova-MRI* device [8] [4] [19].

In research performed by Polliack and Feller, the orientation of the Halbach arrays static magnetic field with respect to the other array results in either an increase or decrease of the B_0 flux density within the *TerraNova* [22]. Experimental research data has shown that when the arrays are orientated 180° out of sync with the other, the resultant B_0 field increases with decreased Halbach array proximity to the *TerraNova* according to Figure 4-7 [22]. Concurrently, when the arrays are aligned with the same orientation, the resultant B_0 field within the detector coil decreases with decreased array proximity to the TerraNova [22].

Due to limited material availability, the bores of the constructed arrays measure 15 mm in diameter. The bore diameter need not be that of an average human limb,

since the setup is designed for a proof of concept. Positioning and orientation considerations for placement of the Halbach arrays is shown in Figure 4-7,

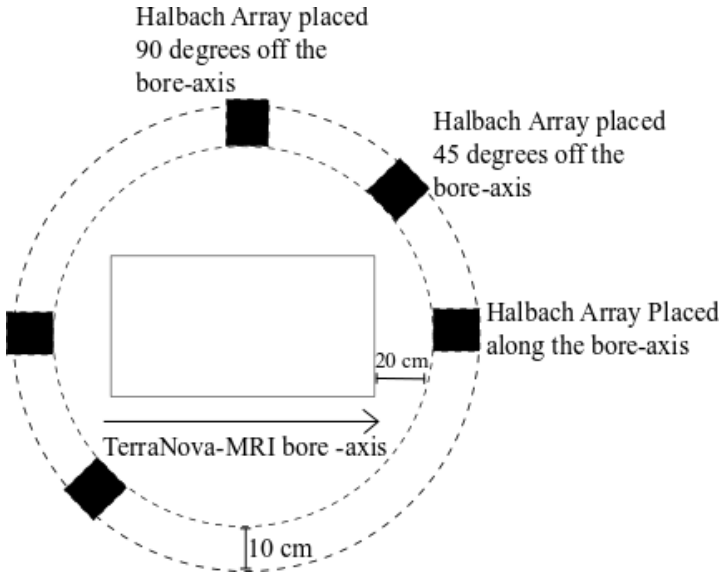

Figure 4-7 Difference between orientation and separation distance between *TerraNova* and Halbach arrays.

Previous experiments show that the orientation of the Halbach arrays with respect to the *TerraNova* have less of an effect on measurements than the distance of the arrays from the *TerraNova* [19]. These effects have been explored in previous works by the author and state that the angular position at a fixed radial distance of the Halbach arrays with respect to the *TerraNova* has negligible effect on the signal magnitude, when compared to the distance of the arrays, along the axis, from the *TerraNova* [19]. The distance between Halbach arrays and the *TerraNova* device determines the maximum signal captured according to the modelled experimental relationship,

$$S_{Max}(x) \cong S_0\left(1 - e^{-\left(\frac{x}{50}\right)^3}\right) \qquad [\mu V], \qquad (10)$$

where S_{Max} is the signal magnitude captured by the *TerraNova* device and is a function of the separation distance between Halbach arrays and the *TerraNova*, S_0 is the signal that would be captured by the device with no Halbach arrays within 50 cm of the *TerraNova* and x is the space between arrays and *TerraNova* in cm. This decrease in signal magnitude is shown in Figure 4-8.

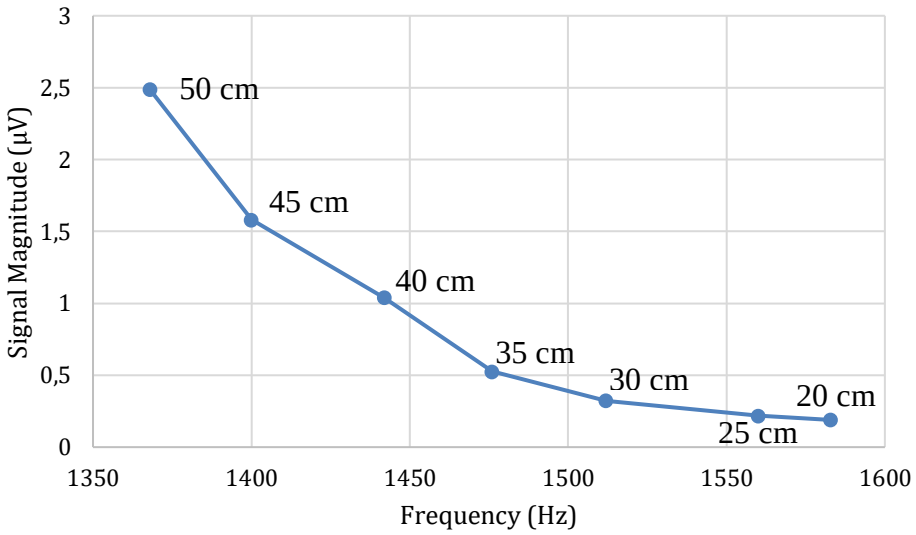

Figure 4-8 Graph showing the signal magnitude vs. the increasing Larmor frequency at different separation distances between the Halbach arrays and *TerraNova*

When the Halbach arrays are brought within 50 cm of the *TerraNova*, there is an observed change in Larmor frequency recorded during static water 1D EFNMR experiments. The rotational orientation of the Halbach arrays with respect to one another determines whether the measured Larmor frequency increases or decreases when the arrays are brought within the 50 cm threshold.

Experiments by Polliack and Feller, have shown that if both arrays are positioned along the bore-axis of the *TerraNova* and both have the same resultant magnetic field direction, the Larmor frequency decreases [22]. A decreased Larmor frequency indicates a weakening of the resultant Earth's magnetic field vector within the *TerraNova*. Conversely, if the arrays have opposite magnetic field directions, the Larmor frequency within the *TerraNova* increases, indicating a strengthening of the Earth's resultant magnetic field vector. The results of Polliack and Feller's experiments have been presented in Appendix C [22].

The final orientation for the arrays and *TerraNova* is with each array placed on either side of the *TerraNova* directly along its bore-axis, 20 cm from the device.

The 20 cm distance is chosen as it results in an overall length of the modelled system of 80-100 cm, which is consistent with the length of the typical human arm [23].

4.4 Pressure and Volume Measurement

In order to calculate pressure and volume from the EFNMR measurement, equations (5), (6) and (7) can be used to modify the signal model of Fridjonnson et al. A solution is then formed where the volume of polarized flow within a vessel is variable. In order to correlate the signal received by the *TerraNova* device and a changing volume, a methodology is devised to measure a change in volume using the measured pressures developed within the idealised model of the upper arm.

The pressure difference measured using the pressure sensor translates to a change in the volume of air within the model according to the Ideal gas law:

$$PV = nRT. \tag{14}$$

Where P is the pressure experienced by the Volume (V) of air in the container, R is the ideal gas constant, T is the absolute temperature of the vessel and n is the number of moles of air which is a known quantity, as the volume of air in the container is known at the temperature and altitude of Johannesburg.

As the right hand-side of equation (14) is approximately a constant, the pressure and volume are observed to be inversely related. Pressures experimentally obtained using the attached pressure sensor are used to calculate a corresponding change in volume of air within the model. This volume is used to calculate the velocity of the flow through the distended vessel according to (10).

In reality the device will be calibrated prior to measurement on a human limb. Calibration will allow for pressure to be calculated given the changing volumes within the artery/vessel at diastole and systole. The pressure will not be directly measured, as it is in this experimental model.

The volumetric flow rate produced by the motor has been experimentally obtained during previous research [19]. The tests were performed again before this research began to ensure that the flow rates produced had not changed.

When equation (5) is manipulated to incorporate these differences, we can see a change in the characteristic shape of the theoretically determined time-domain signal model provided by Fridjonsson et al. as seen in Figure 4-9:

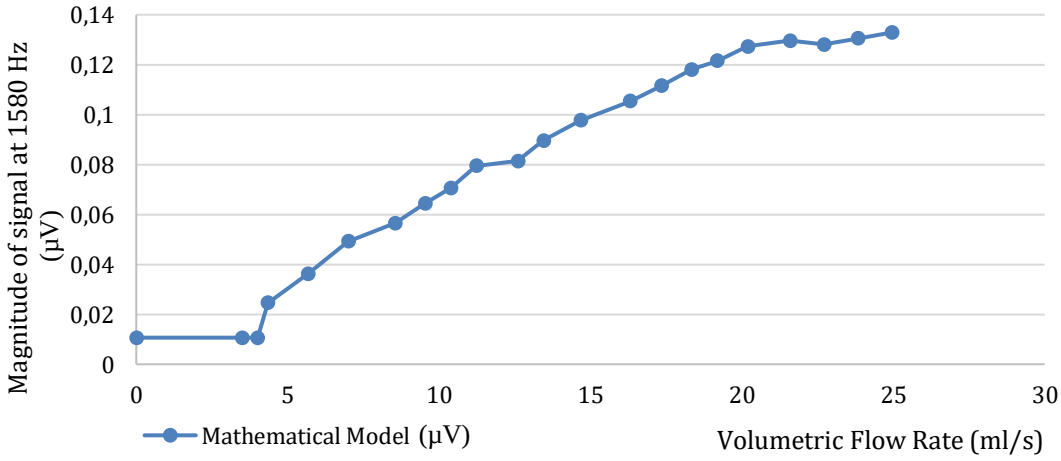

Figure 4-9 Graph illustrating the characteristic shape of the modified signal model vs. volumetric flow rate

Figure 4-9 is not continuous, as would be expected from a mathematical model. The random perturbations of the data points are attributed to the experimentally obtained pressures that are used to determine the volume change within the model. Each experimentally obtained pressure reading has error and is limited by the sensitivity of the pressure sensor, therefore the non-smooth nature of the graph is a direct result of the pressures being experimentally, and not analytically, obtained.

The MATLAB frequency-domain analysis of the signal model also indicates an increased frequency magnitude with an increased volumetric flow rate, when the changing volume and residence time within the detector coil modifications to the model proposed by Fridjonsson et al. are added. The effect of changing internal volumes on the model proposed by Fridjonsson et al. is shown in Figure 4-10.

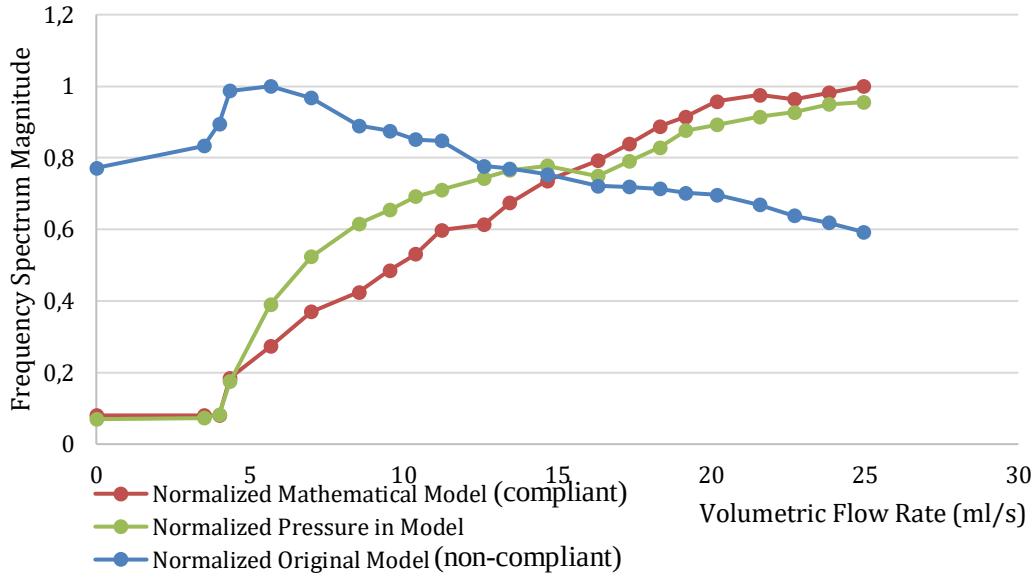

Figure 4-10 Graphs showing the Fridjonsson signal model, the new modified signal model and the Pressure developed in the system.

There is a positive correlation between increasing internal pressure and the modified signal model. Figure 4-10 illustrates the difference between signal models that assume compliant and non-compliant flow carrying tubes.

Chapter 5 – Results and Analysis

The experimental configuration and calibration of the EFNMR device is tested using the layout as described in chapter 4. The balloons used to simulate the lumped model artery and vein are placed within the model. This idealised model of the arm is filled with 500 ml of water leaving an air bubble with a volume of ~150 ml. The model is then placed within the *TerraNova* with the two constructed 12 cm long Halbach arrays on opposite sides of the *TerraNova-MRI* device with 20 cm separation distances.

One-dimensional EFNMR pulse and collect experiments are performed on the model. Initially these tests are performed using the pre-polarising coil of the *TerraNova* on the volume of static water within the model. The initialization is used to locate the Larmor frequency of the water in the bore of the *TerraNova*. Once the Larmor Frequency has been determined, the apparatus is shimmed at this frequency and the polarising coil is turned off for the remaining experiments.

5.1 TerraNova-MRI Parameter Initialisation

The *TerraNova-MRI* apparatus allows for the parameters shown in Figure 5-1 below to be modified in order to determine the most effective setting for EFNMR signal capture.

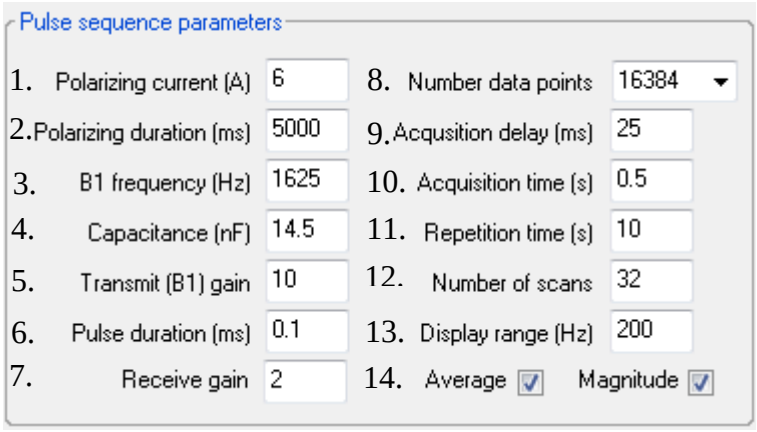

Figure 5-1 *TerraNova* software Prospa, calibration parameters used to initialise the experimental setup.

The Polarizing current and duration in Figure 5-1 define the action of the B_0 polarizing coil built into the *TerraNova-MRI* apparatus. These values are set to zero after calibration.

The capacitance (parameter 4) of the system determines the resonant frequency of the apparatus, which is tuned to the resonant frequency of the precessing hydrogen nuclei in the model. The Larmor frequency (parameter 3) of the static water sample increases according to Figure 4-7 as the Halbach arrays are brought closer to the *TerraNova* device. Therefore the *TerraNova*'s resonant frequency is also adjusted, through use of the capacitance value in the figure above.

The default B_1 pulse length of 1.5 ms is used to "tip" the precessing magnetic vector by 90 degrees. By minimizing the pulse transmission time, the residence time of polarized flow within the *TerraNova* is maximized. The transmit pulse duration used is 0.1 seconds (shown above). This is done by increasing the B_1 gain to 10, as shown above.

The acquisition delay is fixed at a recommended 25 ms (parameter 9) to remove the effect of the B_1 coil ring-down on the time and frequency domain plots. During testing, 64 repetitions (parameter 12) of the 1-Dimensional EFNMR are averaged to reduce noise from the result, using

$$\sigma_{ave} = \frac{\sigma_{signal}}{\sqrt{N}} \quad (15)$$

The repetition time between experiments (parameter 11) defines how long the equipment will take to process one experimental result. Experiments are performed with the minimal repetition time of 1.2 seconds. It therefore takes approximately 80 seconds to perform one complete experimental reading.

5.2 Varied-Volumetric Flow-Rate Experiments

Experiments are performed to measure the frequency magnitude obtained by the *TerraNova* device at differing volumetric flow rates. The acquisition time (parameter 9) is altered (from 0.1 to 0.5 seconds, in increments of 0.05 seconds) between individual EFNMR experiments at the same volumetric flow-rate. The results obtained during each varied acquisition-time experiment at the same flow-rate are averaged to determine the signal level to be used to infer blood pressure.

5.2.1 Signal-to-Noise-Ratio (SNR)

Each individual EFNMR experiment is averaged 64 times to reduce noise, with the SNR increasing by the root of the number of samples (8 times increase with 64 averages) [9].

The signal magnitude at the Larmor frequency (1580 Hz) is recorded. During experiments with lower acquisition times, the spectral resolution in the Frequency domain is diminished. This sometimes prevents selection of the signal magnitude at exactly 1580 Hz. Therefore the signal magnitude selected during these iterations is chosen as the magnitude of the nearest frequency peak to the 1580 Hz Larmor frequency.

All of the experimental results at the same volumetric flow rate (with differing acquisition times) are then averaged. Averaging is performed to obtain a higher noise-reduction in the resultant signal, with 9 experiments, each averaged 64 times individually, being averaged together for a total of a 24 times increase in SNR ($\sqrt{64 \times 9} = 24$).

5.2.2 Static and Flow Measurements

The Larmor frequency of the water is found to be ~1580 Hz with the Halbach arrays being placed on either side of the *TerraNova-MRI* device with 20 cm separation between arrays and the *TerraNova-MRI* device. This is higher than the Larmor frequency of water with no Halbach arrays present (1278 Hz) and shows an increase in the Earth's magnetic field intensity of ~7.2 μT. A calibration experiment showing the Larmor frequency is performed using the polarising coil of the *TerraNova* to pre-polarise the static water within the model of the arm. Due to the polarising coil being active, the repetition time of this experiment is set to 12 seconds between measurements, with a 0.5 s acquisition time and 32 averages being made. The time domain results of this calibration test is shown in Figure 5-2 below.

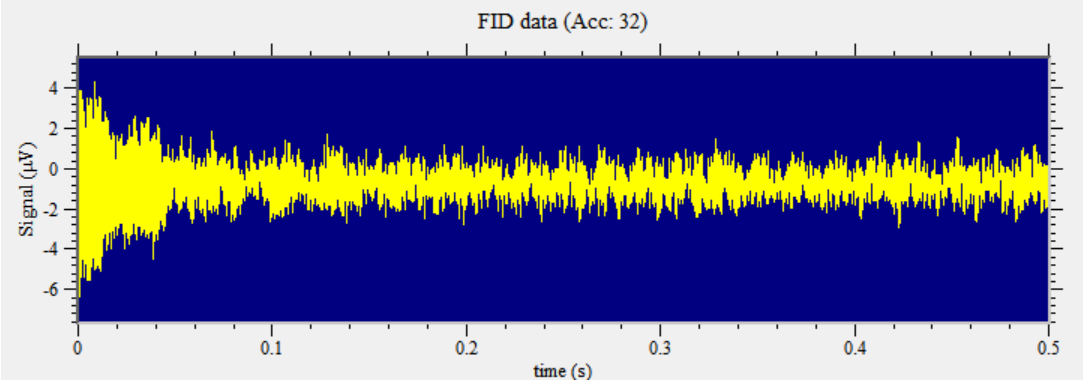

Figure 5-2 FID data recorded with polarization and Halbach arrays at 20cm separation

The time-domain FID response shown above is equatable to the frequency domain response shown in Figure 5-3.

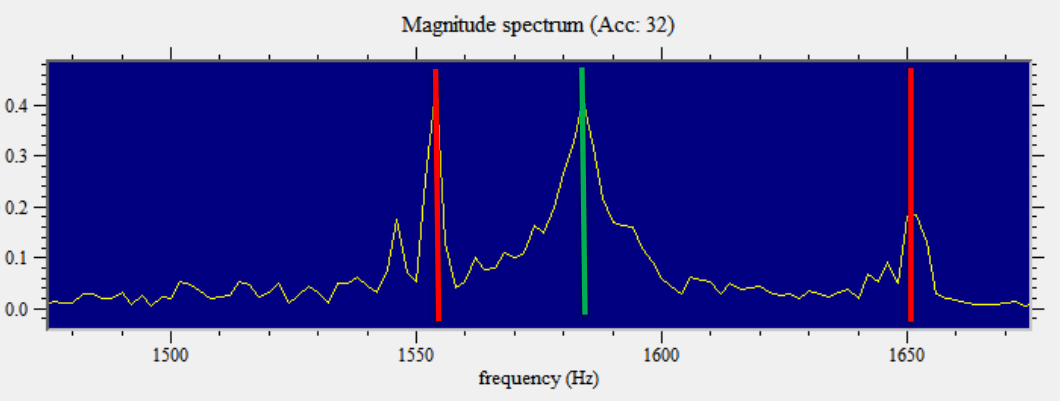

Figure 5-3 Frequency spectrum data of the same experiment with noise peaks marked red and signal in green

The signal peak at 1580 Hz is evident in the above figure and the 1550 Hz noise peak is seen to have comparable magnitude within the frequency spectrum.

Following the calibration and shimming of the *TerraNova* to the 1580 Hz Larmor frequency of the water, experimental data at varied flow rates is obtained according to the procedure mentioned above. At every flow rate, the 9 experiments at the given flow rate (with varied acquisition time) are averaged to produce a final value for the magnitude of signal measured by the *TerraNova* at the given flow rate. The magnitude of the frequency spectrum is then plotted against the volumetric flow rate through the setup, as shown in Figure 5-4.

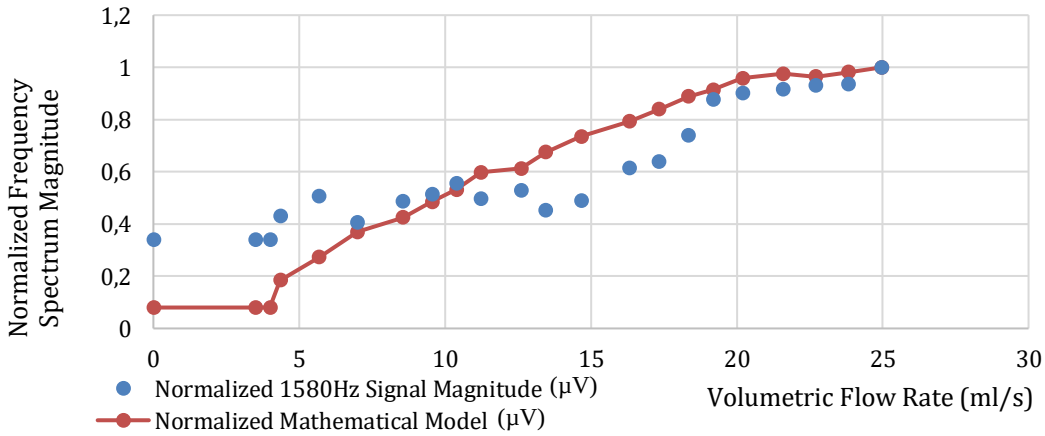

Figure 5-4 Graph showing the signal model and experimental results obtained vs. volumetric flow rate through the system, error bars have been omitted due to their insignificant size when compared to the signal

A clarification of the signal dip and non-linearity between volumetric flow rates of 10-20 ml/s is given in the discussion.

The error bars for each individual measurement are calculated by first obtaining the standard deviation of each experiment with changing acquisition time and constant flow rate. The standard deviation is then divided by the square root of the number of times the experiment is averaged. The resultant approximate average standard error of 0.04 μV is calculated, which is 10% of the smallest signal magnitude measured.

The normalized signal values of both the experimental signal model and the data acquired are shown in the above graph. It can be seen in the above figure that there is an increase in the signal magnitude received by the *TerraNova* device that correlates with the mathematical signal model, with a 0.89 positive correlation coefficient.

The rms noise measured during experimentation is ~3.0 – 3.5 μV. The noise value has been determined by using the *TerraNova*'s built-in MonitorNoise functionality to determine the average noise magnitude in the experimental environment.

It is possible to measure small changing volumes of water comparable to the volumes in vessels with diameters close to real human vascular vessels. The signal captured by the *TerraNova* is embedded within noise in both the time and frequency domains, however averaging allows for data to be extracted. The data correlates well with simulations and a mathematical model of the system ($p = 0.88$).

5.2.3 Pulsatile Flow Experiments

Due to the pulsatile nature of the human cardiovascular cycle, experiments that incorporate pulsatile flow through the setup have been performed using a low pressure resistance (~0.5 kPa) flow valve connected to the flow setup directly after the pump. The valve is toggled open and closed at 1.2 second increments, replicating a standing heart rate of 50 bpm. The 1.2 second increment has been used as this is also the repetition time for an experiment using the *TerraNova-MRI*. This

has been done in an attempt to gate the measurements to the opening and closing of the valve.

The results from these experiments have been omitted from this dissertation as the EFNMR measurements showed no discernible signal at any given flow rate. The reason associated with this lack of evident returned signal from the model, is that the measurements have been inadequately gated with the opening and closing of the implemented valve.

5.3 Compliance of the Idealized Model

The experimental results yield a compliance measurement for the constructed model of 10.9 ml/kPa or 1.46 ml/mmHg using equation (15). According to McVeigh et al. the normal compliance for the major arteries of the arm in young subjects is approximately 2 ml/mmHg [7]. The constructed model more accurately represents a subject with decreased arterial compliance.

Another study by Burattini et al. have estimated the total systemic arterial compliance in canines to be between 0.2 – 1.4 ml/mmHg [24]. The study states that by considering the compliance as a function of mean Aortic pressure, compliance of different arteries can be fitted to a bell curve [24]. Since compliance is a function of both volume and pressure change, the inference is that volume measurement can be used to obtain pressure and compliance information by fitting the compliance measurement to a Gaussian curve as a function of volume according to equation 1.

To calculate compliance, the pressure change within the model is given as the total pressure change measured within the model between minimum (0 ml/s) and maximum flow rate (25 ml/s) tests. The volume change within the vessels is taken as the maximum volume within the vessels, calculated at maximum flow rate, minus the static volume within the patent vessels when there is no flow through the vessel (Hydrostatic Pressure).

The compliance measured for the constructed model is calculated using equation 1. Compliance is typically measured as a volume change within a vessel given a

known change in arterial pressure. The idealized model does not distinguish between arterial and venous flow, as both vessels within the model ideally experience the same pressure and volume changes. An assumption has been made that the air pressure and volume changes within the model represent the changes in fluid volume within the cardiovascular model. The changes in air volume due to temperatures is also assumed to be diabatic due to the relative speed of measurement compared to the changes in temperature.

Chapter 6 – Discussion

The results obtained during experimental analysis deviate from what is expected from the simulations and mathematical model. Phenomena that could result in these deviations are recorded and explored by the author. The detection equipment for EFNMR measurement is limited by the sensitivity of the device to volumes that can be measured and noise induced by other mechanical components in the experimental setup .The following chapter explains some issues that have been encountered during experimentation.

6.1 Volume Limitations

The ability of the *TerraNova* EFNMR device to detect volumes of water smaller than 50 ml has been covered in previous works [19]. The *TerraNova* does not have the ability to consistently measure static water samples smaller than 100 ml if the water is pre-polarised using the built-in *TerraNova* pre-polarising coil [19]. Signal levels of as high as 3 µV have been measured with a 50 ml tap water phantom, but these tests involve manually moving the phantom from within the Halbach arrays (after polarising for longer than 10s) into the *TerraNova* [19]. Results for the manual movement of the static water between Halbach arrays and *TerraNova* is inconsistent. While these tests did not consistently measure the same signal level, the relatively large magnitudes (0.5 - 3 µV) are up to 20 times larger than the signal measured by the *TerraNova* using a 50 ml sample of static water and the built-in polarization coil, with the Halbach arrays in the same orientation.

6.2 Difference in Predicted and Measured Results

When the experimental results and the theoretical signal model results are not normalized as in graph 5-4, the difference between the mathematical model and the acquired results are shown in Figure 6-1.

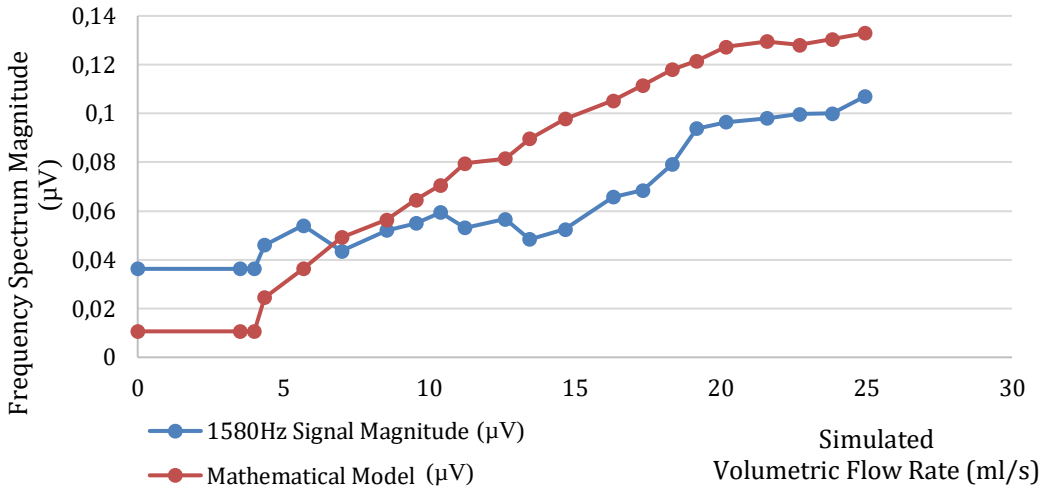

Figure 6-1 Graph showing the non-normalized compliant tube signal model and experimental results

When all of the experimental results are multiplied by a factor of 1.3, there is an approximate alignment, as seen in Figure 6-2.

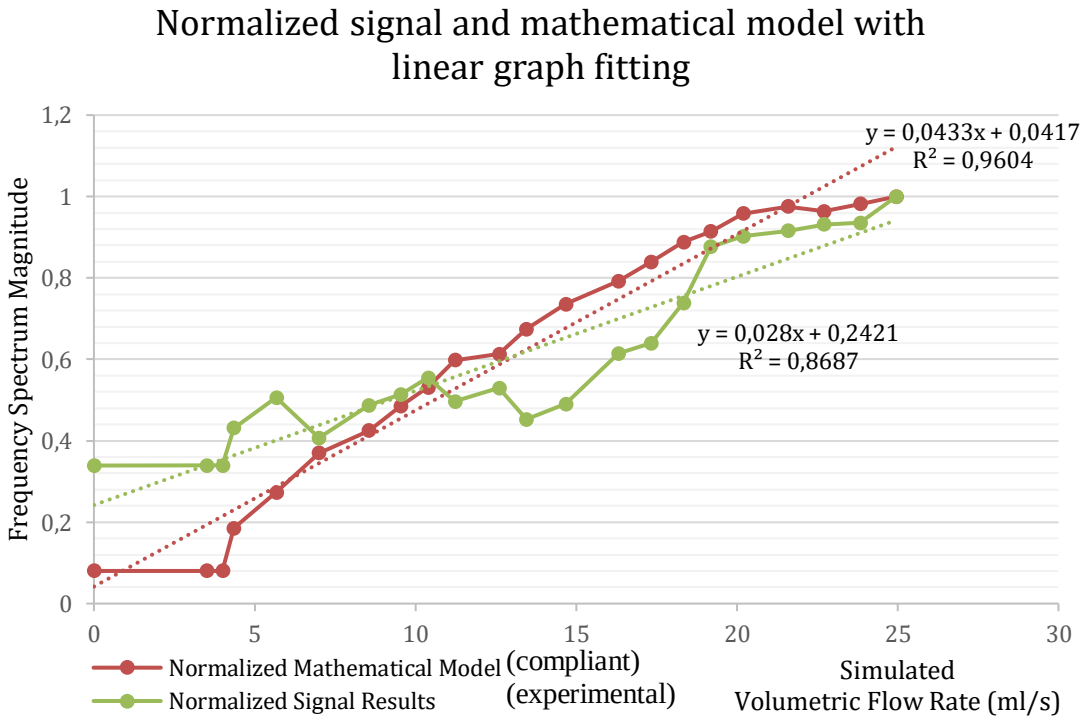

Figure 6-2 Graph showing the normalized compliant tube results with linear trend-lines fitted to both the mathematical model and the results recorded

The relative error between the mathematical model and the results measured can be calculated by fitting a linear approximation to each set of results. The gradients of both linear approximations are then used to calculate relative error using,

$$E = \frac{m_{theory} - m_{measured}}{m_{theory}}, \tag{16}$$

where E is the relative error, m_{theory} is the gradient of the linear approximation to the model results and $m_{measured}$ is the gradient of the linear approximation to the recorded results. Equation (16) yields a relative error of 30%. This approximated relative error is high, however it is observed that the mathematical model does not incorporate a base level of noise in the system. The absence of an added DC rms noise value in the mathematical model results in a steeper theoretical gradient.

The factor of 1.3 can be attributed to the higher-order non-uniform magnetic fields within the *TerraNova* that cannot be corrected for during the shimming process. The shim-coils of the *TerraNova* device are designed to remove irregularities in the magnetic field within the bore that are first order. The irregular fields caused by Halbach arrays that are placed exceptionally close to the device, introduce high order disturbances in the field that are not entirely compensated for in the shim process. Noted through the deterioration of peak signal magnitude that is described in Figure 4-8.

The introduction of a multiplication factor to compensate for the non-ideal magnetic fields within the device can be attributed to a change in 3 variables outlined in equation 6.

Bulk magnetization of a water sample after a polarizing pulse of sufficient length of time can be calculated using the following,

$$M_0 = \frac{N_s \gamma^2 \hbar^2 \frac{B_p}{I}}{4kT_s} I_p \qquad (\mathrm{A/m}), \tag{17}$$

where N_s is the number of spins with the same direction in the sample, $\hbar$ is the reduced Planck's constant, B_p is the magnetic field strength produced by the polarising coil, I_p is the current through the polarising coil, k is the Boltzmann

constant and T_s is the absolute temperature of the sample. Since we are not using the polarising coil we can cancel the currents in the above equation and substitute B_p with the field strength produced by a Halbach array.

6.3 Halbach Array Proximity Distortion

The bulk magnetization M_0 of water could also be estimated using the proportionality relationship to the static magnetic field strength $B_0^{7/4}$ [8] [4]. This static magnetic field strength increases with increased Halbach array proximity to the *TerraNova*, as noted by the increasing Larmor frequency. When no arrays are near the device, the B_0 field strength is approximately 30 µT, with a Larmor frequency of 1277 Hz. The B_0 value increases to 37.2 µT when the arrays are placed 20 cm away from the *TerraNova*.

The increased field strength is determined using equation 2 and the observed new Larmor frequency of 1580 Hz. The Earth's magnetic field strength B_E, seen in equations 5 and 6, is also increased to 37.2 µT, with the increased proximity of the Halbach arrays to the *TerraNova* device.

The T_2^*, effective spin-spin relaxation time constant, also changes with increased inhomogeneity of the static magnetic field described by Magritek Ltd. [9]:

$$\frac{1}{T_2^*} = \frac{1}{T_2} + \gamma \Delta B_0. \tag{18}$$

Where T_2^* is the effective spin-spin relaxation time constant, T_2 is the spin-spin relaxation time constant, γ is the gyromagnetic ratio of Hydrogen and ΔB_0 is the magnetic field inhomogeneity. The change in the effective relaxation time is calculated using (18) for when the Halbach arrays are 20 cm away from the *TerraNova* (T_2^* = 0.631 ms) and for when the Halbach arrays are placed >50 cm from the *TerraNova* (T_2^* = 0.783 ms).

The proximity distortion effects have not been accounted for in the modelling of the signal and could attribute to the 1.3 times multiplication factor required to adjust the experimentally obtained signal to the mathematical model.

6.4 Halbach Arrays Optimal Placement

As shown in Figure 4-7 that when the Halbach arrays are moved closer to the *TerraNova*, the Larmor frequency of the signal increases while the signal magnitude decreases. Ideally, we would like to place the Halbach arrays as close to the *TerraNova* as possible. This ensures that the proposed BP measurement device can be used on patients with short limbs.

Finding the shifted Larmor frequency is performed through an iterative procedure. Knowing that the Larmor frequency increases with increased proximity of the two Halbach arrays to the *TerraNova*, the arrays are moved closer to the device while performing Pulse and Collect tests using a static water sample. This iterative procedure helps locate the approximate location of the Larmor frequency peak. The *TerraNova* auto-shimming process is then used to maximise the static water peak magnitude.

A decrease in SNR accompanies an increase in Larmor frequency signal strength. When the arrays are brought within the 20 cm threshold, the SNR becomes too low for the auto-shimming calibration procedure to adequately "lock onto" the Larmor frequency of the water sample.

6.5 Frequency Shifting Versus Flow Rates

The experimental results are obtained when the Halbach arrays are placed 20 cm from the bore of the *TerraNova*, with opposite polarity. In order to obtain an averaged signal result for each flow rate tested, 8 tests are performed at each flow rate. Each test averages the signal obtained over 64 individual measurements. The acquisition time is the only varied parameter between each test at a constant flow rate and is varied from 0.1 to 0.5 seconds in increments of 0.05 seconds. The peak frequency recorded for each experiment is the largest peak frequency magnitude within 10 Hz of the 1582 Hz Larmor frequency.

The Larmor frequency is obtained using the polarising coil of the *TerraNova*, a static water sample, the Halbach arrays at a distance of 20 cm and an acquisition

time of 1 second. The frequency resolution of this measurement is 1 Hz which gives us an accurate location of the signal.

It has been observed that when the flow rate through the model is increased, the location of the peak frequency can shift by up to ±10 Hz. The shifting is attributed to the varying acquisition times between individual experimental data recording. When the acquisition time is decreased, the resolution of the frequency spectrum also decreases. It is noted, through use of the Prospa software provided by *Magritek*, that with an acquisition time of 0.1 seconds, the resolution of the frequency spectrum only allows for signal measurement at 10 Hz intervals while an acquisition time of 0.3 seconds provides a frequency resolution of 3.33 Hz.

6.6 Noise

Noise produced by the water pump becomes evident in the measurements obtained by the *TerraNova* when testing using flow rates higher than 15 ml/s. The noise is attributed to the mechanical noise induced by the vibration of the motor with a frequency component in the measured spectrum. The motor produces noise at lower flow rates, but at lower flow rates the frequency of vibrations produced by the motor do not lie within the frequency sensitive region of the *TerraNova*.

The following figures that are used to illustrate this interaction are recorded using a flow rate of 24 ml/s through the Halbach arrays, acquisition time of 0.5 seconds and using the polarisation coil of the *TerraNova* to polarise the static water locate the Larmor frequency. Figure 6-3 shows the frequency spectrum of a result captured by the *TerraNova-MRI* apparatus and highlights the signal of interest and the noise peaks induced by ambient noise sources.

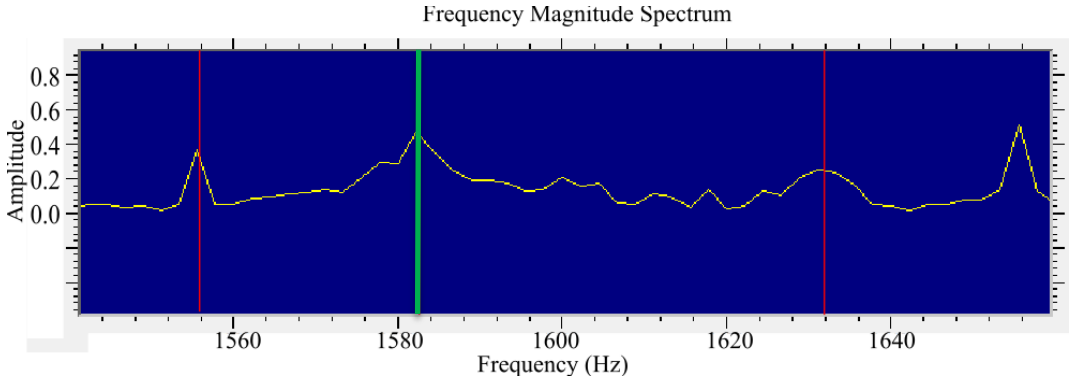

Figure 6-3 Prospa software magnitude spectrum highlighting noise sources and the signal of interest with the built-in polarizing coil activated

The 3 lines in the figure above (from left to right) are the 1550 Hz noise peak, the signal returning from the static water sample and the noise artefact produced by the motor respectively. The two noise artefacts are still visible in the same experiment performed without the polarising coil of the *TerraNova*, shown in Figure 6-4:

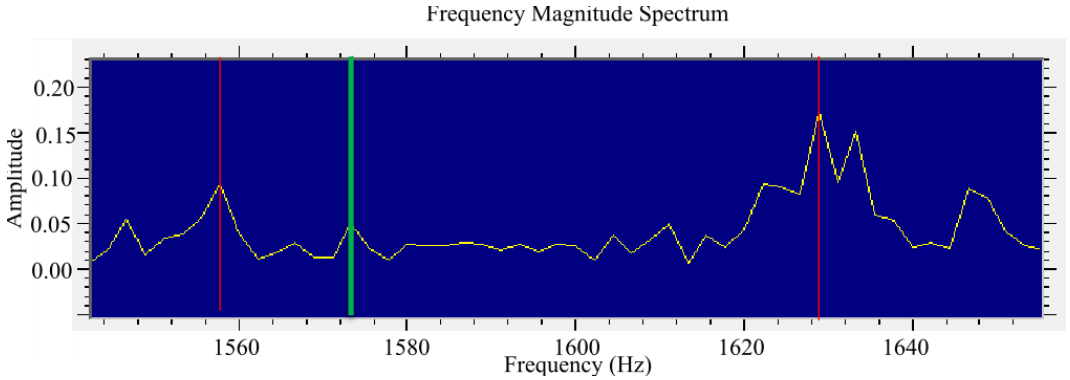

Figure 6-4 Magnitude spectrum highlighting noise sources and the signal of interest with the no built-in polarizing coil

The first red line on the left is the 1550 Hz noise that has not been entirely eliminated. The green line is the peak of interest that is recorded. The second red line is the noise induced in the *TerraNova* by the motor. The peak of interest is half the magnitude of the 1550 Hz resonant noise peak and one third the magnitude of the noise induced by the motor.

In order to ensure that no measurement that is recorded is due to noise alone, every experiment has been performed with the polarising coil switched on. The

experiment performed while using the polarizing coil helps isolate the errant noise peaks. The experimental result recorded must then adhere to the rule that the selected peak must not lie within 20 Hz of a noise peak induced by the motor.

6.7 Error Induced by Delayed and Uncontrolled Pulsatile Flow

There is a deviation that is noted for flow rates between 10-20 $ml \cdot s^{-1}$, where the experimental results are seen to be 30% lower than those that the model predicts, even including the 1.3 times correction factor. A lower than expected signal magnitude could be attributed to the uncontrolled pulsatile nature of flow through the model at volumetric flow rates lower than 20 $ml \cdot s^{-1}$.

The error induced by pulsatile flow arises due to the physical setup of the model itself. Flow through the model begins through one distensible tube. The tube expands and creates a positive gauge pressure within the model before the flow can fully develop through the second distensible tube. Due to this increased external pressure on the second distensible tube, the "venous return" analogous tube can be seen collapsing as the initial distensible tube becomes filled with water. The "venous return" tube then begins to fill with water and expand until the tube becomes fully patent, at which point the outlet side of the "venous return" tube collapses again. The interaction is illustrated in the Causal Loop Diagram Figure 6-5 below:

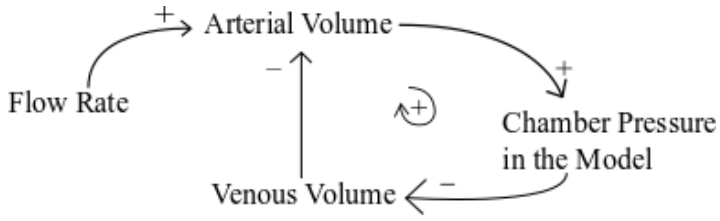

Figure 6-5 Causal Loop Diagram showing positive pressure feedback within the model that leads to undesired dynamic pulsatile effects within the flow carrying vessels

The pressure developed by the motor that drives volumetric flow through the second tube first needs to become greater than the positive pressure exerted by the

expansion of the “arterial” analogous tube. Once this happens, the “venous return” analogue becomes fully patent and the pressure built up within the analogue drops, causing the tube to collapse again. As a result, an undesired positive feedback oscillation effect within the model is observed.

The uncontrolled pulsatile effect does not occur with flow rates below 10 ml/s. This is attributed to the “arterial” analogous tube not becoming fully patent at these lower volumetric flow rates. The arterial analogue does not exert a large enough pressure within the model to collapse the venous return analogue. The decreased pressure within the arterial analogue explains the non-pulsatile, constant flow that is achieved at flow rates sub 10 ml/s.

The pulsatile effect also does not occur when flow rates through the model are sufficiently high (the effect disappears at average flow rates > 20 ml/s, as the pulsatile effects disappear). This is recognized as being the flow rate at which the pressure developed within the secondary venous return analogue becomes great enough to not collapse under the combined gauge pressure developed by both tubes within the model.

The pulsatile effect can explain the decrease in signal amplitude captured by the *TerraNova* device for flow rates sub 20 ml/s. The conservation of fluid flow states that the volumetric flow rate is always consistent through a closed system. If the flow is pulsed then there is a portion of time where fluid resides within the Halbach array longer and hence magnetize for a longer period of time. This should lead to a larger signal than expected. However, the rate at which the venous return analogue collapses cannot be measured and therefore the measurement cannot be gated effectively.

Without being able to exactly time each measurement, the volume of water within the second tube is inconsistent between measurements. It is considered that the pulsatile flow is incorrectly gated to the measurement and 30% of the polarised flow does not reside within the detector during detection. The effect of the extended polarisation time in the Halbach arrays vs. the unknown volume at time of

measurement is what is believed to cause the up to 30% deviation from the mathematical model.

6.8 Volume, Pressure and Signal Magnitude

Using the idealized model of the human arm it is noted that there is a relationship between the pressure developed within the model, the volume within the cardiovascular analogues and the signal captured by the *TerraNova* device.

The pressure has been measured in order to calculate the change in volume and the change in velocity of flow through the model. In order to create a system that will determine the blood pressure within a vessel, both automatically and non-invasively, a methodology for the inference of Blood Pressure values from the signal gathered by the *TerraNova-MRI* needs to be developed.

Stanwix and Fridjonsson et al. have proposed a methodology for the inference of flow velocity in rigid pipes based on the time-domain characteristic shape of the captured signal [4]. They have done this using Tikhonov regularisation, which is a statistical method for regularization of problems that could have more than one solution for a given question. In the case proposed by Stanwix et al. the uncertainty of the solution depends on the velocity through the system and the acquisition time of the signal.

In their problem the signal level captured by the *TerraNova* device can be the same for two different velocities through the model, dependant on the acquisition time or vice versa. This means that the question “what is the velocity of the fluid through the system?” can have multiple valid answers based on the acquisition time.

A similar problem is encountered in the model for this research. The signal level received by the *TerraNova* is dependent on a changing volume within the vessel, which also infers a change in the flow velocity through the system according to (7). A change in volume is also related to the changing pressure in the vessel according to (1). The change in volume, pressure and velocity of flow within the model is shown in Figure 6-6.

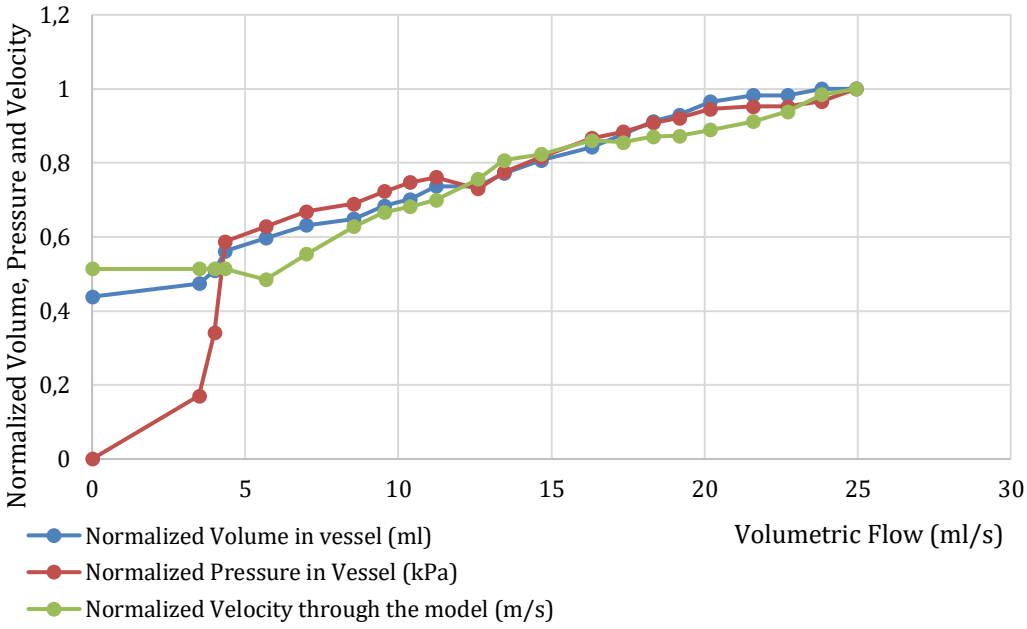

Figure 6-6 Graph showing the normalized values of the metrics of interest within the model

We can see that the volume/pressure and velocity through the model all increase at approximately the same rate when normalized. The result shows that it is possible to relate just one of these quantities to the signal retrieve through testing and infer the effect this change in quantity would have on the other parameters. Regularization of the problem and signal model needs to be performed before we can start interpolating accurate blood pressure and compliance measurements from recorded signal readings.

6.8.1 Real-World Differences from the Model

Human blood is approximately 50% water. If this experiment is to be performed on a human limb, the results can be expected to be half the magnitude of the results captured with the idealised model.

Other differences between the model and a real human limb have already been discussed. However, it can be noted that some of these differences may improve the signal captured by the *TerraNova*.

In a real human limb, blood is distributed to different muscles along the route of the arteries. The model created differs, as none of the polarised flow can disperse from the simulated vessels. In a real human limb, polarised flow can accumulate in the muscular compartment that is placed within the EFNMR detector without being ejected.

The residence time in the detector and volume terms from equation 6 will be larger than it is in the experiment. The τ_d in the equation 6 defines how long the polarised flow resides within the EFNMR apparatus. If polarised flow can perforate into the muscular compartment within the EFNMR apparatus, the residence time of the polarised flow within the apparatus is increased. Perforating flow also infers a larger polarised volume of spins within the detector, leading to an increased signal received by the *TerraNova*, as there is a larger volume of net polarised flow lying within the detector.

6.9 Future Improvements

As previously mentioned, the *TerraNova-MRI* device created by *Magritek* is constructed for hands-on learning of NMR principles and is generally used for 1D, 2D or 3D imaging of static water samples. In order to maximise the efficacy and consistency of measurements for diagnostic processes, it is proposed that a device, similar in origin and design of the *TerraNova*, be designed and manufactured. The new device must be constructed specifically with the purpose of applying NMR measurement principles to applications for the human body.

6.9.1 Pre-Polarisation

The pre-polarisation of water samples will be done using Halbach arrays instead of the large pre-polarisation coil distributed with EFNMR devices like the *TerraNova*. The Halbach arrays used for the purposes of this dissertation have center-bore uniform magnetic field intensities of 250-320 mT. This field is 10 times larger than that produced by the pre-polarization coil of the *TerraNova* (~30 mT).

The larger polarizing field intensity allows for smaller volumes of water to emit a more robust FID in response to an RF stimulus according to equations 6 and 12.

The Halbach arrays used for these experiments have been constructed using cost-effective 20x20x5 mm Neodymium rare earth magnets. The bore of these arrays is too small to be used for medical purposes. For future experimentation, Halbach arrays with bores large enough to fit a human limb will need to be constructed. This reduces the cost effectiveness of the solution and also introduces the problem of magnetic interference with the RF emission and detection coils.

Halbach Array Shielding

During this research the effect of decreased proximity between Halbach arrays and the *TerraNova* has been explored. It is noted that the orientation of the Halbach arrays, when placed on either side of the *TerraNova*, can either reinforce or oppose the Earth's magnetic field. The higher order magnetic field perturbations which decrease homogeneity within the bore of the detector can either be removed by implementing shielding between arrays and detector, or through designing new shimming coils.

An automated system can also be developed that will calibrate the device to obtain the largest possible signal level. This can be done by automating the rotation of each Halbach arrays with respect to the *TerraNova* device. Automated calibration techniques will rotate the Halbach arrays and perform measurements to ascertain the ideal rotational orientation of each array in order to maximize signal measured by the *TerraNova* with either a static volume of water.

In order to mitigate the effects of fringe fields emanating from the Halbach arrays, magnetic shielding can be constructed to house either the RF/shimming coils or the individual Halbach arrays. The use of magnetic shielding to decrease the effect of fringe fields on the *TerraNova* has been tentatively breached in previous works by the author. Fridjonsson et al. have also implemented mu-metal shielding around their Halbach arrays in research involving flowing water experiments using the *TerraNova-MRI* [8] [4].

6.9.2 Shimming Coils

New alternatice shimming coils can be designed to minimize the effect of the fringe fields attributed with the use of permanent magnets to polarise volumes of flowing water. The coils can be designed using software suites like *CST studio* and *Flux*. Software suites like those mentioned above allow for simulation of static (produced by magnetic materials) and dynamic magnetic fields (created using coils with known current flow).

The *TerraNova-MRI* device makes use of 3 gradient coils (x, y and z-axis) to eliminate first-order (linear) inhomogeneity in the Earth's magnetic field. In order to eliminate higher order inhomogeneity that can arise through use of Halbach arrays, more than 3 coils need to be constructed. 5 coils are required to obtain second order shimming with even more coils required for higher order fields of correction [25].

6.9.3 RF – Coils

The RF B_1 coil used in the *TerraNova-MRI* is a transceiver for both excitation and detection of an NMR signal [9]. It is the innermost coil of the apparatus and is also sensitive to external RF fields [9]. New RF coils can be designed as a gradiometer, which would consist of two separate coils for excitation and direction. The RF coils can be wound opposite directions to further decrease radiofrequency interference from external sources and the shimming coils.

Passive filters can be added to the RF coils in order to filter out the 50 Hz power line frequency and its harmonics in the low frequency region of the signal (below 2 kHz, with the signal of interest at around 1600 kHz). Passive filters can also be used to eliminate unwanted high frequency noise above 1 kHz. If required the RF and gradient coils can be placed within additional RF shielding to mitigate the effect of leakage flux lines from Halbach arrays at close proximity to the device.

Chapter 7 – Conclusion

Current methodologies for indirect blood pressure measurement are subjective in nature due to the reliance on the Korotkoff Auscultatory Method throughout all measurement techniques. A new objective methodology for blood pressure measurement has been proposed that makes use of EFNMR techniques.

A model has been constructed that mimics the behaviour of the major blood carrying vessels of the upper arm. Experiments have been performed using this model and the *TerraNova-MRI* EFNMR apparatus from *Magritek*. The measurement technique makes use of Halbach arrays placed co-axially along the bore of the *TerraNova* on either side of the machine. The Halbach arrays are rotated 180° out of sync, which results in a B_0 field increase of ~7.2 μT within the bore of the detector coil. This B_0 field increase corresponds to a shift in the Larmor frequency of the precessing Hydrogen from 1370 Hz (Halbach arrays placed 50 cm from the detector) to 1580 Hz (Halbach arrays placed 20 cm from the detector).

The arrays have inner bore flux densities of 300 mT and are used to polarise flowing water inside 5mm radius indistensible PVC tubing. Within the TerraNova detector coil, the water flows into distensible, compliant balloons within the model of the human upper limb. Inside the *TerraNova*, excitation and detection of the precessing hydrogen nuclei in the polarised water is detected.

Pressure within the model is measured using a MPX10DP series gauge pressure sensor that measures the changing air pressure within the model. The changing pressure within the model is directly proportional to the flow rate through the fluid flow setup. The slowest flow rate achieved by the pump through the model is 4 ml/s, which corresponds to an internal pressure of 1.65 kPa gauge. The fastest flow rate achieved by the pump through the model is 25 ml/s, corresponding to an internal pressure within the model of 3.15 kPa gauge. At steady-state the volume within both cardiovascular analogues at minimum flow rate is ~25 ml of polarized flowing water. At max flow rate this volume increases to ~47 ml.

The increased volume with increasing flow rate correlates with increased compliant vessel diameters within the model. According to the conservation of fluid flow equation (7), the increased vessel diameters within the detector coil leads to a decrease of flow velocity through the analogues in the model. Through non-compliant pipes the flow velocity through the model at maximum flow rate would be ~0.32 m/s. The vessel compliance and change in volume correlates to a flow velocity, at maximum flow rate, of ~0.11 m/s.

The decreased flow velocity increases the residence time of polarised flow within the detector coil by a factor of 3. The increased residence time of polarised flow within the detector, coupled with the increased polarised volume in the detector, allows for small volumes of flowing water to be measured using the EFNMR apparatus.

Results indicate that there is a 0.88 positive correlation between the signal received by the *TerraNova* and theoretical signal model developed through modification of the model proposed by Fridjonsson et al. The compliance of the model's vessel analogues is calculated to be 1.46 ml/mmHg. It is noted that the compliance is below the average compliance of a healthy young individual and indicates that the model more accurately represents a person with poor cardiovascular compliance.

Suggestions for future improvement of the experiment have been provided. These include manufacturing of new EFNMR RF and shimming coils that are built with dimensions fit for human use. New Halbach arrays that have large internal bore diameters need to be constructed. Methodologies for the mitigation of stray fields emitted from the Halbach arrays have been proposed.

References

[1] C. Höcht, “Blood Pressure Variability: Prognostic Value and Therapeutic Implications,” *ISRN Hypertension*, vol. 2013, p. 16, 2013.

[2] R. Leca and V. Groza, “Why Are We Still Measuring Blood Pressure by Ear?,” in *Measurement Technology Conference*, Victoria, Vancouver Island, 2008.

[3] L.-w. H. Lehman, M. Saeed, D. Talmor, R. Mark and A. Malhotra, “Methods of Blood Pressure Measurement in the ICU,” *Crit Care Med.*, vol. 1, no. 41, pp. 34-40, 2013.

[4] K. O'Neill, P. Stanwix, M. Johns and E. Fridjonsson, “Online Multiphase Flow Measurement using Earth's Field Nuclear Magnetic Resonance,” in *20th Australasian FLuid Mechanics Conference*, Perth, 2016.

[5] J. Perez, R. M. Lang and S. G. Shroff, “Noninvasive Evaluation of Aortic Elastic Properties,” in *Echocardiography and Cardiovascular Function: Tools for the Next Decade*, New York, Springe Science and Business Media, 2012.

[6] C. F. Babbs, “Oscillometric measurement of systolic and diastolic blood pressures validated in a physiologic mathematical model,” BioMedical Engineering Online, 2012.

[7] G. E. McVeigh, A. J. Bank and J. N. Cohn, “Arterial Compliance,” in *Cardiovascular Medicine*, Springer, 2007, pp. 1811-1831.

[8] E. O. Fridjonsson, P. L. Stanwix and M. L. Johns, “Earth’s field NMR flow meter: Preliminary quantitative measurements,” *Journal of Magnetic Resonance,* vol. 245, pp. 110-115, 2014.

[9] Magritek Ltd., Hands-on learning MRI and NMR principles, Wellington: Magritek Ltd., 2006.

[10] E. Fukushima, "Nuclear Magnetic Resonance as a tool to study flow," *Annual Review of Fluid Mechanics,* vol. 31, pp. 95-123, 1999.

[11] N. Westerhof, J.-W. Lankhaar and B. E. Westerhof, "The arterial Windkessel," *Medical and Biological Engineering and Computing,* vol. 47, no. 2, pp. 131-141, 2009.

[12] B. Seyithanoglu, A. Zaki Masud, O. Ergene, W. Morris, O. Kozan, J. Corbelli and M. Wilson, "Compliant vs non-compliant balloons. A prospective randomized study.," *Japan Heart Journal,* vol. 39, no. 1, pp. 45-54, 1998.

[13] G. Gamble, J. Zorn, G. Sanders, S. MacMahon and N. Sharpe, "Estimation of Arterial Stiffness, Compliance, and Distensibility from M-Mode Ultrasound Measurements of the Common Carotid Artery," *Stroke,* vol. 25, no. 1, pp. 11-16, 1998.

[14] T. Yuuki, Y. Keiichiro, F. Satoshi, O. Noriki, I. Mamiko, N. Mutumi, A. Kumi, H. Tatsunori, K. Chietsugu and N. Tamaki, "Accurate quantitative measurements of brachial artery cross-sectional vascular area and vascular volume elastic modulus using automated oscillometric measurements: comparison with brachial artery ultrasound," *Hypertension Research,* vol. 38, no. 7, pp. 478-484, 2015.

[15] Y. Keiichiro, F. Satoshi, T. Yuuki, T. Keisuke and T. Nagara, "Anatomical and Functional Estimations of Brachial Artery Diameter and Elasticity Using Oscillometric Measurements with a Quantitative Approach," *Pulse,* vol. 4, no. 1, pp. 1-10, 2016.

[16] AZoMaterials, "Silicone Rubber," AZoNetwork Site, 2018.

[17] L. Sherwood, Fundamentals of physiology : a human perspective, Minneapolis: West Publishing Co., 1995.

[18] Mantech Electronics, “RS-360SH,” Mantech, 2018. [Online]. Available: http://www.mantech.co.za/ProductInfo.aspx?Item=15K0485-+KZN. [Accessed September 2017].

[19] S. R. Frohlich and V. Kuverjee, “EFNMR FLOW MEASUREMENTS AND FINDINGS ON AN ARTERIAL MODEL,” Johannesburg, 2016.

[20] Ventana Systems inc., “Vensim Personal Learning Environment,” Ventana Systems Inc., 2015. [Online]. Available: http://vensim.com. [Accessed July 2017].

[21] Motorola Inc., “MPX10 Series Datasheet,” Motorola Inc., 1997.

[22] J. Polliack and S. Feller, “Effect of Halbach Arrays on EFNMR measurement,” University of the Witwatersrand, Johannesburg, 2017.

[23] S. Johnson and K. McPherson, “Size of a Human: Body Proportions,” The Physics Factbook, 2005. [Online]. Available: https://hypertextbook.com/facts/2006/bodyproportions.shtml. [Accessed 21 November 2017].

[24] R. Burattini, G. Gnud, N. Westerhof and S. Fioretti, “Total systemic arterial compliance and aortic characteristic impedance in the dog as a function of pressure: a model based study.,” *Computers and Biomedical Research,* vol. 20, no. 2, pp. 154-165, 1987.

[25] P. Jezzard, “Shim Coil Design, Limitations and Implications,” 2006 May 2006. [Online]. Available: http://mriquestions.com/uploads/3/4/5/7/34572113/shim_coil_design_jezzard.pdf. [Accessed 9 September 2018].

[26] J. Bramwell and H. A.V., “The Velocity of the Pulse Wave in Man,” *Proceedings of the Royal Society,* vol. 93, no. 652, pp. 298-306, 1922.

[27] M. Townsend, “Superconducting magnets: The heart of NMR,” *ingenia online*, no. 18, pp. 15-19, 2004.

[28] T. M. Osán, J. M. Ollé, M. Carpinella, L. M. C. Cerioni, D. J. Pusiol, M. Appel, J. Freeman and I. Espejo, “Fast measurements of average flow velocity by Low-Field 1H NMR,” *Journal of Magnetic Resonance,* vol. 209, pp. 116-122, 2011.

[29] E. O. Fridjonsson, P. L. Stanwix and M. L. Johns, “Earth’s field NMR flow meter: Preliminary quantitative measurements,” *Journal of Magnetic Resonance,* vol. 245, pp. 110-115, 2014.

[30] K. T. O’Neill, A. Klotz, P. L. Stanwix, E. O. Fridjonsson and M. L. Johns, “Quantitative Multiphase Flow Characterisation using an Earth's Field NMR Flow Meter,” *Flow Measurement and Instrumentation,* 2017.

[31] K. T. O’Neill, P. L. Stanwix, M. L. Johns and E. O. Fridjonsson, “Application of Earth’s Field Nuclear Magnetic Resonance to Multiphase Flow Metering,” in *FLOMEKO 2016*, Sydney, 2016.

[32] Magritek, “Student Guide,” in *Terranova-MRI: Hands-on learning MRI & NMR principles,* Magritek, 2009, pp. 2-2.

[33] O. Winter, C. Kral and E. Schmidt, “Design study of magnet shapes for axial Halbach arrays using 3D Finite Element Analyses,” *IEEE Electrical Machines (ICEM), 2012 XXth Int.l Conf,* pp. 2660-2665, 2012.

[34] M. C. Tayler and D. Sakellariou, “Low-cost, pseudo-Halbach dipole magnets for NMR,” *Journal of Magnetic Resonance,* vol. 277, p. 143–148, 2017.

[35] C. R. Nave, “Relative Permeability,” Hyperphysics, [Online]. Available: http://hyperphysics.phy-astr.gsu.edu/hbase/Solids/ferro.html#c5. [Accessed 21 October 2017].

[36] S. Fröhlich and V. Kuverjee, “EFNMR Flow Measurement and Findings on an Arterial Model,” School of Electrical and Information Engineering, University of the Witwatersrand, Johannesburg, 2016.

[37] D. Meeker, *Finite Element Method Magnetics (FEMM),* Aladdin Free Public License, 2016.

[38] P. Callaghan, Principles of NMR microscopy, Oxford: Clarendon Press, 1991.

[39] S. Frohlich and V. Kuverjee, “Arterial Compliance using EFNMR,” Johannesburg, 2016.

[40] Magritek Ltd., “Hands-on learning MRI & NMR principles,” Magritek, Ltd., Wellington, 2006.

[41] P. Blumler, “Dipolar Halbach magnet stacks made from identically shaped permanent magnets for magnetic resonance,” *Concepts in Magnetic Resonance,* vol. 36A, no. IV, pp. 211-222, 2010.

[42] T. Sandgren, B. Sonesson, A. Ahlgren and T. Lanne, “The diameter of the common femoral artery in healthy human: Influence on sex, age and body size,” *Journal of Vascular Surgery,* vol. 29, no. 3, pp. 503-510, 1999.

[43] E. Fridjonsson, P. Stanwix and M. Johns, “Earth's Field NMR Flow Meter: Preliminary Quantitative Measurements,” *Journal of Magnetic Resonance,* no. 245, pp. 110-115, 2014.

[44] I. Herman, “Fluid Pressure, Fluid Flow in the Body, and Motion in Fluids,” in *Physics of the Human Body*, New York, Springer, 2006, pp. 405-425.

[45] J. Jackson, Classical Electrodynamics 3rd edition, New York: Wiley, 1999.

[46] C. Luo, M. Li, Q. Li, X. Quan, L. Gu, M. Zhao and Z. Wang, “Measurement and Clinical Study of Arterial Compliance,” 2008 World Automation Congress, Hawaii, 2008.

[47] C. Liu, S. Xin, C. Liu, J. J. Gu and M. Yu, “Non-invasive Measurement of Arterial Pressure-Dependant Compliance,” 2007 Canadian Conference on Electrical and Computer Engineering, Vancouver, 2007.

[48] J. Jararaj, T. Emy Anu, M. Sivaprakasam and S. S, “ARTSENS - An image-free system for noninvasive evaluation of arterial compliance,” 35th Annual International Conference of IEEE EMBS, Osaka, 2013.

[49] Magritek Limited, Hands-on learning MRI and NMR principles, MAgritek Ltd., 2006.

[50] A. Tsanas, J. Y. Goulermas, V. Vartela, D. Tsiapras, G. Theodorakis, A. C. Fisher and P. Sfirakis, “The Windkessel model revisited: a qualitative analysis of the circulatory system,” Medical Engineering and Physics, 2009.

[51] J.-W. Lankhaar and B. E. Westerhof, “The Arterial Windkessel,” Springer, 2008.

[52] T. J. Brinton, M. T. Kailasam, R. A. Wu, J. H. Cervenka, S.-S. Chio, R. J. Parmer, A. N. DeMaria and D. T. O'Connor, “Arterial Compliance by Cuff Sphygmomanometer,” Springer , San Diego, 1996.

[53] J. Shoemaker, M. MacDonald and R. Hughson, “Time course of brachial artery diameter responses to rhythmic handgrip exercise in humans,” European Society of Cardiology, 1997.

[54] G. Beevers, G. Y. Lip and E. O'Brien, “Blood Pressure Measurement: Part 1-Sphygmomanometry: factors common to all techniques,” BMJ, 2001.

[55] E. Fukushima, “Nuclear Magenetic Resonance as a Tool to Study Flow,” *Annual Reviews: Fluid Mech.,* vol. 31, pp. 95-123, 1999.

[56] P. Callaghan, Director, *Video 03: How the Terranova-MRI works.* [Film]. New Zealand : Magritek Ltd.2009.

[57] Magritek Ltd, “Science: Exciting the scientific community,” magritek, 2015. [Online]. Available: http://www.magritek.com/support/science/. [Accessed 13 July 2017].

[58] X. Zhang, V. Mahesh, D. Ng, R. Hubbar, A. Ailiani, B. O’Hare, A. Benesi and A. Webb, “Design, construction and NMR testing of a 1 tesla Halbach Permanent Magnet for Magnetic Resonance,” in *COMSOL Users Conference* , Boston, 2005.

[59] B. Manz , M. Benecke and F. Volke, “A simple, small and low cost permanent magnet design to produce homogeneous magnetic fields,” *Journal of Magnetic Resonance*, vol. 192, p. 131–138, 2008.

[60] D. Meeker, *Finite Element Method Magnetics (FEMM).*

[61] H. Raich and P. Blumler, “Design and Construction of a Dipolar Halbach Array with a Homogeneous Field from Identical Bar Magnets: NMR Mandhalas,” *Concepts in Magnetic Resonance Part B Magnetic Resonance Engineering* , vol. 23B, no. 1, p. 16–25, 2004.

[62] K&J Magnetics, “K&J Magnetics, Inc,” [Online]. Available: https://www.kjmagnetics.com/blog.asp?p=shielding-materials. [Accessed 20 July 2017].

[63] T. Ashraf, Z. Panhwar, S. Habib, M. A. Memon and J. Arif, “Size of radial and ulnar artery in local population,” *JPMA*, vol. 60, no. 10, pp. 817-819, 2010.

Appendix A – **Research Proposal**

Steven Ronny Fröhlich ***(538380)***

Research Question:

> To what extent can we use Earth Field Nuclear Magnetic Resonance (EFNMR) to extract blood pressure and arterial compliance metrics from an arterial model of a human limb?

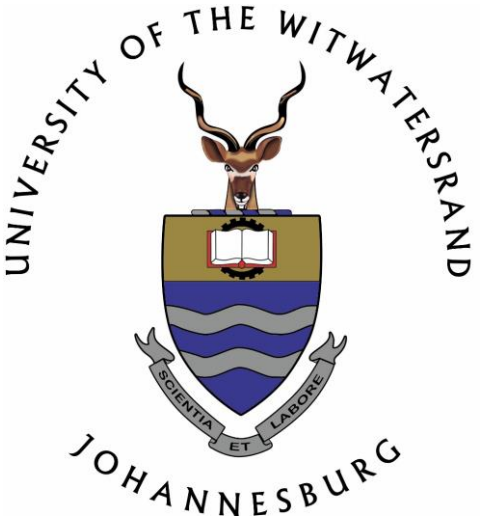

Abstract:

An experimental method using an Earth Field Nuclear Magnetic Resonance (EFNMR) measurement device to determine blood pressure, pulse wave velocity and arterial compliance is proposed within this report. The mathematical modelling and reasoning behind the concept are provided. Simulation and testing results are obtained using the *Vensim PLE* software package. The simulation results indicate that the precision of the *TerraNova* readings should be 0.001 μV or smaller in order to obtain measurements from volumes of water typical to that of human arteries. A proposed initial experimental setup in order to extract the desired metrics is then discussed and provided.

1. Introduction

The following report will detail the proposed research into the use of EFNMR experiments to determine arterial compliance and blood pressure. Blood Pressure (BP) and arterial compliance are important metrics that are required by doctors in order to diagnose a patient successfully [1]. The following sub-sections detail the assumptions made and how the problem has been broken up into 3 categories in order to address the research question.

2. Assumptions

The following assumptions have been made with respect to the experimental setup:

- The device is setup with a pre-polarising Halbach array situated upstream of the flow and the EFNMR device.
- The pulse rate and pressure of the artery/model must be continuous with no instantaneous changes.
- In order to take measurements, the EFNMR device is gated to synchronise measurements using a pulse waveform measured using a pulse oximeter.
- The EFNMR device has sufficient resolution to distinguish signal magnitude differences between changing volumes typical of the radial and ulnar arteries.

3. Compliance and BP

Current indirect methodologies to estimate arterial compliance and blood pressure in localised arteries of the human body make use of the Korotkoff Auscultatory

Method (KAM) techniques [2]. Current methodologies for estimation of blood pressure includes use of either invasive (Invasive Arterial Pressure (IAP)) or non-invasive (Non-Invasive Blood Pressure (NIBP)) methods of determining the systolic/diastolic/mean pressure within the artery. Invasive determination of arterial pressure is undesirable as it is an operation which may not be required [3]. These invasive surgeries also present risks associated with bleeding and infection which are undesirable.

Lehman et al. shows that current non-invasive measurements of systolic and diastolic BP's in hypotensive and hypertensive patients are clinically and significantly different from the intra-arterial BP's [2]. A study by Lehman et al. showed that systolic blood pressure measurements performed using NIBP for hypotensive patients in the ICU is higher than measurements obtained using IAP by an average offset of 10.05 mmHg [3]. The same study also showed that these systolic BP measurements in the hypotensive range can be indicators for acute kidney injury (AKI). The study shows that there is a higher prevalence of AKI in hypotensive patients (systolic pressures < 70mmHg) whose systolic BP threshold is measured non-invasively (~51%) as opposed to IAP (~34%) [3].

Current non-invasive methods for BP measurement require either a sphygmomanometer or calibrated subclavian pulse tracing to obtain blood pressures within major arteries of the upper limb. Both of the aforementioned non-invasive techniques make use of Korotkoff Auscultatory Method (KAM) techniques to estimate blood pressure.

The use of Korotkoff's sounds to non-invasively determine blood pressure was first implemented in 1905 and has been held as the golden standard of BP measurement [2]. These sounds are generally used in all methods of non-invasively determining blood pressures around the body. Oscillometry is an automated technique that has been developed to automatically measure BP using similar Korotkoff sounds to aid in the measurements [3, 2, 1]. Leca and Groza have put forth that the Korotkoff Auscultatory Method (KAM) is unscientific and hence inaccurate to be considered as the gold standard [2]. In order to consider a measurement objective and correct, the measurement must have a basis for the measurement in science. KAM is

subjective to the measurer, which automatically rejects the possibility of the measurement being objective. In addition to this most of the procedures to ensure correct auscultation may not be followed by practitioners [2].

Compliance is typically obtained through either direct (angiography, MRI or transcutaneous intravascular ultrasound) or indirect (Stroke Volume over pulse pressure and pulse wave velocity) methods [7]. These techniques for arterial compliance estimation all in some way require blood pressure measurements to be used according to the relationship in equation 1.

Compliance can then be calculated using the equation below.

$$Compliance = \frac{\Delta V}{\Delta P} \tag{1}$$

Therefore it is required to create a scientific methodology for the determination of both blood pressure and arterial compliance. The proposed research will attempt to show the extent to which we can determine BP and Compliance can be determined using measurements obtained using the TerraNova-MRI equipment belonging to the University of the Witwatersrand.

4. Flow Measurement

In order to determine the blood pressure, and with it compliance, within an artery, the basic understanding and modelling of the arteries must be covered. For this research proposal, the two-element WindKessel (WK) model is used to describe arterial flow. This is represented in Figure 1 below as an electric circuit consisting of a capacitance (compliance) in parallel with a load resistance (resistance to blood flow at the capillary bed) [11].

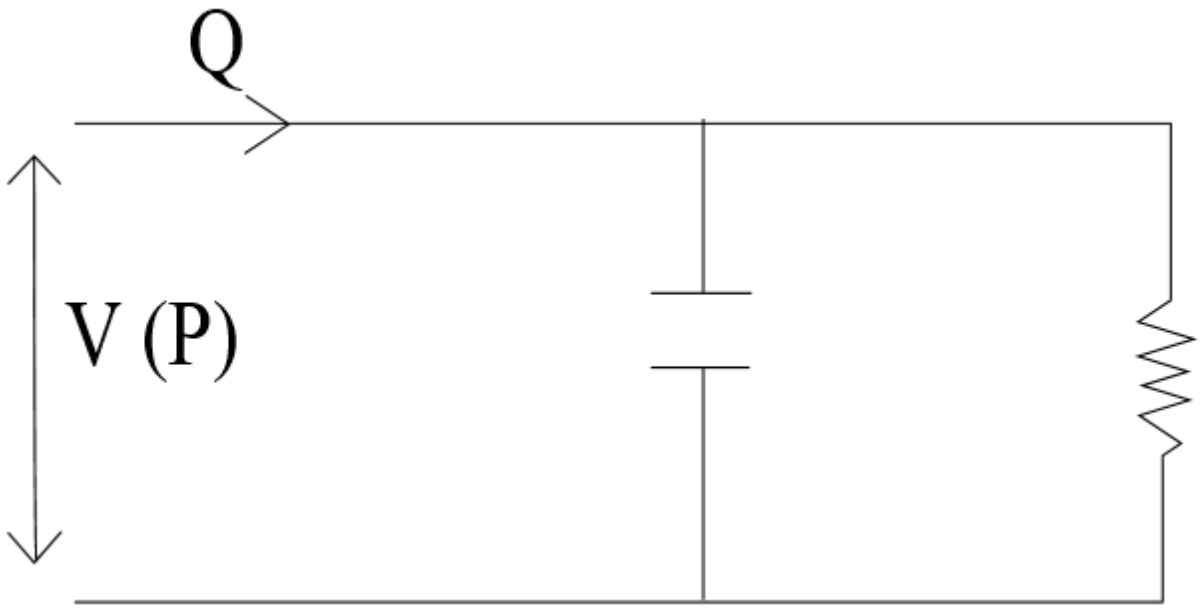

Figure 1-1- Windkessel model of an artery

According to equation 1, compliance and the change of volume are implicitly related. The set of equations that determine this system's behaviour are obtained using standard circuit analysis equations.

$$Q \propto I \tag{2}$$

$$V \propto P \tag{3}$$

$$V_{in} = V_c = V_R \tag{4}$$

$$I = I_c + I_R \tag{5}$$

According to the two element WK model. The change in voltage is proportional to a differential pressure within an artery. Logically this pressure is the radial pressure within the artery, which causes the deformation of the arterial walls. The full WK model lumps all arteries together and assumes that the valves and peripheral resistance result in a consistent peripheral flow rate [11]. Using this assumption, it is possible to lump various arteries within regions of the upper limb. The lumped model allows the use of the axial pressure difference across the artery in the determination of compliance.

The change in volume term is to be determined by the EFNMR device, discussed under the next subheading. The change in pressure term can be determined using the equation describing Pulse Wave Velocity (PWV) as derived by Moens-Korteweg and using the relevant substitutions performed by Bramwell and Hill [26].

$$v = \sqrt{\frac{V \cdot dP}{\rho \cdot dV}} \tag{6}$$

Where v is the PWV, ρ is the density of blood, V is the diastolic volume of the artery, dP is the change in pressure within the artery over a known area and dV is the change of volume in the same area. It can be noted that the dP/dV term is the inverse of compliance. This equation implicitly makes a connection between arterial compliance and the pulse wave velocity in the artery. Figure 2 below illustrates this concept.

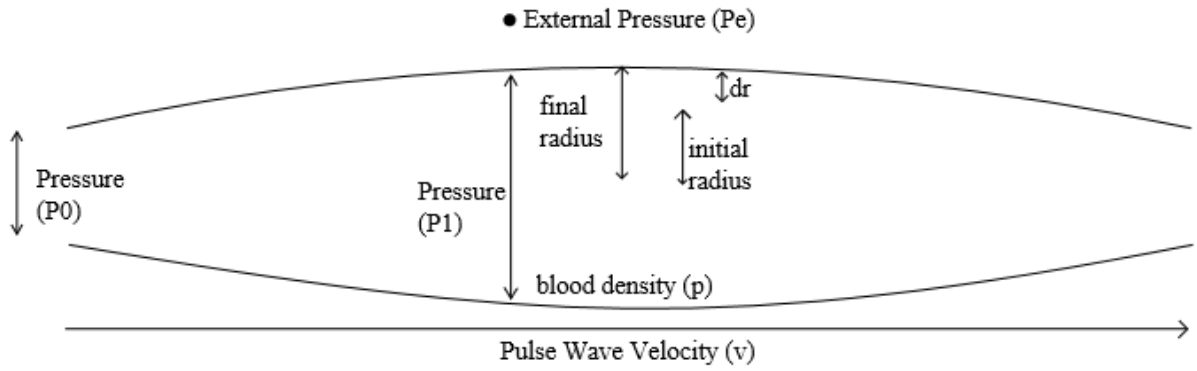

Figure 1-2- Simplified diagram illustrating the variables and relationships in equation 6

We therefore have a method that allows for the determination of change in volume using the methods described in the following section. In order to determine the change in pressure we therefore need to obtain the other terms in the equation above. The diastolic volume can also be estimated using the EFNMR method described below, the density of blood is known to fluctuate around 1025 kilograms per meter cubed. Therefore the only term we require in order to find the change in pressure is the Pulse Wave Velocity.

This will be performed by utilising a pulse oximeter to gate the measurements obtained using the TerraNova-MRI apparatus. The Terranova will be made to take a measurement only when the peak of the pulse is registered by the pulse oximeter. This measurement does not reflect the true peak value of volume within the artery, this is due to the fact that the pulse-wave has travelled down the arm inducing a time delay between peaks. Therefore we can create an algorithm that will delay the measurements taken by the NMR device, whilst gated to the pulse oximeter, until the peak signal measurement is found. Once a peak in the NMR signal has been located we can then compare the times at which each peak occurred in order to determine the PWV.

.

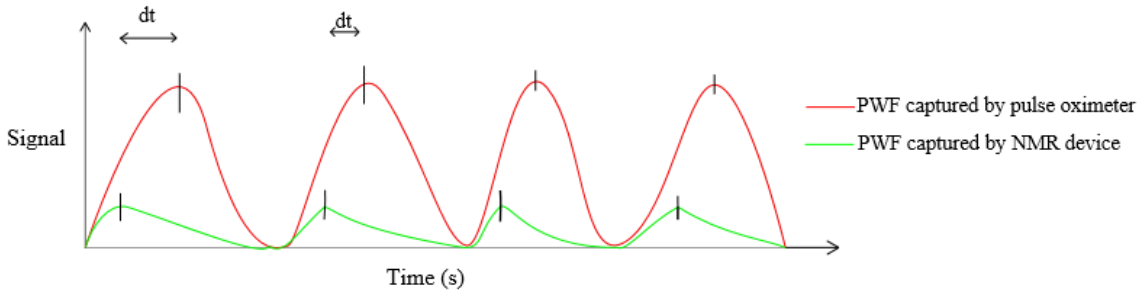

Figure 1-3- Graph showing the time displacement between signals obtained wih a pulse oximeter and the EFNMR device

$$v = \frac{dx}{dt} \tag{7}$$

The velocity can then be determined using the known Newtonian relationship above. The following section describes how the EFNMR device operates in order to obtain a changing volume.

5. Earth-Field NMR

Evidence for the use of Nuclear Magnetic Resonance (NMR) principles in measuring volumes of water is well documented [3]. If we want to determine the compliance of an artery we will need to relate these NMR equations and principles to information and equations linking flow, pressure and compliance.

EFNMR experiments mostly pertain to static sample tests with recent advances into its uses on the determination of flow characteristics [8]. Fridjonsson et al. have put forth preliminary results detailing the possibility of using EFNMR equipment for the measurement of flow [8]. Their experiments implemented a pre-polarisation permanent magnet upstream from the detector coil, with fluid velocities of 0-1 m/s. The equation below is presented in the mentioned paper and relates the signal magnitude received to the time taken for the sample to pass from pre-polarising magnet to the measurement equipment:

$$S_d = S_0 \left(1 - \frac{t_D}{\tau_d}\right) e^{\frac{t_D}{T_2^*}} \left(1 - e^{-\frac{\tau_p}{T_1}}\right) e^{-\frac{\tau_{pd}}{T_1}}$$

Where S_d is the signal detected by the device (in μV), S_0 is the original signal magnitude under static conditions in a magnetising field after an infinite time, t_D is the time taken between excitation and detection of the signal (in order to reduce the B1 coil ring-down time), τ_d is the fluid residence time within the detector, T_2^* is the combination of spin-spin relaxation and magnetic field inhomogeneity, τ_p is the residence time inside the polarising coil, T_1 is the fluid spin-lattice relaxation time and τ_{pd} is the time taken for the fluid to travel between polariser and detector. Furthermore, according to the paper by Fridjonsson et al. the spins within the detector must still be accounted for because the residence time within the detector is close to the residence time of the water between polarisation and detection [8].

We know the distance between the polarising magnetic field and the EFNMR device and the rate at which this magnetization decays [8]. A simulation has been developed of a simple fluid flow system with the signal detection element added to the system. The simulation shows a peak in signal magnitude when the fluid is flowing at a specified velocity. This is shown in figures 4, 5 and 6 below. The maximum signal occurs when the fluid flow rate through the simulation is 0.00007 L/s or the fluid velocity is 0.7m/s through a 6mm radius pipe.

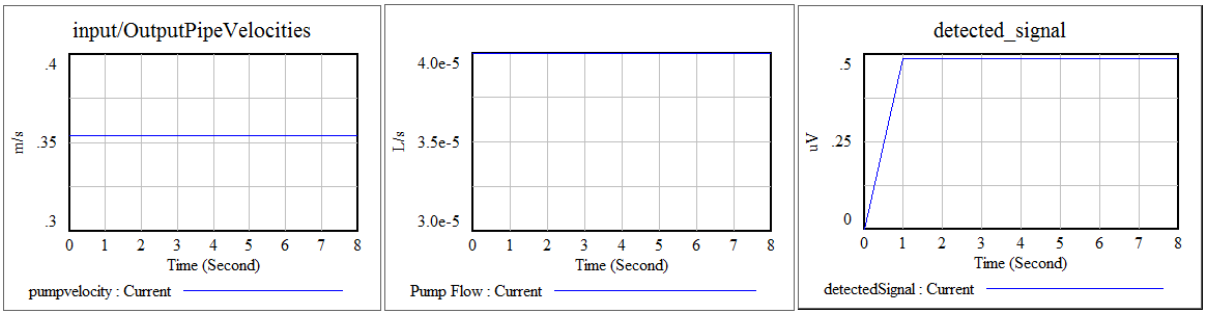

Figure 1-4- Figures showing volumetric flow rate, fluid velocity and detected signal magnitude at a speed of 0.35 m/s

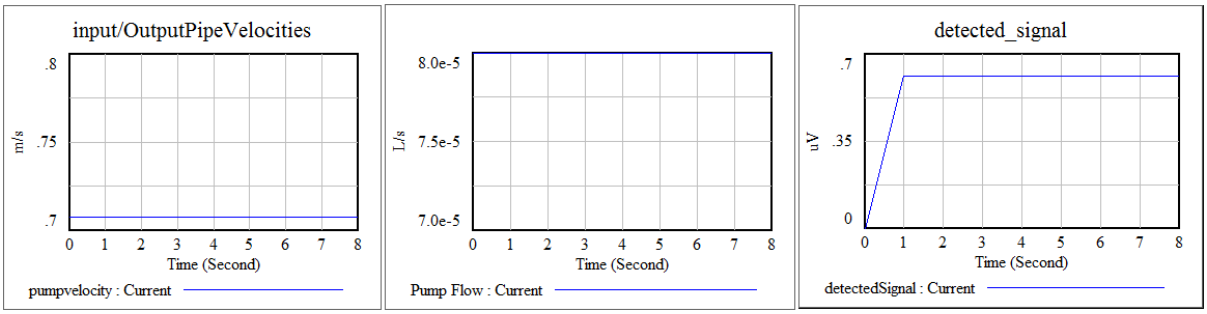

Figure 1-5- Graphs showing that the signal magnitude decreases as the fluid velocity is decreased

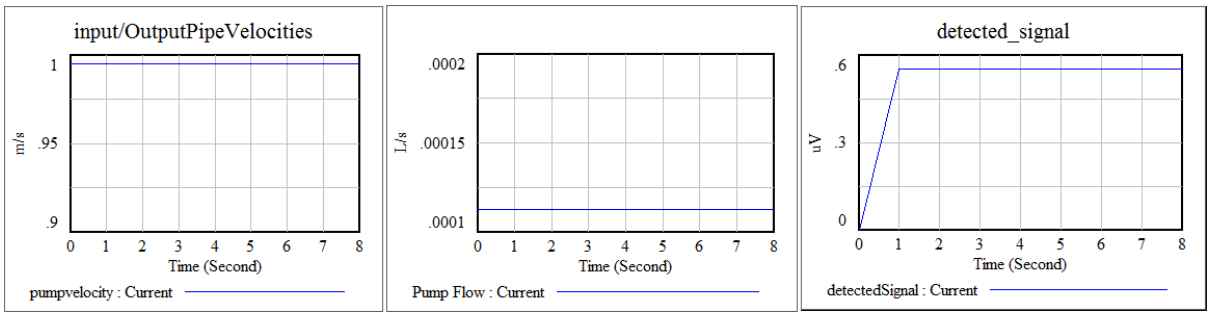

Figure 1-6-Graphs showing that the signal magnitude increases as the fluid velocity increases

Once we optimise this distance we will know the velocity of the blood as it enters the machine. From the previous subsection we will be able to determine an estimate for change in pressure in the arteries within the detector.

Bulk magnetization of the water sample entering a static magnetic field is developed according to [8] [9]:

$$M = M_0\left(1 - e^{-\frac{t}{T_1}}\right)$$

Where $M_0 \propto B_0^{\frac{7}{4}}$ [10], t is time and T_1 is as before. For this experiment we say that the initial signal magnitude that is present in the artery is equal to this magnetization term above multiplied by the volume within the artery within the polarizing field [9].

$$S_0 = M_0 \gamma B_E V_{artery} \frac{B_1}{I}$$

Where M_0 is the bulk magnetization of water, γ is the gyromagnetic ration for hydrogen, $\frac{B_1}{I}$ is the ratio of the magnetic field produced by the B_1 coil to the current through the polarisation coil x and V is the volume within the detector. The product of the B1/I and Earth's magnetic flux density (B_E) increase the efficacy of the measurement and can therefore not be omitted from the above equation [9]. This gives us the volume term that we require in order to determine the changing volume in order to determine arterial compliance.

In order to calculate a change in volume we can use the gated signal capturing of the device with a pulse oximeter. We take signal measurements at the peak of the signal and at the trough of the signal to determine the change in volume within the artery over the pressure difference (Compliance).

Assuming that the only changing variable in the system is the volume within the artery, we can derive the change in signal term:

$$\Delta S_d = M_0 \gamma B_E \Delta V_{artery} \frac{B_1}{I}\left(1 - \frac{t_D}{\tau_d}\right) e^{\frac{t_D}{T_2^*}}\left(1 - e^{-\frac{\tau_p}{T_1}}\right) e^{-\frac{\tau_{pd}}{T_1}}$$

6. Simulations

We have now developed a mathematical relationship for determining change in pressure and change in volume within an artery using a theoretical setup. We can therefore begin creating an experimental setup and model to define the system. This

section describes the creation of a simulation that will be used to model the pressure waveform through the major arteries of a human arm.

6.1 Preliminary Results

The first step to proving whether EFNMR can be used to detect blood flow is to investigate whether the device can detect the small volumes of polarised blood.

The ability of the *TerraNova-MRI* to detect small volumes of flowing water has been tentatively breached in my honours project for Electrical Engineering [19], where detectable signal levels (0.1 ~ 1 µV) from tap water were obtained from water in lengths of 12mm diameter PVA pipe [19]. The paper states that a 300 mT annular Halbach array is used to polarise the flowing water upstream from the *TerraNova-MRI*.

Vensim PLE simulations have been constructed to model this honours project experiment in order to verify that the software can accurately determine what has been experimentally measured. This model is given in the figure below.

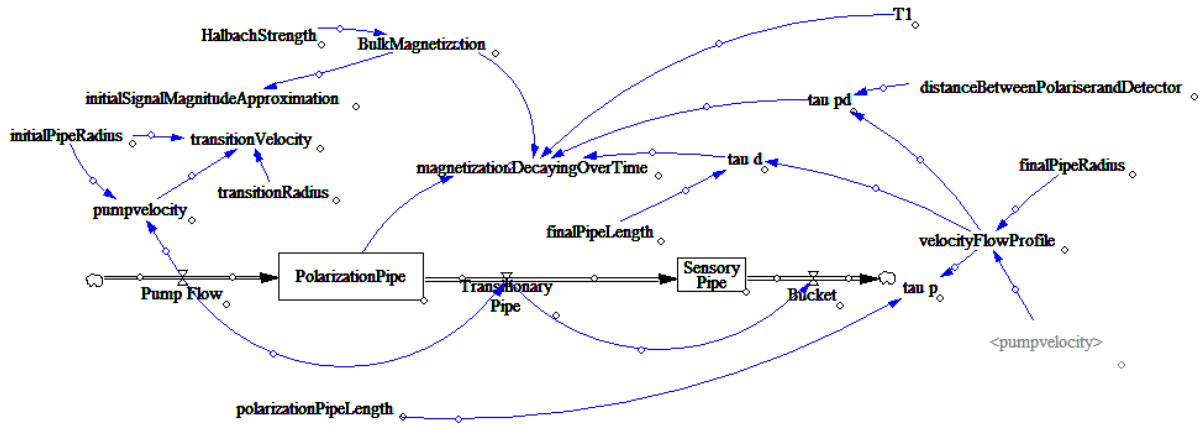

Figure 1-7- VENSIM implementation of an experimental EFNMR fluid flow setup

Using this model it is possible to then simulate the experiment and check whether the results correlate with the experimentally obtained results. The results obtained in the honours report showed signal amplitudes of between 0.2 – 1 μV, which are replicated by the simulation model. The model output for detected signal magnitude at a travelling velocity of ~ 1 m/s is given below.

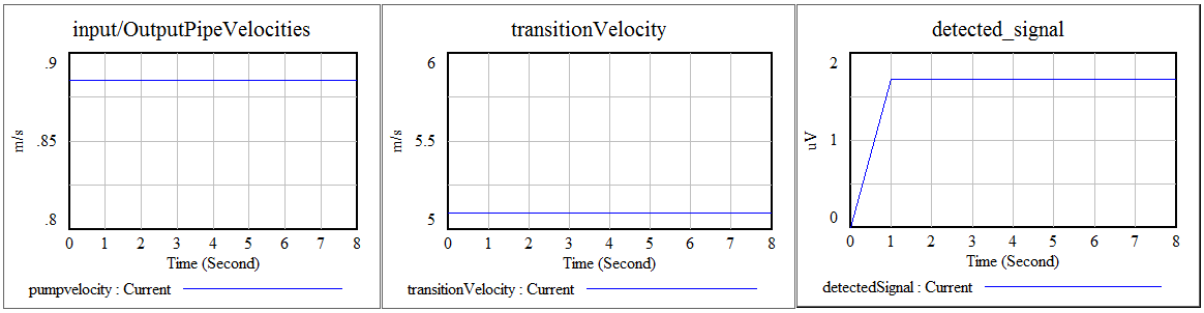

Figure 1-8- VENSIM generated graphs showing signal magnitude and relative travelling velocities through the experimental setup

6.2 Experimental Simulations

An experimental simulation is used to see the relationship between pulsatile polarised blood flow and EFNMR signal. The simulation will be used to see the signal magnitude ranges received by the EFNMR device in response to volumes typical of the human Brachial, Radial and Ulnar arteries. The simulation model is constructed using the *Vensim PLE x32* software package. The model only takes into account oxygenated blood flowing through the arterial system.

As stated in section 4, the model being used to describe the characteristics of blood flow through arteries of interest is the 2-element Windkessel. The simulation makes use of a given pressure waveform equation. This is applied as an activation input for the left ventricle. Blood then flows from the left ventricle into the aorta, then into the axillary arteries, followed by the brachial artery which then splits into radial and ulnar arteries as illustrated below.

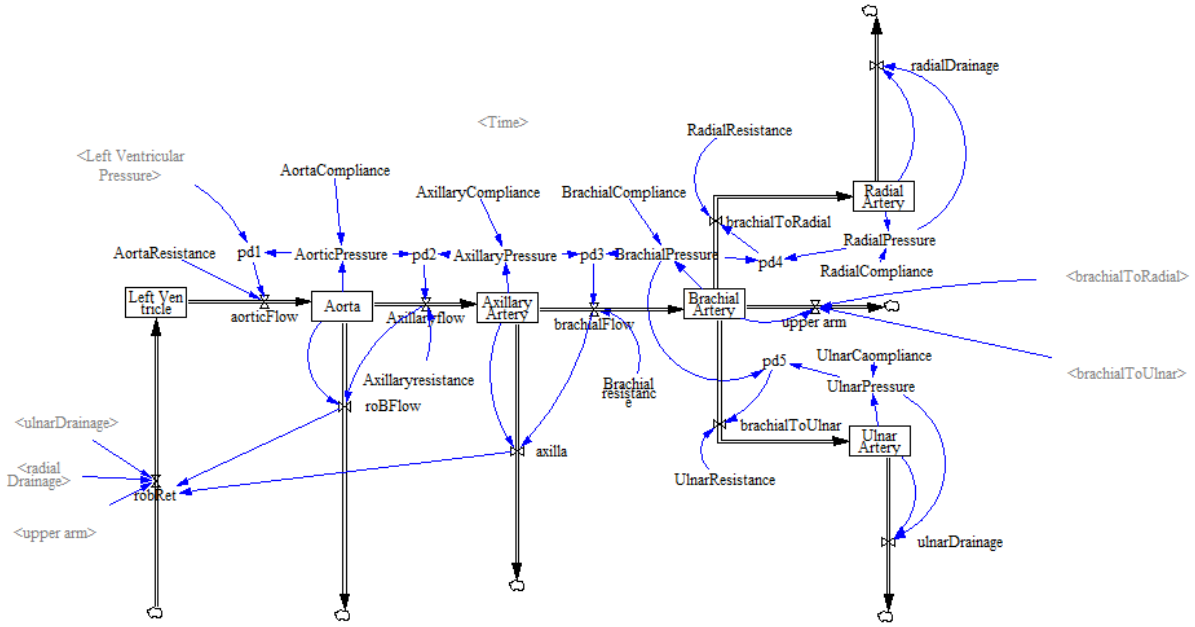

Figure 1-9- VENSIM model implementation of the main arteries in the upper limb

In addition to this model, a model describing the EFNMR signal expected to be obtained from the arteries are then overlaid into the simulation using the shadow variable functionality of *Vensim PLE*. The implementation of this functionality is shown below.

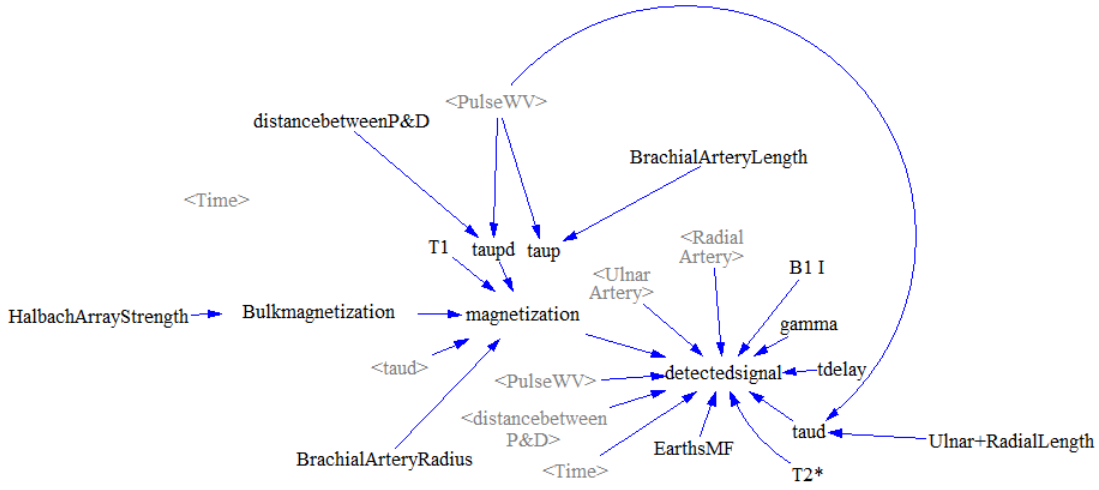

Figure 1-10- Model implementation of the signal detection equipment

The above figure shows how the EFNMR equations in section 5 have been implemented into the *Vensim PLE* environment. The final equation required to be implemented is the Pulse Wave Velocity calculations. As shown in the figure

below, this is done by varying the change in distance and time between pulse oximeter and EFNMR device.

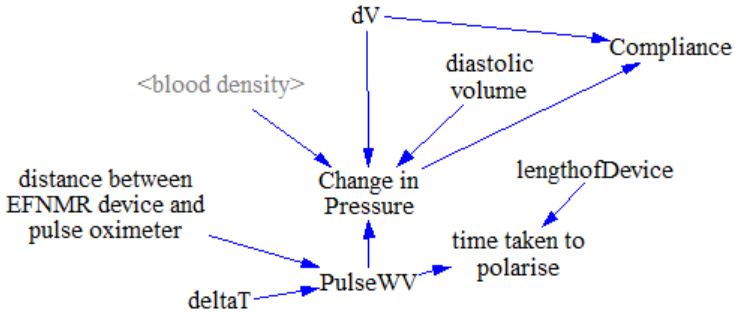

Figure 1-11- Model implementation of Pulse Wave Velocity equation

The output from the simulation is within the range experimentally obtained in the honours project research report. The model for EFNMR signal detection in *Vensim PLE* is then applied to the model of the major arteries in the arm and forearm according to the figures above. The following figure illustrates the changing signal magnitude received by the *TerraNova-MRI* from the polarised blood flowing within the radial and ulnar arteries.

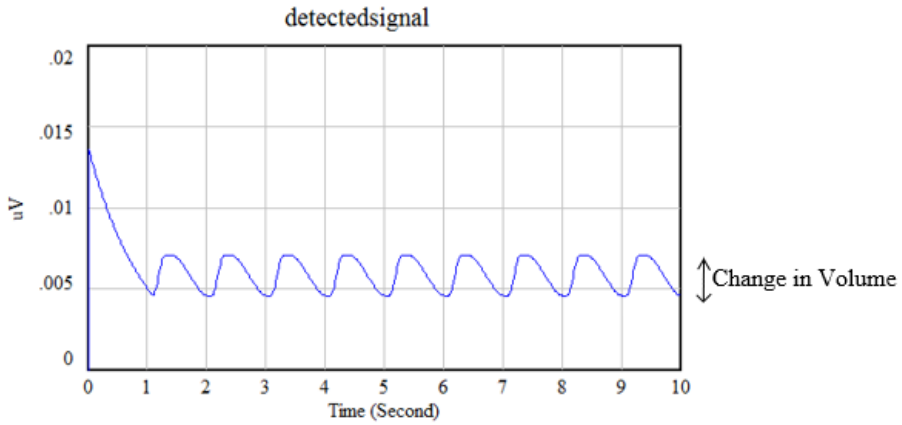

Figure 1-12- Model simulation results on pulsatile flow within the radial and ulnar arteries

These simulation results indicate that the device will be able to detect changes in signal based on these changing volumes during a blood pulsatile flow. The above

simulation of the detected signal indicates that the resolution of the TerraNova need to be set to 0.001 µV or less to obtain the pulse waveform.

7. Methodology

The following section lays out a proposed design and methodology for the determination of arterial compliance and blood pressure using the *TerraNova-MRI* and a pulse oximeter to gate the *TerraNova* measurements.

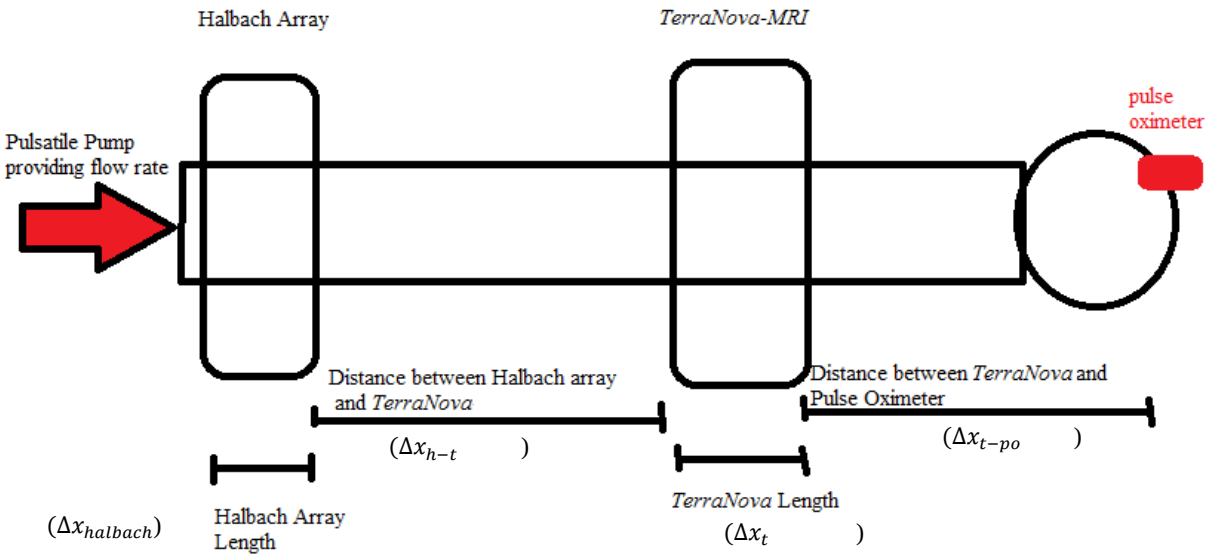

The arterial system will be experimentally setup and tested using medical piping with diameters near to those of the arteries of interest (radius = 2~5mm). The only arteries of interest for initial testing are the arteries mentioned above (Brachial, radial and ulnar).

A centrifugal pump will be used to provide the flow through the system. The choice of pump has been made in order to try and limit the noise induced onto the system. It is known from the honours project report that the pump introduces a lot of noise on the measurement through mechanical vibration of the equipment [19]. In order to create the pulsatile flow, a PWM input to the pump will be used to recreate the pulsatile nature of blood flow at approximately 70 beats per minute (bpm).

Once the flow has been calibrated to within normal human arterial ranges, experimental testing of the setup can begin. Measurements will ideally be taken by gating the collection of data by the *TerraNova* with the data obtained with the pulse

oximeter. The experiment will initially be performed using tap water to avoid the need to obtain medical and ethical clearance to use blood. This means that a pulse oximeter cannot be used to gate the measurements. During testing this can be replaced by gating the measurements to the PWM controlling the pump as described in section 4. This could also be achieved by placing an inline pressure sensor (catheter) near the end of the tube.

The measurements obtained using the *TerraNova* apparatus needs to be stored for further use in determination of blood pressure and compliance. Software can then be written to use the measurement data and the equations laid out above in order to calculate and display the measured systolic and diastolic blood pressures, pulse wave velocity and average compliance of the arteries within the arm.

8. Conclusion

An experiment to test the extent at which blood pressure and arterial compliance metrics can be obtained using Earth Field Nuclear Magnetic Resonance techniques has been described. A new technique is required in order to mathematically model compliance, blood pressure, pulsatile flow measurement and earth-field NMR. Arterial models have been implemented in simulations using *Vensim PLE*. The simulations indicate that blood pressure measurement is possible using a *TerraNova-MRI* with a measurement precision of at least 0.001 μV.

9. References

[1] C. Höcht, "Blood Pressure Variability: Prognostic Value and Therapeutic Implications," *ISRN Hypertension*, vol. 2013, p. 16, 2013.

[2] R. Leca and V. Groza, "Why Are We Still Measuring Blood Pressure by Ear?," in *Measurement Technology Conference*, Victoria, Vancouver Island, 2008.

[3] L.-w. H. Lehman, M. Saeed, D. Talmor, R. Mark and A. Malhotra, “Methods of Blood Pressure Measurement in the ICU,” *Crit Care Med.,* vol. 1, no. 41, pp. 34-40, 2013.

[4] K. O'Neill, P. Stanwix, M. Johns and E. Fridjonsson, “Online Multiphase Flow Measurement using Earth's Field Nuclear Magnetic Resonance,” in *20th Australasian FLuid Mechanics Conference*, Perth, 2016.

[5] J. Perez, R. M. Lang and S. G. Shroff, “Noninvasive Evaluation of Aortic Elastic Properties,” in *Echocardiography and Cardiovascular Function: Tools for the Next Decade*, New York, Springe Science and Business Media, 2012.

[6] C. F. Babbs, “Oscillometric measurement of systolic and diastolic blood pressures validated in a physiologic mathematical model,” BioMedical Engineering Online, 2012.

[7] G. E. McVeigh, A. J. Bank and J. N. Cohn, “Arterial Compliance,” in *Cardiovascular Medicine*, Springer, 2007, pp. 1811-1831.

[8] E. O. Fridjonsson, P. L. Stanwix and M. L. Johns, “Earth’s field NMR flow meter: Preliminary quantitative measurements,” *Journal of Magnetic Resonance,* vol. 245, pp. 110-115, 2014.

[9] Magritek Ltd., Hands-on learning MRI and NMR principles, Wellington: Magritek Ltd., 2006.

[10 E. Fukushima, “Nuclear Magnetic Resonance as a tool to study flow,” *Annual Review of Fluid Mechanics,* vol. 31, pp. 95-123, 1999.

[11 N. Westerhof, J.-W. Lankhaar and B. E. Westerhof, “The arterial Windkessel,” *Medical and Biological Engineering and Computing,* vol. 47, no. 2, pp. 131-141, 2009.

[12 B. Seyithanoglu, A. Zaki Masud, O. Ergene, W. Morris, O. Kozan, J. Corbelli and M. Wilson, "Compliant vs non-compliant balloons. A prospective randomized study.," *Japan Heart Journal,* vol. 39, no. 1, pp. 45-54, 1998.

[13 G. Gamble, J. Zorn, G. Sanders, S. MacMahon and N. Sharpe, "Estimation of Arterial Stiffness, Compliance, and Distensibility from M-Mode Ultrasound Measurements of the Common Carotid Artery," *Stroke,* vol. 25, no. 1, pp. 11-16, 1998.

[14 T. Yuuki, Y. Keiichiro, F. Satoshi, O. Noriki, I. Mamiko, N. Mutumi, A. Kumi, H. Tatsunori, K. Chietsugu and N. Tamaki, "Accurate quantitative measurements of brachial artery cross-sectional vascular area and vascular volume elastic modulus using automated oscillometric measurements: comparison with brachial artery ultrasound," *Hypertension Research,* vol. 38, no. 7, pp. 478-484, 2015.

[15 Y. Keiichiro, F. Satoshi, T. Yuuki, T. Keisuke and T. Nagara, "Anatomical and Functional Estimations of Brachial Artery Diameter and Elasticity Using Oscillometric Measurements with a Quantitative Approach," *Pulse,* vol. 4, no. 1, pp. 1-10, 2016.

[16 AZoMaterials, "Silicone Rubber," AZoNetwork Site, 2018.

[17 L. Sherwood, Fundamentals of physiology : a human perspective, Minneapolis: West Publishing Co., 1995.

[18 Mantech Electronics, "RS-360SH," Mantech, 2018. [Online]. Available: http://www.mantech.co.za/ProductInfo.aspx?Item=15K0485-+KZN. [Accessed September 2017].

[19 S. R. Frohlich and V. Kuverjee, “EFNMR FLOW MEASUREMENTS AND FINDINGS ON AN ARTERIAL MODEL,” Johannesburg, 2016.

[20 Ventana Systems inc., “Vensim Personal Learning Environment,” Ventana Systems Inc., 2015. [Online]. Available: http://vensim.com. [Accessed July 2017].

[21 Motorola Inc., “MPX10 Series Datasheet,” Motorola Inc., 1997.

[22 J. Polliack and S. Feller, “Effect of Halbach Arrays on EFNMR measurement,” University of the Witwatersrand, Johannesburg, 2017.

[23 S. Johnson and K. McPherson, “Size of a Human: Body Proportions,” The Physics Factbook, 2005. [Online]. Available: https://hypertextbook.com/facts/2006/bodyproportions.shtml. [Accessed 21 November 2017].

[24 R. Burattini, G. Gnud, N. Westerhof and S. Fioretti, “Total systemic arterial compliance and aortic characteristic impedance in the dog as a function of pressure: a model based study.,” *Computers and Biomedical Research,* vol. 20, no. 2, pp. 154-165, 1987.

[25 P. Jezzard, “Shim Coil Design, Limitations and Implications,” 2006 May 2006. [Online]. Available: http://mriquestions.com/uploads/3/4/5/7/34572113/shim_coil_design_jezzard.pdf. [Accessed 9 September 2018].

[26 J. Bramwell and H. A.V., “The Velocity of the Pulse Wave in Man,” *Proceedings of the Royal Society,* vol. 93, no. 652, pp. 298-306, 1922.

[27 M. Townsend, “Superconducting magnets: The heart of NMR,” *ingenia online,* no. 18, pp. 15-19, 2004.

[28 T. M. Osán, J. M. Ollé, M. Carpinella, L. M. C. Cerioni, D. J. Pusiol, M. Appel, J. Freeman and I. Espejo, "Fast measurements of average flow velocity by Low-Field 1H NMR," *Journal of Magnetic Resonance,* vol. 209, pp. 116-122, 2011.

[29 E. O. Fridjonsson, P. L. Stanwix and M. L. Johns, "Earth's field NMR flow meter: Preliminary quantitative measurements," *Journal of Magnetic Resonance,* vol. 245, pp. 110-115, 2014.

[30 K. T. O'Neill, A. Klotz, P. L. Stanwix, E. O. Fridjonsson and M. L. Johns, "Quantitative Multiphase Flow Characterisation using an Earth's Field NMR Flow Meter," *Flow Measurement and Instrumentation,* 2017.

[31 K. T. O'Neill, P. L. Stanwix, M. L. Johns and E. O. Fridjonsson, "Application of Earth's Field Nuclear Magnetic Resonance to Multiphase Flow Metering," in *FLOMEKO 2016,* Sydney, 2016.

[32 Magritek, "Student Guide," in *Terranova-MRI: Hands-on learning MRI & NMR principles,* Magritek, 2009, pp. 2-2.

[33 O. Winter, C. Kral and E. Schmidt, "Design study of magnet shapes for axial Halbach arrays using 3D Finite Element Analyses," *IEEE Electrical Machines (ICEM), 2012 XXth Int.l Conf,* pp. 2660-2665, 2012.

[34 M. C. Tayler and D. Sakellariou, "Low-cost, pseudo-Halbach dipole magnets for NMR," *Journal of Magnetic Resonance,* vol. 277, p. 143–148, 2017.

[35 C. R. Nave, "Relative Permeability," Hyperphysics, [Online]. Available: http://hyperphysics.phy-astr.gsu.edu/hbase/Solids/ferro.html#c5. [Accessed 21 October 2017].

[36 S. Fröhlich and V. Kuverjee, “EFNMR Flow Measurement and Findings on an Arterial Model,” School of Electrical and Information Engineering, University of the Witwatersrand, Johannesburg, 2016.

[37 D. Meeker, *Finite Element Method Magnetics (FEMM),* Aladdin Free Public License, 2016.

[38 P. Callaghan, Principles of NMR microscopy, Oxford: Clarendon Press, 1991.

[39 S. Frohlich and V. Kuverjee, “Arterial Compliance using EFNMR,” Johannesburg, 2016.

[40 Magritek Ltd., “Hands-on learning MRI & NMR principles,” Magritek, Ltd., Wellington, 2006.

[41 P. Blumler, “Dipolar Halbach magnet stacks made from identically shaped permanent magnets for magnetic resonance,” *Concepts in Magnetic Resonance,* vol. 36A, no. IV, pp. 211-222, 2010.

[42 T. Sandgren, B. Sonesson, A. Ahlgren and T. Lanne, “The diameter of the common femoral artery in healthy human: Influence on sex, age and body size,” *Journal of Vascular Surgery,* vol. 29, no. 3, pp. 503-510, 1999.

[43 E. Fridjonsson, P. Stanwix and M. Johns, “Earth's Field NMR Flow Meter: Preliminary Quantitative Measurements,” *Journal of Magnetic Resonance,* no. 245, pp. 110-115, 2014.

[44 I. Herman, “Fluid Pressure, Fluid Flow in the Body, and Motion in Fluids,” in *Physics of the Human Body*, New York, Springer, 2006, pp. 405-425.

[45 J. Jackson, Classical Electrodynamics 3rd edition, New York: Wiley, 1999.

[46 C. Luo, M. Li, Q. Li, X. Quan, L. Gu, M. Zhao and Z. Wang, “Measurement and Clinical Study of Arterial Compliance,” 2008 World Automation Congress, Hawaii, 2008.

[47 C. Liu, S. Xin, C. Liu, J. J. Gu and M. Yu, “Non-invasive Measurement of Arterial Pressure-Dependant Compliance,” 2007 Canadian Conference on Electrical and Computer Engineering, Vancouver, 2007.

[48 J. Jararaj, T. Emy Anu, M. Sivaprakasam and S. S, “ARTSENS - An image-free system for noninvasive evaluation of arterial compliance,” 35th Annual International Conference of IEEE EMBS, Osaka, 2013.

[49 Magritek Limited, Hands-on learning MRI and NMR principles, MAgritek Ltd., 2006.

[50 A. Tsanas, J. Y. Goulermas, V. Vartela, D. Tsiapras, G. Theodorakis, A. C. Fisher and P. Sfirakis, “The Windkessel model revisited: a qualitative analysis of the circulatory system,” Medical Engineering and Physics, 2009.

[51 J.-W. Lankhaar and B. E. Westerhof, “The Arterial Windkessel,” Springer, 2008.

[52 T. J. Brinton, M. T. Kailasam, R. A. Wu, J. H. Cervenka, S.-S. Chio, R. J. Parmer, A. N. DeMaria and D. T. O'Connor, “Arterial Compliance by Cuff Sphygmomanometer,” Springer , San Diego, 1996.

[53 J. Shoemaker, M. MacDonald and R. Hughson, “Time course of brachial artery diameter responses to rhythmic handgrip exercise in humans,” European Society of Cardiology, 1997.

[54 G. Beevers, G. Y. Lip and E. O'Brien, “Blood Pressure Measurement: Part 1-Sphygmomanometry: factors common to all techniques,” BMJ, 2001.

[55 E. Fukushima, “Nuclear Magenetic Resonance as a Tool to Study Flow,” *Annual Reviews: Fluid Mech.,* vol. 31, pp. 95-123, 1999.

[56 P. Callaghan, Director, *Video 03: How the Terranova-MRI works.* [Film]. New Zealand : Magritek Ltd.2009.

[57 Magritek Ltd, “Science: Exciting the scientific community,” magritek, 2015. [Online]. Available: http://www.magritek.com/support/science/. [Accessed 13 July 2017].

[58 X. Zhang, V. Mahesh, D. Ng, R. Hubbar, A. Ailiani, B. O’Hare, A. Benesi and A. Webb, “Design, construction and NMR testing of a 1 tesla Halbach Permanent Magnet for Magnetic Resonance,” in *COMSOL Users Conference* , Boston, 2005.

[59 B. Manz , M. Benecke and F. Volke, “A simple, small and low cost permanent magnet design to produce homogeneous magnetic fields,” *Journal of Magnetic Resonance,* vol. 192, p. 131–138, 2008.

[60 D. Meeker, *Finite Element Method Magnetics (FEMM).*

[61 H. Raich and P. Blumler, “Design and Construction of a Dipolar Halbach Array with a Homogeneous Field from Identical Bar Magnets: NMR Mandhalas,” *Concepts in Magnetic Resonance Part B Magnetic Resonance Engineering* , vol. 23B, no. 1, p. 16–25, 2004.

[62 K&J Magnetics, “K&J Magnetics, Inc,” [Online]. Available: https://www.kjmagnetics.com/blog.asp?p=shielding-materials. [Accessed 20 July 2017].

[63 T. Ashraf, Z. Panhwar, S. Habib, M. A. Memon and J. Arif, “Size of radial and ulnar artery in local population,” *JPMA*, vol. 60, no. 10, pp. 817-819, 2010.

Appendix B – **Matlab Code**

This appendix contains the code that has been used to convert the Fridjonsson et al. signal model in the frequency domain. The code is modified with the calculated polarised water flow velocity and volume within the detector.

```
%Model Paramters that change with increased volumetric flow rate
velocityFlow = 0.108;
LengthDetector = 0.2;
LengthPolarising = 0.24;
Transition = 0.2;
%Model Paramters that change with increased volumetric flow rate
%Physical constants
t2Star = 3;
T1 = 2;
B0 = 0.0000372;
Magnetization = B0^(7/4)*(exp(-t/tauPolarising));
GammaHydrogen = 42580000;
EarthB = 30*10^-6;
ArteryVolume = 55;
B1OverI =0.3;
%Physical constants
%Residence times at detector, Halbach array and transition between
tauDetector = LengthDetector/velocityFlow;
tauPolarising = LengthPolarising/velocityFlow;
tauTransition = Transition/velocityFlow;
%Residence times at detector, Halbach array and transition between
%Modelling the TerraNova's capturing of the signal
SamplingFrequency = 10000;
SamplingPeriod = 1/SamplingFrequency;
TimeStep = 1; %ms
t = (0:TimeStep:tauDetector*SamplingFrequency)*SamplingPeriod;
%Building the Signal model
Component1 = 1-((t+0.025)/tauDetector);
Component2 = exp(-(t+0.025)/t2Star);
Component3 = cos(B0*GammaHydrogen*t);
Component4 = 1-exp(-tauPolarising/T1);
Component5 = exp(-tauTransition/T1);
S0 = Magnetization*GammaHydrogen*EarthB*ArteryVolume*B1OverI;
s =
S0.*Component1.*Component2.*Component3.*Component4.*Component5;
%Building the Signal model
%Modelling the TerraNova's capturing of the signal
%Fourier Transform and plotting
FourierSignal = fft(s);
P2 = abs(FourierSignal/tauDetector);
P1 = P2(1:((tauDetector*SamplingFrequency)/2)+1);
P1(2:end-1)=2*P1(2:end-1);
f =
SamplingFrequency*(0:(tauDetector*SamplingFrequency/2))/(tauDetect
or*SamplingFrequency);
%plot(t,s);
plot(f,P1);
%Fourier Transform and plotting
```

Appendix C - Honour's project report of Shani Feller and Jethro Polliack

EFFECTS OF HALBACH ARRAYS ON EFNMR MEASUREMENT

Shani Feller 669874 **Partner: Jethro Polliack 670872**

School of Electrical & Information Engineering, University of the Witwatersrand, Private Bag 3, 2050, Johannesburg, South Africa

Abstract: The effects that Halbach arrays have on Earth's Field Nuclear Magnetic Resonance (EFNMR) measurements are presented. A modified circular Halbach array with a measured magnetic field strength of 320 mT is designed and constructed. Static water tests note that the ideal distance between the probe and the *Terranova* EFNMR device is 0.3 m and that the relative orientation of the array effect the signal strength. Placing Halbach arrays on either side of the probe minimizes the interference of the system, increasing the signal to noise ratio by up to 50 %. The upstream Halbach array pre-polarises the fluid flow, while the downstream Halbach array serves to cancel the fringe field interference. A flow rate of 806.6 ml/min and a polarisation length of six Halbach arrays yields the greatest signal strength of 0.59 μV.

Key words: Earth's Field Nuclear Magnetic Resonance, Halbach Array, Homogeneity, Pre-polarisation.

1.Introduction

In recent advances Nuclear Magnetic Resonance (NMR) devices have been used to detect fluid flow. This has aided many diagnostic techniques due to its non-invasive nature. As a result it can be used in many biomedical applications such as the potential measurement of blood pressure

The Earth's magnetic field is homogenous which makes it an ideal static magnetic field for NMR devices as it allows for sufficient signal detection. This is known as Earth's Field Nuclear Magnetic Resonance (EFNMR). However the Earth's magnetic field is approximately 100 000 times weaker than the magnetic field of superconducting magnets which are used in high frequency NMR [27]. Therefore the magnetic field is amplified. Despite the amplification of the static magnetic field a pre-polarising stage is required for the detection of fluid flow [28]. This ensures that the fluid flow is sufficiently magnetised before entering the EFNMR device and a signal can be detected [28]. Halbach arrays are positioned to produce a stronger static magnetic field that can also pre-polarise the fluid. The addition of these arrays introduce inhomogeneities in the system which interfere with the EFNMR device. As a result, methods are determined to minimize the fringe field interference on the EFNMR device while increasing the signal to noise ratio (SNR).

A flow system based on Fridjonsson et al., [29] is implemented using the *Terranova* EFNMR device. This allows for monitoring the effects of different flow rates on signal strength as well as investigating the different methods available to decrease the fringing field.

It is assumed that constant pressure and velocity is applied to the sample and that the temperature of the sample remains constant throughout the laboratory experiment.

The laboratory experiment is constrained by a six week time frame and a budget of R 1000. The project is also limited by the working hours available in the control laboratory. Furthermore the sample sizes and flow rates used are restricted by the device and the experimental setup.

Success is achieved if the effects of the Halbach arrays on EFNMR device are demonstrated. Various placements and orientations of the array must be explored in order to illustrate the full effects on the device. Furthermore progression on the experiment is required. This includes an improved Halbach array design with a stronger magnetic field strength, a reduction in the interference experienced by the EFNMR device, as well as an increase in the SNR.

Background relating to the problem is discussed in Section 2 while Section 3 describes the Halbach array design. The experimental setup and testing procedure is detailed in Section 4, results are illustrated in Section 5 while the discussion is found in Section 6.

2.Background

EFNMR is advantageous in fluid flow studies as there is no physical contact with the flow during the measurement [28]. This ensure that the flow pattern is not altered and accurate results are achieved. During the measurement the EFNMR probe detects and measures the free induction decay (FID) signal of the sample [30]. The signal received is dependent on the magnitude of signal growth during pre-polarisation (S_P); the amount the signal attenuates as it travels to the EFNMR probe (S_{PD}), and the magnitude of signal attenuation before signal detection occurs (S_D) [31]. Therefore the placement of the pre-polarising magnet as well as its strength is important to ensure that the sample is sufficiently magnetised as it will improve the SNR.

During static water tests the polarising coil of the EFNMR device produces a magnetic field with a strength of 18mT [32], which sufficiently magnetises the sample, ensuring a signal can be detected. During fluid flow the sample does not get sufficiently magnetised as it flows through the EFNMR probe. As a result a Halbach array with a strong magnetic field is required for upstream polarisation. This will ensure that the fluid flow is sufficiently magnetised when it reaches the EFNMR probe.

The principles of NMR as well as the composition of the *Terranova* device are described in Appendix B.

2.1. Halbach Array

A Halbach array is an arrangement of permanent magnets that focuses the magnetic field in a particular direction. In a circular configuration the magnetic field is concentrated through the centre of the array and is minimized on the outside of the array [33].

A Halbach array is a vital element for flow detection as it ensures that the sample is sufficiently magnetised and that static magnetic field is amplified. Thus improving the SNR.

Tayler et al., [34] proposes a modified circular Halbach array design, using rectangular block type magnets. This orientation allows for stacking of multiple magnets in one orientation, thereby increasing the strength of the magnetic field produced. It was noted that as the number of magnets in the array increased the strength of the magnetic field increased [34]. A maximum field strength of 1.95 T was measured through the centre of the array when 24 magnets are used [34].

2.2. Fluid Flow Measurement

Fridjonsson et al., [29] presents a system comprised of a Halbach array and *Terranova* probe to detect fluid flow at different flow rates. The Halbach array has a magnetic field strength of 300 mT and is positioned to provide upstream polarisation [29]; this ensures that the fluid is sufficiently magnetised for signal detection [28]. Osán et al., [28] noticed that by setting the distance between the probe and the pre-polarizing magnet (L_{pd}) a range of flow velocities can be measured with a reasonable SNR. When a 330 mT pre-polarizing magnet is placed 0.5 m away from probe optimal results are yielded.

O'Neill et al.; [31] designed a two-phase flow measurement system using an EFNMR device and an upstream pre-polarising magnet which is located 0.65 m away from the probe. This set up allows for the detection of the ^1H signal from the fluid flow which is then analysed and the velocity flow distribution determined [31].

Fridjonsson et al., [29] modelled the relationship between the detected signal and fluid flow rate. This relationship is illustrated in Equation 1.

$$S_d = S_0\left(1-\frac{t_{delay}}{\tau_d}\right)e^{\frac{t_{delay}}{T*_2}}\left(1-e^{-\frac{\tau_p}{T_1}}\right)e^{-\frac{\tau_{pd}}{T_1}} \qquad (1)$$

Where S_d is the detected NMR signal, S_0 is the detected signal under no flow conditions. τ_d is the time the fluid spends in the device, t_{delay} is the acquisition time delay. T_2* is the observed response of the transverse relaxation time. T_1 is the longitudinal relaxation time. τ_p is the time the fluid is polarised, for while τ_{pd} is the time taken for the fluid flow to travel form the Halbach array to the device.

2.3. Magnetic field interference

In order to minimize the fringe field effects on the *Terranova* probe O'Neill et al.; [30] suggests using Mu metal sheets to shield the Halbach array. Mu metal sheets are the ideal material for magnetic shielding as it has a relative permeability of 20 000 $H.m^{-1}$ which is 100 times stronger than magnetic iron which has a relative permeability of 200 $H.m^{-1}$ [35].

3.Halbach design

The Halbach array is designed with the aim of improving on the design of Fröhlich and Kuverjee [36], which had a magnetic field strength of approximately 300 mT [36]. In order to increase the magnetic field strength of the array, a modified circular Halbach array based on Taylor et al., [34] is designed. Sixteen 20x10x6.8 mm N35H neodymium rare earth magnets are arranged in a modified circular arrangement. Due to the dimension of the magnets used, this array has a rectangular bore with the dimensions 20x14.6 mm. The configuration of the magnets is illustrated in Appendix C Figure C-1.

A finite element modelling software *FEMM 4.2* [37] is used to simulate the design. A magnetic field strength of approximately 450 mT is achieved through the centre of the bore while the fringing field on the outside of the array has a strength of approximately 200 mT. This is shown in Appendix C Figure C-2.

The simulated magnetic field is roughly 1.5 times stronger than the array designed by [36] and is approximately 25 times stronger than the magnetic field produced by *Terranova* polarising coil. A Gaussmeter is used to measure the strength of the magnetic field of the constructed Halbach array. A strength of approximately 320 mT is measured indicating that the simulated results are incorrect. This discrepancy can be attributed to the difference in magnetic properties of the simulated magnets and the purchased magnets.

Due to financial constraints only two Halbach arrays are constructed. As a result the circular Halbach arrays (CHA) which were designed and built by [36] are used in conjunction with the newly designed modified circular Halbach arrays (MCHA). This ensures that the fluid flow is sufficiently pre-polarised during the testing procedure as a total of six arrays are constructed (4 CHA and 2 MCHA). Furthermore the interaction between the fringing fields of the different Halbach arrays may have a significant effect on EFNMR measurements.

The *Terranova* device is highly sensitive therefore the large fringe fields of the Halbach array described above introduce inhomogeneities into the system. The amount of inhomogeneity in the magnetic field (ΔB) is dependent on the placement of the array. This relationship is illustrated in Equation (2).

$$\Delta B = \frac{\mu_0 \times 2\mu}{4\pi(L_{pd})^3} \qquad (2)$$

Where μ_0 is the permeability of free space, μ is the magnetic moment, and L_{pd} is the distance between the device and the array.

4.experimental setup and testing procedure

A two-Halbach array system is designed to minimize the fringe field effects of the arrays on the *Terranova* probe without the use of magnetic shielding. One array is placed on either side of the probe as illustrated in Figure 1 and Figure 2. The upstream array serves to pre-polarise the fluid flow, while the downstream Halbach array serves to cancel the fringe field interference.

In order to determine the correct placement and orientation of the array static water tests are first conducted. Once the optimal placement is determined fluid flow tests are carried out.

4.1. Static Water Tests

The experimental setup for static water tests is shown in Figure 1. The experiment serves to investigate whether the magnetic fringe field of one array interferes destructively with the other, thereby reducing the resultant fringe field and the interference experienced by the probe. In order to have a baseline for comparison tests are also conducted with only one array placed upstream.

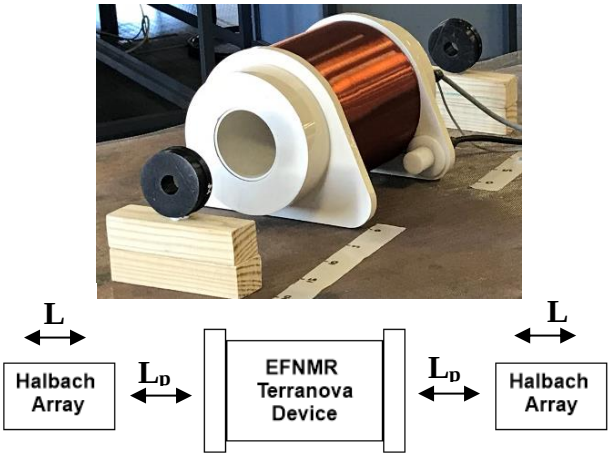

Figure 4-1: Static water test configuration

The distance between the probe and the array (L_{pd}) is important as it affects the strength of the signal detected. This is illustrated in Equation 2. If the arrays are placed too close to the probe, the inhomogeneity of the system becomes too great to detect a signal and the SNR is minimal. However for fluid flow detection, if the distance is too large, the fluid demagnetises before reaching the probe thus decreasing the SNR. The optimal distance of 0.3 m is found to through an iterative approach using *Pulse and Collect* tests, described in Appendix D Section 2. For every distance investigated the optimal orientation of the array is also noted.

Pulse and Collect tests are conducted on a 500 ml water bottle. 32 tests are averaged per iteration in order to cancel out the noise. The heat generated by the polarising current limited the number of tests conducted per iteration.

The orientation of one array relative to the other is important in order to maximize the destructive interference that occurs between the both arrays. One array is kept constant, with its North Pole pointing upwards. The second array starting in the same position, is then rotated clockwise in 30° increments until 180° is achieved. This ensures that the full range is covered.

The length of polarisation L_p is an important factor for fluid detection. As L_p is increased the magnetisation of the fluid flow is increased thereby increasing the SNR. Various arrays are stacked together in order to increase L_p. The array stacks are treated as a singular unit and called an array collection. Since the ideal distance L_{pd} = 0.3 m is known, static water tests described above are conducted to determine the optimal orientation of the stacked arrays. The results can be found in Appendix D Section 3.

The optimal orientation for the different array collections are summarised in Table 1. It can be seen that each array collection has a different ideal orientation. This can be attributed to the fringe field interaction between each array in the collection. Two arrays of the same type result in the same ideal orientation, as their fringe field are similar.

While a combination of different arrays have a different resultant fringe field thereby changing the optimal orientation.

Table 1: Optimal orientation of different array collections at a distance 0.3 m away from the probe

Types of Arrays per Collection	Relative Orientation (°)	Signal Strength (μV)
1 CHA	30	7.3
1 MCHA	150	7.2
2 CHA	30	5.8
2 CHA + 1 MCHA	90	6.5

4.2. Flowing Water Tests

The experimental setup for fluid flow is illustrated in Figure 2. It consists of 15 mm diameter PVC piping, a 12 V flow pump and a bucket serving as a water source. Due to the lack of a flow meter, the flow rates are calculated manually. These calculations are detailed in Appendix E.

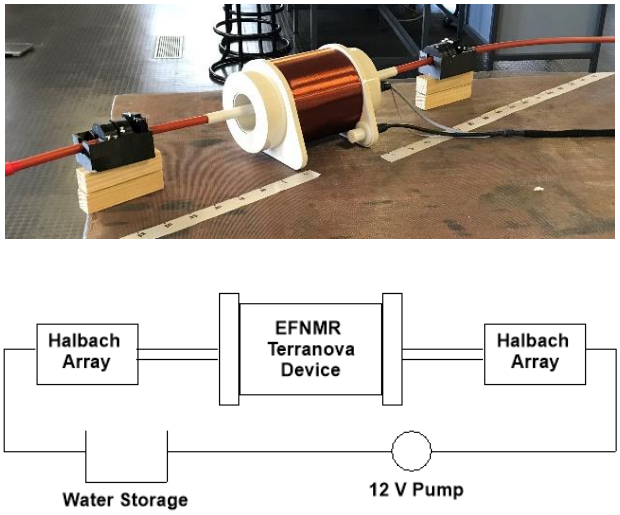

Figure 4-2: Flowing water test configuration

For flow detection tests, the fluid flow relies solely on the upstream pre-polarisation supplied by the Halbach arrays. Therefore the magnitude of the polarising current as well as its duration is set to zero. As a result heat generation is not a limiting factor and 64 tests are averaged per iteration in order to average out the noise.

The device is shimmed using a 500 ml bottle of static water. Since the optimal placement and orientation of the arrays are known, shimming only occurs once between placements of different arrays as this alters the magnetic field of the system.

The effects of increasing L_p on signal strength is illustrated by placing array collections of different lengths on one side of the probe. At first an array collection of one array is placed on one side of the probe, a *Pulse and Collect* test is conducted and the results are recorded for varying flow rates. This process is repeated until a collection of six arrays are tested.

Array collections consisting of two and three arrays respectfully are combined. At a time each collection type is placed on either side of the probe. *Pulse and Collect* tests are then conducted at varying flow rates before the next array collection is tested. These tests illustrate the fringe field interaction among the collections and the effect on the interference experienced by the device.

5.Results

The static water results in Table 2 shows that the fringe field of each array interacts destructively with one another thereby reducing the interference experienced by the probe and increasing the SNR by at least 30 %.

Table 2: Signal strength for varying array configurations at 0.3 m distance

Array Type	Array Configuration	Signal Strength (μV)
CHA	One side	5.6
CHA	Both sides	7.3
MCHA	One side	3.6

Both sides 7.2

MCHA

This effect is further illustrated in flowing water tests where an array collection of three arrays are placed on either side of the probe. The results obtained are depicted in Figure 3. It is clearly evident that the SNR has increased by 50 % when the arrays are placed on either side of the probe.

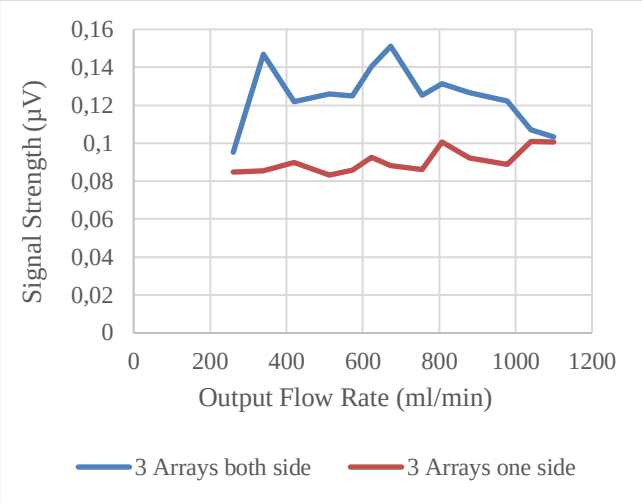

Figure 5-1: Signal strengths at varying flow rates for two different array configurations

The effect of increasing the length of polarisation (L_p) is clearly evident in Figure 4. As the number of arrays are added to one side of the probe, the L_p increases, and the signal strength rises. The effect of the flow rate on signal strength is also shown. If the flow rate is too slow it loses magnetisation before it reaches the probe, however if it is too quick it does not polarise sufficiently. The optimal flow rate is approximately 800 ml/min.

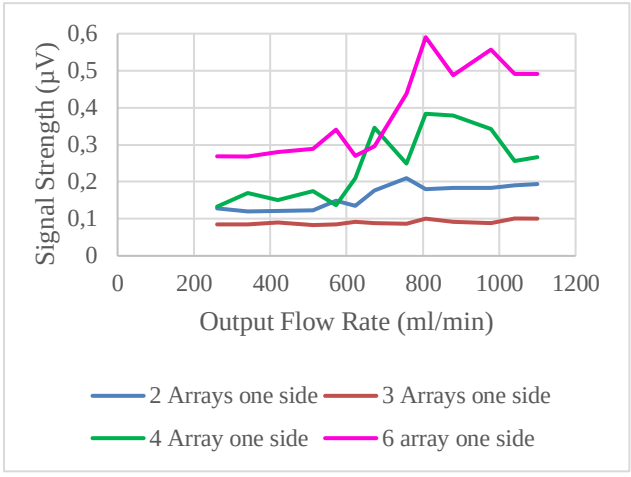

Figure 5-2: Signal strength for various polarisation lengths at different flow rates

The greatest signal amplitude is detected when six arrays are placed on one side of the probe at a flow rate of 806.6 ml/min. Table 3 contains the results for this measurement, while Figure 5 shows the frequency response obtained using the *Terranova-Prospa* software.

Table 3: Results achieved using six arrays on one side of the probe

Flow Rate (ml/min)	Maximum Amplitude (µV)	Frequency (Hz)	Integral
806.6	0.5904	1294	2.7

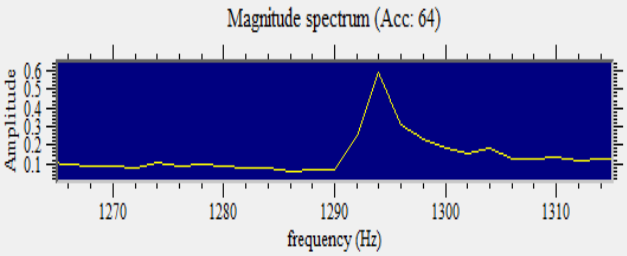

6.discussion

6.1. Critical Analysis

The optimal distance between the Halbach arrays and the probe is 0.3 m. If the array is too close to the probe, the inhomogeneity of the system becomes too great to detect a signal. However if the distance is too far the fluid flow

loses its magnetisation before reaching the probe.

The different array configurations (CHA and MCHA) yield similar results as shown in Table 1. The results obtained when using one CHA is approximately 1.4 % stronger than the signal received when using on MCHA. Different magnets are used in the construction of the different array types. As a result the different magnetic properties may affect the homogeneity of the system effecting the strength of the signal received.

The length of polarisation is the most important factor when discussing the strength of the received signal. This is clearly evident as six arrays placed on one side of the probe yields the greatest signal magnitude. Figure 4, however shows that improved results are achieved when two arrays of the same type are used instead of three arrays of different types, despite the increase in L_p. This implies that the different types of arrays in a collection have different fringe field which interact with each other. This results in an increase in the resultant fringe field decreasing the SNR.

Due to financial constraints the effects of six arrays of the same type placed on either side of the probe was not investigated. It is assumed that this configuration will produce the greatest results as L_p is maximized and the fringe fields will interact in a destructive manner.

6.2. Trade-offs

The budget was a main factor in a few trade-offs that occurred. Due to the cost incurred in the construction of a Halbach array, which can be seen in Appendix F, only two modified circular arrays are built. As a result different array geometries are used which have affected the results obtained. Furthermore the cost of a magnetic shield constructed from material with a high relative permeability such as Mu metal was too great. Therefore no magnetic shielding is used.

A trade-off occurred between accuracy and time taken to complete a test. Sufficient heat is generated when current is passed though the polarising coil during *Pulse and Collect* tests. The number of tests conducted per iteration is therefore limited to 32 in order to reduce the time taken for the device to cool down. As a result the accuracy of the readings obtained are reduced.

6.3. Recommendations

Surrounding the *Terranova* device with a faraday cage will limit the interference experienced by the probe thereby improving the SNR. Furthermore shielding the Halbach array with a high permeability metal will limit the interaction of its fringe field.

In order to improve the quality of the signal detected, the number of arrays used to pre-polarise the fluid flow must be increased. Additionally, the Halbach array should be constructed using long rectangular rod shaped magnets, which are magnetised through their length. This results in one elongated Halbach array which is long enough to sufficiently pre-polarise the fluid flow. As a result the fringe field interaction among the arrays in a collection is no longer a concern.

7.Conclusion

The effects of Halbach arrays on EFNMR measurements have been presented. Through static water tests the ideal placement and orientation of the Halbach arrays are determined. Placing arrays on either side of the *Terranova* probe minimizes the interference experienced by the probe. The ideal length of polarisation as well as optimal flow rate is noted through flowing water tests. Recommendations to improve the SNR are discussed.

ACKNOWLEDGEMENT

The author would like to thank Dr. S Dinger for his guidance and supervision throughout the project, as well as Mr. S Fröhlich for his advice. The author is appreciative to Mr. J Polliack for his contribution to the laboratory project.

References

[1 C. Höcht, "Blood Pressure Variability: Prognostic Value and Therapeutic Implications," *ISRN Hypertension*, vol. 2013, p. 16, 2013.

[2 R. Leca and V. Groza, "Why Are We Still Measuring Blood Pressure by Ear?," in *Measurement Technology Conference*, Victoria, Vancouver Island, 2008.

[3 L.-w. H. Lehman, M. Saeed, D. Talmor, R. Mark and A. Malhotra, "Methods of Blood Pressure Measurement in the

ICU," *Crit Care Med.,* vol. 1, no. 41, pp. 34-40, 2013.

[4 K. O'Neill, P. Stanwix, M. Johns and E. Fridjonsson, "Online Multiphase Flow Measurement using Earth's Field Nuclear Magnetic Resonance," in *20th Australasian FLuid Mechanics Conference*, Perth, 2016.

[5 J. Perez, R. M. Lang and S. G. Shroff, "Noninvasive Evaluation of Aortic Elastic Properties," in *Echocardiography and Cardiovascular Function: Tools for the Next Decade*, New York, Springe Science and Business Media, 2012.

[6 C. F. Babbs, "Oscillometric measurement of systolic and diastolic blood pressures validated in a physiologic mathematical model," BioMedical Engineering Online, 2012.

[7 G. E. McVeigh, A. J. Bank and J. N. Cohn, "Arterial Compliance," in *Cardiovascular Medicine*, Springer, 2007, pp. 1811-1831.

[8 E. O. Fridjonsson, P. L. Stanwix and M. L. Johns, "Earth's field NMR flow meter: Preliminary quantitative measurements," *Journal of Magnetic Resonance*, vol. 245, pp. 110-115, 2014.

[9 Magritek Ltd., Hands-on learning MRI and NMR principles, Wellington: Magritek Ltd., 2006.

[1 E. Fukushima, "Nuclear Magnetic Resonance as a tool to study flow," *Annual Review of Fluid Mechanics*, vol. 31, pp. 95-123, 1999.

[1 N. Westerhof, J.-W. Lankhaar and B. E. Westerhof, "The arterial Windkessel," *Medical and Biological Engineering and Computing*, vol. 47, no. 2, pp. 131-141, 2009.

[1 B. Seyithanoglu, A. Zaki Masud, O. Ergene, W. Morris, O. Kozan, J. Corbelli and M. Wilson, "Compliant vs non-compliant balloons. A prospective randomized study.," *Japan Heart Journal*, vol. 39, no. 1, pp. 45-54, 1998.

[1 G. Gamble, J. Zorn, G. Sanders, S. MacMahon and N. Sharpe, "Estimation of Arterial Stiffness, Compliance, and Distensibility from M-Mode Ultrasound Measurements of the Common Carotid Artery," *Stroke*, vol. 25, no. 1, pp. 11-16, 1998.

[1 T. Yuuki, Y. Keiichiro, F. Satoshi, O. Noriki, I. Mamiko, N. Mutumi, A. Kumi, H. Tatsunori, K. Chietsugu and N. Tamaki, "Accurate quantitative measurements of brachial artery cross-sectional vascular area and vascular volume elastic modulus using automated oscillometric measurements: comparison with brachial artery ultrasound," *Hypertension Research,* vol. 38, no. 7, pp. 478-484, 2015.

[1 Y. Keiichiro, F. Satoshi, T. Yuuki, T. Keisuke and T. Nagara, "Anatomical and Functional Estimations of Brachial Artery Diameter and Elasticity Using Oscillometric Measurements with a Quantitative Approach," *Pulse,* vol. 4, no. 1, pp. 1-10, 2016.

[1 AZoMaterials, "Silicone Rubber," AZoNetwork Site, 2018.

[1 L. Sherwood, Fundamentals of physiology : a human perspective, Minneapolis: West Publishing Co., 1995.

[1 Mantech Electronics, "RS-360SH," Mantech, 2018. [Online]. Available: http://www.mantech.co.za/ProductInfo.aspx?Item=15K0485-+KZN. [Accessed September 2017].

[1 S. R. Frohlich and V. Kuverjee, "EFNMR FLOW MEASUREMENTS AND FINDINGS ON AN ARTERIAL MODEL," Johannesburg, 2016.

[2 Ventana Systems inc., "Vensim Personal Learning Environment," Ventana Systems Inc., 2015. [Online]. Available: http://vensim.com. [Accessed July 2017].

[2 Motorola Inc., "MPX10 Series Datasheet," Motorola Inc., 1997.

[2 J. Polliack and S. Feller, "Effect of Halbach Arrays on EFNMR measurement," University of the Witwatersrand, Johannesburg, 2017.

[2 S. Johnson and K. McPherson, "Size of a Human: Body Proportions," The Physics Factbook, 2005. [Online]. Available: https://hypertextbook.com/facts/2006/bodyproportions.shtml. [Accessed 21 November 2017].

[2 R. Burattini, G. Gnud, N. Westerhof and S. Fioretti, "Total systemic arterial compliance and aortic characteristic impedance in the dog as a function of pressure: a model based study.,"

Computers and Biomedical Research, vol. 20, no. 2, pp. 154-165, 1987.

[2 P. Jezzard, "Shim Coil Design, Limitations and Implications," 2006 May 2006. [Online]. Available: http://mriquestions.com/uploads/3/4/5/7/34572113/shim_coil_design_jezzard.pdf. [Accessed 9 September 2018].

[2 J. Bramwell and H. A.V., "The Velocity of the Pulse Wave in Man," *Proceedings of the Royal Society,* vol. 93, no. 652, pp. 298-306, 1922.

[2 M. Townsend, "Superconducting magnets: The heart of NMR," *ingenia online,* no. 18, pp. 15-19, 2004.

[2 T. M. Osán, J. M. Ollé, M. Carpinella, L. M. C. Cerioni, D. J. Pusiol, M. Appel, J. Freeman and I. Espejo, "Fast measurements of average flow velocity by Low-Field 1H NMR," *Journal of Magnetic Resonance,* vol. 209, pp. 116-122, 2011.

[2 E. O. Fridjonsson, P. L. Stanwix and M. L. Johns, "Earth's field NMR flow meter: Preliminary quantitative measurements," *Journal of Magnetic Resonance,* vol. 245, pp. 110-115, 2014.

[3 K. T. O'Neill, A. Klotz, P. L. Stanwix, E. O. Fridjonsson and M. L. Johns, "Quantitative Multiphase Flow Characterisation using an Earth's Field NMR Flow Meter," *Flow Measurement and Instrumentation,* 2017.

[3 K. T. O'Neill, P. L. Stanwix, M. L. Johns and E. O. Fridjonsson, "Application of Earth's Field Nuclear Magnetic Resonance to Multiphase Flow Metering," in *FLOMEKO 2016*, Sydney, 2016.

[3 Magritek, "Student Guide," in *Terranova-MRI: Hands-on learning MRI & NMR principles,* Magritek, 2009, pp. 2-2.

[3 O. Winter, C. Kral and E. Schmidt, "Design study of magnet shapes for axial Halbach arrays using 3D Finite Element Analyses," *IEEE Electrical Machines (ICEM), 2012 XXth Int.l Conf,* pp. 2660-2665, 2012.

[3 M. C. Tayler and D. Sakellariou, "Low-cost, pseudo-Halbach dipole magnets for NMR," *Journal of Magnetic Resonance,* vol. 277, p. 143–148, 2017.

[3 C. R. Nave, "Relative Permeability," Hyperphysics, [Online]. Available: http://hyperphysics.phy-

astr.gsu.edu/hbase/Solids/ferro.html#c5. [Accessed 21 October 2017].

[3 S. Fröhlich and V. Kuverjee, "EFNMR Flow Measurement and Findings on an Arterial Model," School of Electrical and Information Engineering, University of the Witwatersrand, Johannesburg, 2016.

[3 D. Meeker, *Finite Element Method Magnetics (FEMM)*, Aladdin Free Public License, 2016.

[3 P. Callaghan, Principles of NMR microscopy, Oxford: Clarendon Press, 1991.

[3 S. Frohlich and V. Kuverjee, "Arterial Compliance using EFNMR," Johannesburg, 2016.

[4 Magritek Ltd., "Hands-on learning MRI & NMR principles," Magritek, Ltd., Wellington, 2006.

[4 P. Blumler, "Dipolar Halbach magnet stacks made from identically shaped permanent magnets for magnetic resonance," *Concepts in Magnetic Resonance*, vol. 36A, no. IV, pp. 211-222, 2010.

[4 T. Sandgren, B. Sonesson, A. Ahlgren and T. Lanne, "The diameter of the common femoral artery in healthy human: Influence on sex, age and body size," *Journal of Vascular Surgery*, vol. 29, no. 3, pp. 503-510, 1999.

[4 E. Fridjonsson, P. Stanwix and M. Johns, "Earth's Field NMR Flow Meter: Preliminary Quantitative Measurements," *Journal of Magnetic Resonance*, no. 245, pp. 110-115, 2014.

[4 I. Herman, "Fluid Pressure, Fluid Flow in the Body, and Motion in Fluids," in *Physics of the Human Body*, New York, Springer, 2006, pp. 405-425.

[4 J. Jackson, Classical Electrodynamics 3rd edition, New York: Wiley, 1999.

[4 C. Luo, M. Li, Q. Li, X. Quan, L. Gu, M. Zhao and Z. Wang, "Measurement and Clinical Study of Arterial Compliance," 2008 World Automation Congress, Hawaii, 2008.

[4 C. Liu, S. Xin, C. Liu, J. J. Gu and M. Yu, "Non-invasive Measurement of Arterial Pressure-Dependant Compliance," 2007 Canadian Conference on

Electrical and Computer Engineering, Vancouver, 2007.

[4 J. Jararaj, T. Emy Anu, M. Sivaprakasam and S. S, "ARTSENS - An image-free system for noninvasive evaluation of arterial compliance," 35th Annual International Conference of IEEE EMBS, Osaka, 2013.

[4 Magritek Limited, Hands-on learning MRI and NMR principles, MAgritek Ltd., 2006.

[5 A. Tsanas, J. Y. Goulermas, V. Vartela, D. Tsiapras, G. Theodorakis, A. C. Fisher and P. Sfirakis, "The Windkessel model revisited: a qualitative analysis of the circulatory system," Medical Engineering and Physics, 2009.

[5 J.-W. Lankhaar and B. E. Westerhof, "The Arterial Windkessel," Springer, 2008.

[5 T. J. Brinton, M. T. Kailasam, R. A. Wu, J. H. Cervenka, S.-S. Chio, R. J. Parmer, A. N. DeMaria and D. T. O'Connor, "Arterial Compliance by Cuff Sphygmomanometer," Springer , San Diego, 1996.

[5 J. Shoemaker, M. MacDonald and R. Hughson, "Time course of brachial artery diameter responses to rhythmic handgrip exercise in humans," European Society of Cardiology, 1997.

[5 G. Beevers, G. Y. Lip and E. O'Brien, "Blood Pressure Measurement: Part 1- Sphygmomanometry: factors common to all techniques," BMJ, 2001.

[5 E. Fukushima, "Nuclear Magenetic Resonance as a Tool to Study Flow," *Annual Reviews: Fluid Mech.*, vol. 31, pp. 95-123, 1999.

[5 P. Callaghan, Director, *Video 03: How the Terranova-MRI works.* [Film]. New Zealand : Magritek Ltd.2009.

[5 Magritek Ltd, "Science: Exciting the scientific community," magritek, 2015. [Online]. Available: http://www.magritek.com/support/science/. [Accessed 13 July 2017].

[5 X. Zhang, V. Mahesh, D. Ng, R. Hubbar, A. Ailiani, B. O'Hare, A. Benesi and A. Webb, "Design, construction and NMR testing of a 1 tesla Halbach Permanent Magnet for Magnetic Resonance," in *COMSOL Users Conference* , Boston, 2005.

[5 B. Manz , M. Benecke and F. Volke, “A simple, small and low cost permanent magnet design to produce homogeneous magnetic fields,” *Journal of Magnetic Resonance,* vol. 192, p. 131–138, 2008.

[6 D. Meeker, *Finite Element Method Magnetics (FEMM).*

[6 H. Raich and P. Blumler, “Design and Construction of a Dipolar Halbach Array with a Homogeneous Field from Identical Bar Magnets: NMR Mandhalas,” *Concepts in Magnetic Resonance Part B Magnetic Resonance Engineering* , vol. 23B, no. 1, p. 16–25, 2004.

[6 K&J Magnetics, “K&J Magnetics, Inc,” [Online]. Available: https://www.kjmagnetics.com/blog.asp?p=shielding-materials. [Accessed 20 July 2017].

[6 T. Ashraf, Z. Panhwar, S. Habib, M. A. Memon and J. Arif, “Size of radial and ulnar artery in local population,” *JPMA,* vol. 60, no. 10, pp. 817-819, 2010.